Tribhuvan University
INSTITUTE OF ENGINEERING
PULCHOWK, LALITPUR

Dissertation No: 074phme602

Sediment Erosion in Guide Vanes of Francis Turbine

Shekhar Aryal

A DISSERTATION SUBMITTED IN FULFILLMENT OF THE REQUIREMENTS FOR THE DEGREE OF DOCTOR OF PHILOSOPHY IN MECHANICAL ENGINEERING

DEPARTMENT OF MECHANICAL AND AEROSPACE ENGINEERING

November, 2023

Dedicated to my Family and Parents ...

Late. Bhim Prasad Aryal and Lila Devi Aryal (Great Grand Father/Mother)

Late. Krishna Prasad Aryal and Bhagwati Aryal (Grand Father/Mother)

Late. Gopal Prasad Bhattarai and Bidhya Manjari Bhattarai (Grand Father/Mother)

Late. Sabitri Aryal (Grand Mother)

Late. Gyanu Devi Aryal (Grand Aunty)

Shankar Prasad Aryal (Father)

Sudha Aryal (Mother)

Sandhya Aryal (Sister)

Pawan Lamichhane (Uncle)

Copyright

Declaration of Authorship

The dissertation entitled "**Sediment Erosion in Guide Vanes of Francis Turbine**", which is being submitted to the Department of Mechanical and Aerospace Engineering, Pulchowk Campus, IOE, TU, Nepal, for the award of the degree of Doctor of Philosophy (PhD) is a research work carried out by me under the supervision of Prof. Dr. Rajendra Shrestha, Department of Mechanical and Aerospace Engineering, IOE, Pulchowk Campus, TU, Nepal, Assoc. Prof. Dr. Ajay Kumar Jha, Department of Mechanical and Aerospace Engineering, IOE, Pulchowk Campus, TU, Nepal and Asst. Prof. Dr. Sailesh Chitrakar, Department of Mechanical Engineering, Kathmandu University (KU), Nepal, between May 2017 to November 2023. I declare that this is my work and has not been previously submitted by me at any university for any academic award.

Shekhar Aryal

Signed:

_____

Date: **November, 2023**

Recommendation

The undersigned certify that they have read and recommended for acceptance, a dissertation entitled "**Sediment Erosion in Guide Vanes of Francis Turbine**", submitted by **Shekhar Aryal** in partial fulfillment of the requirement for the award of the degree of **Doctor of Philosophy in Mechanical Engineering (Hydro Mechanical and Renewable Energy)**.

Prof. Dr. Rajendra Shrestha,
Supervisor,
Dept. of Mechanical and Aerospace Engg.,
IOE, Pulchowk Campus, TU, Nepal

Assoc. Prof. Dr. Ajay Kumar Jha,
Supervisor
Dept. of Mechanical and Aerospace Engg.,
IOE, Pulchowk Campus, TU, Nepal

Asst. Prof. Dr. Sailesh Chitrakar
Supervisor
Dept. of Mechanical Engineering, Kathmandu University, Nepal

November, 2023

Tribhuvan University
INSTITUTE OF ENGINEERING

The dissertation **"Sediment Erosion in Guide Vanes of Francis Turbine"** submitted by **Shekhar Aryal** for partial fulfillment of the requirement for the degree of Doctor of Philosophy in Mechanical and Aerospace Engineering has been accepted by the IOE Research Committee (IERC) upon the recommendation of the supervisor and Departmental Research Committee (DRC) with the approval by the following examiners.

Dr. Baoshan Zhu,
Professor, Department of Engegy and Power Engineering,
Tsinghua University, China

Dr. Hari Prasad Neopane
Professor, School of Engineering,
Kathmandu University, Nepal

Dr. Suman Pradhan,
Nepal YantraShala Energy,
Kathmandu, Nepal

Prof. Dr. Shashidhar Ram Joshi
Committee Chairperson,
Dean, Institute of Engineering
November, 2023

Tribhuvan University
INSTITUTE OF ENGINEERING

The undersigned certify that they have evaluated the dissertation entitled **"Sediment Erosion in Guide Vanes of Francis Turbine"** submitted by **Shekhar Aryal** and have external oral presentation for the partial fulfillment of the requirement for the degree of Doctor of Philosophy and recommended to IOE for the acceptance of this dissertation.

Dr. Baoshan Zhu,
Professor, Department of Engegy and Power Engineering,
Tsinghua University, China

Dr. Hari Neopane
Professor, School of Engineering,
Kathmandu University, Nepal

Dr. Suman Pradhan,
Nepal YantraShala Energy,
Kathmandu, Nepal
November 2023

Departmental Acceptance

The doctoral dissertation entitled "**Sediment Erosion in Guide Vanes of Francis Turbine**", submitted by **Shekhar Aryal** in partial fulfillment of the requirement for the award of the degree of **Doctor of Philosophy in Mechanical Engineering (Hydro Mechanical and Renewable Energy)** has been accepted as a bonafied record of work carried out by him in the department.

Asst. Prof. Dr. Sudip Bhattrai,
DRC Chairman and Head of Department,
Department of Mechanical and Aerospace Engineering, Pulchowk Campus,
Institute of Engineering,
Tribhuvan University,
Nepal

November, 2023

Research Motivation

My journey into the realm of research was shaped by my position as an assistant researcher in the Department of Computational Engineering at Ruhr University Bochum Germany. I did my Master's thesis on Large Eddy Simulation of Hydrogen Combustion with Star-CD simulations under the supervision of Prof. B. Rogg in 2009 from the Institute for Thermo and Fluid Dynamics in the field of computational fluid dynamics (CFD). My active participation in that research project encouraged me to carry out research activities in next-generation CFD. From 2009 to 2012, I served as a research assistant at the Interdisciplinary Centre for Advanced Materials Simulation (ICAMS) specializing in micro mechanical-and-macroscopic-modeling. I carried out the research on Computation of Back Stress Due To Strain Gradient under the supercision of Prof. Anxin Ma and Texture evolution during uniaxial creep in a ferritic power-plant steel under Prof. Victoria Yardely in Bochum Germany. My first poster presentation was held T National Physical Laboratory, london UK.
Additionally, I worked as a research assistant at Bundesanstalt für Materialforschung und -prüfung (BAM) to research on The development of a model for calculating the damage development in concrete due to fatigue loading under the guidance of Prof. A. Rogge. All these technical researches are the mild stone of my career towards Ph-D-research and analysis. My Master's thesis has especially served as a connecting link to my Ph-D-research indirectly.
The development of new hydro-power projects, including sediment erosion, poses significant technical hurdles. The deteriorating performance of hydroelectric turbines has emerged as a serious technical challenge in the development of hydroelectric power facilities. Sediment transfer from rivers is not a natural phenomenon, and it cannot be totally managed or prevented. Extracting clean water from the river for generating electricity is an expensive process since sediment-settling basins must be designed, built, and maintained. Removing fine sediments completely is neither practical nor cost effective. When dealing with sediment issues in hydro-power plants, a three-dimensional strategy is preferable: silt-resistant equipment (SRE) to withstand the sediment, effective desilting arrangements (EDA) to prevent sediment, and catchment area treatment (CAT) to reduce the sediment load.

Turbine guide vanes' erosion by sediment is a complicated process that is influenced by a number of factors, including the size, concentration, hardness of the silt, water's velocity, and the characteristics of the base material. As sediment wear there increases the turbine's efficiency decreases. Many scholars have carried out research on the impact of these parameters on sediment wear; however, the majority of these studies use small-scale samples in various test rigs designed to mimic the turbine's flow conditions. As a result, simulating real flow conditions and the sediment wear phenomenon is too difficult.

In order to create an erosion model, a great deal of study has been done on the material properties involved; nevertheless, the turbulent flow regime of guide vanes hasnot received adequate attention. The available formulas are more intricate. The main causes of this conditions are the intricacy of wear and the numerous factors influencing the result.

All rivers that flow through Nepal have a high concentration of quartz and a sediment load, according to a research done at the Department of Mechanical Engineering, Kathmandu University, and the Department of Mechanical and Aerospace Engineering, Institute of Engineering (IOE), Tribhuvan University (TU), Nepal. This implies that silt erosion will affect any turbines erected in these rivers. This suggests that a wide range of elements impact the erosion damage process. To accurately anticipate the rate of erosion, it is imperative to investigate and determine the impact of varying sediment particle sizes and shapes. As a result, issues are solved with sediment erosion calls for a multidisciplinary strategy. The interaction between the erosion inside the turbine and the movement of the particles has to be further studied and developed.

As I got inrolled for my PhD at the IOE, TU at hydro-power sectors, my first duty was to find out the laboratory to do my research with experiments. I visited Turbine Testing Lab (TTL), of Kathmandu University (KU) frequently to know about the lab's facility. I met Sailesh Chitrakar, the Asst. Prof. and TTL in-charge of KU there. After I discussed with him about my immense interest about the hydro-mechanical sector, he accepted to supervise me to carry out the research. He liked my idea and assured me to hint the signposts needed to pursue my Ph-D. That was the turning point of my life as a researcher to begin my work and experiment at TTL, KU.

The relation between the motion of sediment particles and the erosion of the turbine components has been investigated, studied and experimented at the Department of Mechanical And Aerospace Engineering (DMAE), Institute of Engineering, TU, and TTL, KU, and Hydro Laboratory Nepal (HLN). This indicates that the volume and concentration of quartz are high in all the rivers flowing across Nepal. Furthermore, the flow phenomena are responsible for causing damage in turbine components. The researches conducted so far have discovered that the primary and the secondary flow

including the vortex filament are responsible for damaging the surface of GVs and runner blades. Adequate attention has not been paid in understanding the impact of various sediment particles and slow dynamics for predicting erosion. So, it is quite crucial to conduct a research on this area.

Abstract

The hydro-power plants under Himalayan basins are mostly characterized by heavy sediment load due to geographical and metamorphic constraints. Run-off-river projects with the limited size of the desilting basins allow suspended sediments to be carried into the turbine components, causing wear due to sediment erosion. In the case of high-head power plants consisting of Francis turbines, a large portion of the hydraulic energy is transformed into kinetic energy within the guide vanes. This causes various instabilities in the flow due to high acceleration and velocity. Some recent studies have shown that due to the combined effect of the secondary flow around the guide vanes and sediment carrying flow, the clearance gap increases, further aggravating the performance of the turbine. This study takes a reference from one of the power plants in Nepal containing Francis turbines. An in-depth analysis of the effect of the sediment in this power plant and sediment erosion in the turbine components has been performed. A CFD analysis of the guide vanes and runner blades corresponding to the same turbine has been conducted and the results are used to analyze the erosion pattern on the actual turbine. The detailed erosion analysis is made possible with a 3D scanner, such that the eroded regions can be captured and classified based on the flow behavior at those regions. Guide vanes and runner blades are found to be the predominant components affected by erosion. It has been seen that most affected regions are erosion-affected regions that originated from increasing clearance gaps between the guide vanes and facing plates caused by continuous leakage flow within the two sides of the guide vanes.

The broad range of dependent parameters, such as sediment characteristics, base materials and flow conditions, limits estimation of sediment erosion in hydraulic turbines. Some mathematical models have been proposed in the past literature and some of them have been incorporated in a CFD tool for predicting erosion and flow conditions. Rotating Disc Apparatus is a simplified experimental setup initially developed targeting erosion studies in Francis turbines. However, the closeness of the results obtained from this apparatus with the actual turbine remains uncertain. This thesis also investigates the flow phenomena inside the guide vanes region using RDA, and compares them with the actual turbine. A reference case of Jhimruk hydro-power plant has been taken in

this study, which has been scaled down with a factor of 1:4 from its original size. The numerical fluid domain consists of four rotating blades distributed around the disc uniformly. The GVs were designed as symmetrical NACA0012 hydrofoils. The pressure distribution around the guide vanes inside RDA and the tip-vortices' development have been compared with the results from the past research works. It is found that the flow field around guide vanes inside RDA matches closely with that of the real turbine. The stagnation point and development of the pressure and suction sides are similar to the actual guide vanes, which make the apparatus suitable for investigating the erosion after including the sediment particles. However, more investigations might be needed to determine whether to use the same apparatus for the runner blades or guide vanes under different operating conditions.

Scanning electron microscopy (SEM) has been used to analyze erosion in various regions of guide vanes constructed of two different materials, Brass and Mild Steel. The mechanism of erosion in various parts of guide vanes is found to be highly related to the flow pattern in that part. Mild steel guide vanes displays corrosion attack and crack formation as material is removed, but Brass guide vanes shows plastic deformation during ploughing, cutting, and pitting. The weight of two Brass and two Mild Steel guide vanes before and after 390 minutes experiment were 249.44g, 241.27g, 283.89g and 276.78g and 244.5g, 236.0g, 280.9g, and 274.9g respectively.

Acknowledgement

This Ph.D. is a single degree offered by Tribhuvan University's Pulchowk Campus' Institute of Engineering. My supervisors for this study are: Prof. Rajendra Shrestha from the Institute of Engineering, Assoc. Prof. Ajay Kumar Jha from the Institute of Engineering, and Asst. Prof. Sailesh Chitrakar from KU. I appreciate their confidence in me and superb assistance throughout the endeavor. I want to thank them from the bottom of my heart.

I am proud to record that I had the opportunity to work with an exceptionally experienced professor like Prof. Bhola Thapa the Vice-Chancellor of KU, Prof. Shashidhar Ram Joshi the Dean of the Institute of Engineering, Prof. Arun Kumar from the Indian Institute of Technology (IIT), Roorkee, Prof. Thomas Staubli from the Swiss Federal Institute of Technology (ETH), Prof. Ravindra Nath Shrestha, Prof. Triratna Bajracharya, Prof. Gokrana Motra, Prof. Bhola Nath Sharma Ghimire, Asst. Dean and Prof. Sushil Bahadur Bajracharya, Asst. Dean and Prof. Binod Kumar Bhattarai, Prof. Sudha Shrestha, Prof. Laxman Poudel, Prof. Mahesh Chandra Luintel, Prof. Sangeeta Singh, Prof. Surya Raj Acharya, Prof. Hari Neopane, Prof. Yogen Pant, Asst. Dean and Assoc Prof. Suraj Lamichhane, Assoc. Prof. and Campus Chief Indra Prasad Acharya, Assoc. Prof. Bishwo Prasanna Amatya, Assoc. Prof. Surya Prasad Adhikari, Assoc. Prof. Rajesh Kaji Kayestha, Assoc. Prof. Shree Raj Shakya, Assoc. Prof. Nawraj Bhattarai, Assoc. Prof. Hari Bahadur Darlami, Asst. Prof. Prashant Kumar Ghimire, Asst. Prof. Sanjeev Maharjan, Asst. Prof. Deu Kaji Gurung, Asst. Prof. Biraj Singh Thapa, Asst. Prof. Anant Rai, Asst. Prof. Hari Dura, Asst Prof. and Department Research Committee (DRC) chair Sudip Bhattrai, Asst. Prof. Bijendra Prajapati, Asst. Prof. Anita Prajapati, Asst. Prof. Laxman Motra, Asst. Prof. Sanjay Neupane, Asst. Prof. Tek Raj Subedi, Asst. Prof. Neeraj Adhikari, Asst. Prof. Navin Kumar Jha, Asst. Prof. Basanta Adhikari, Asst. Prof. Baburam Dawadi, Asst. Prof. Basanta Joshi, Asst. Prof. Santosh Giri, Er. Rudra Ghimire, Er. Upendra Bhatta, Er. Atmaram kayestha, Er. Amul Ghimire, Er. Nischal Pokahrel, Er. Prajwal Sapkota, Er. Bhim Ghale, Instructors. Bal Prusottam Shakya, Govinda Maharjan, Administrative Officers Bidhur Dhakal, Sunita Dhungel, Rili Pradhan, Yesodha Adhikari, Nhuchha Narayan Shrestha, Krishna Bhatta, Krishna Karki,

Ram Chandra Awal and all the Institute of Engineering, TU members and Turbine Testing Lab, KU members for their essential assistance with my research.
I especially acknowledge Nepal Electricity Authority (NEA) Managing-Director Kul Man Ghising, Er. Pramod Rijal, Er. Rajendra Koirala, Er. Avas Ojha, Er. Pashupati Gautam, Er. Ram Kumar Yadav, Er Atmesh Poudel, Er. Subrath Aryal, Mr. Tilak Rana, and Mr. Tej Jirel for their assistance with my work. Hydro Lab Nepal (HLN) General-Manager Meg Bahadur Bishowkarma, Er. Ishwar Joshi, Mr. Yogesh Khakda, and Mr. Bhagwan Basnet deserve my special thanks for their assistance with my lab work.
I would like to express my gratitude to the vice president of operations Prakash kumar Shrestha of Butwal Power Company (BPC), Mr. Shyam Thapa, Mr. Sundar Poudel, and Mr. Dhan Bahadur Gaha of Jhimruk Hydro Electric Project (JHEP), Puythan for their assistance with my lab work. I'd like to thank Nepal Hydro Electric (NHE), Butwal's Er. Purushottam Panti, and Mr. Shiva Chaudhary for their assistance with my lab work.
I am equally indebted to the entire team of Zehner Technology's Er. Ram Chandra Thapa and Er. Bishal Poudel, as well as Pro-Mech-Minds and Engineering's Er. Nilesh Pradhan, Er. Sunny Tuladhar, and Er. Nashla Shakya, for their technical assistance during my work. I would like to thank the University Grant Commission (UGC) and Nepal Academic of Science and Technology (NAST) for their partial financial support to fulfill my Ph.D. program. My sincere thanks go to Assco. Prof. Rena Thapa, Asst. Prof. Madhav Prasad Dahal, Asst. Prof. Dr. Bharat Neupane and Asst. Prof. Punya Prasad Koiral for supporting my thesis work with editing. I thank Shambhu Bhattarai (Uncle), Chandra Bahadur Lama (Uncle), Madhav Khanal (Uncle), Yadav Raj Mainali (Uncle), Sabitra Upreti (Sister), Kreepa Shrestha, Mona Shrestha, Axit Raj Poudyal, Dambar Bahadur Tamang (Province's MP), Surya Man Dong, Kersing Tamang, Lakpa Tsering lama, Tsering Dorji Lama (Province's MP), John Carr, Anil Pokhrel, Shushant Limbu, Region Poudel and Damodar Kandel for encouraging me during my entire work.
Finally, any attempt at any level cannot be satisfactorily completed without the support of my parents, sister, sister-in-law and nephew for their unending love and support throughout my career.

Shekhar Aryal
074phme602

List of Figures

List of Tables

List of Abbreviations

AD	After Death (Jesus)
ADB	Asian Development Bank
ASTM	American Society for Testing and Materials
BAM	Bundesanstalt für Materialforschung und -prüfung
BPC	Butwal Power Company
BSL	Baseline Two Equation Model
CAT	Catchment Area Treatment
CNC	Computer Numeric Control
CFD	Computational Fluid Dynamics
DMAE	Department of Mechanical and Aerospace Engineering
DT	Draft Tube
EDA	Effective Desilting Arrangements
EDS	Energy Dispersive Spectroscopy
ETH	Eidgenossische Technische Hochschule (Swiss Federal Institute of Technology)
FSI	Fluid Structure Interaction
GCI	Grid Convergence Index
GON	Government of Nepal
GVs	Guide Vanes
GW	Gigawatt
GWh	Gigawatt Hour
HLN	Hydro Lab Nepal
HPP	Hydro Power Plant
HVOF	High Velocity Oxygen Fuel
Hz	Hertz
ICAMS	Interdisciplinary Centre for Advanced Materials Simulation
ICEM	Integrated Computer Engineering and Manufacturing
IEC	International Electrotechnica Commission
IDA	International Development Association
IIT	Indian Institute of Technology
INPS	Integrated Nepal Power System
IOE	Institute of Engineering
KM	Kilometer
KU	Kathmandu University
MSDM	Micro-Scale Dynamic Model
MW	Megawatt
MWh	Megawatt Hour
NACA	National Advisory Committee for Aeronautics
NEA	Nepal Electricity Authority

NHE	Nepal Hydro Electric
N-S	Naviers-Stokes
OM	Optical Microscope
PIV	Particle Image Velocimetry
PS	Pressure Side
RANS	Reynold's Average Navier-Stokes
RDA	Rotating Disc Apparatus
SEM	Scanning Electron Microscope
SRE	Silt Resistance Equipment
SS	Suction Side
SST	Shear Stress Transport
TTL	Turbine Testing Lab
TU	Tribhuvan University
USD	United States Dollar
U/S	Upper Stream
3-D	Three Dimenison

List of Symbols

a	distance	m
P	power	W ($\mathrm{J\,s^{-1}}$)
W	Wear	-
V	Velocity	$\mathrm{m\,s^{-1}}$
n	Number of materials	-
U	Characteristic speed	$\mathrm{m\,s^{-1}}$
ρ	Density of the particle	$\mathrm{kg/m^3}$
D	Characteristics Size of the machine	mm
p	Particle count per unit surface	-
K	Experimental coefficient of particle	-
E'	Erosion of the particle	-
m	Mass of the particle	kg
C	Average translation rate	-
α	Coefficient dependent on flow conditions, particles and materials	-
N	Number of abrasive particles	-
t	Time interval	s
β	Flow condition over the plate	-
v	Mean velocity of the plate	$\mathrm{m\,s^{-1}}$
ϵ	Particle concentration	-
c	Average velocity	$\mathrm{m\,s^{-1}}$
C_w	Solid weight	kg
η_m	Efficiency of mixture	-
η_w	Efficiency of clean water	-

Contents

This page is left intentionally blank...

Chapter 1

Introduction

The research works introduce in this chapter with background and a statement of the problem. After designing research questions, scopes and limitations, research objectives define. A list of publications throughout the study period is presented, and the overall structure of the thesis is outlined.

1.1 Background

Despite the promising future potential for hydro-power development in the Asian region, geological problems appears to be a serious impediment. Hydro-power is one of the most efficient and cleanest forms of energy and has been used in many countries as a principal source of electricity. However, it has been reported that two-third of the world's feasible hydro power resources are still undeveloped. Out of these potential resources, more than 55% lies in Asia alone [1]. Despite the future prospects for hydro-power development in this region, the geological problem seems to be a major obstacle. The study shows that out of 20 billion tons of global sediment flux from rivers to the oceans per year, around 6 billion tons are contributed by Asian rivers, particularly from the Indian subcontinent [2]. The problem of sediment handling, maintenance and operation of the power plants has become a serious issue. The total installed capacity in 2017-18 was 1016 MW but the peak demand was 1508 MW. This power deficit during the peak period was compensated through power purchase from India, with a total of 2581 GWh in one year [3].
Nepal Electricity Authority (NEA) also emphasizes the participation of the private sector in hydro-power development by raising the posted power purchase rate. However, developing a hydro-power requires a large investment and has a longer gestation period compared to other power production. Besides, the import of technologies and manpower from abroad multiplies the cost numerous times. The risks and uncertainty

factors create economic barriers for further development. The erosion rate density parameter (kg/s/m^2), which correlates to flow pressure and shear stress, provides a fair indication of erosion. The impacts of silt concentrations on the erosion rate density of the turbine blade were calculated using the Tabakoff erosion model simulation results. One major obstacle to current hydro-power development in Nepal is the run-of-the river type schemes in most projects. This type of scheme not only ceases the generation in the dry season, but also induces maintenance and operation challenges due to excessive sedimentation in the wet season. Some efforts have been made in developing more reservoir-type projects, with initiatives from the 140 MW Upper Seti (Tanahun), 600 MW Budhi Gandaki and 530 MW Dudh Koshi Storage Development Projects. It was reported that in Nepalese rivers, nearly 70% of the constituent are hard particles, including Quartz [4].

The other sediment parameters (sediment size, shape, turbine operating condition, and impingement angle) remained constant. It can be shown that as the concentration rate increases, so does the erosion rate density, although this is not the case at all for guide vane apertures. This is to be expected because, at full load, the fluid velocity increases and, as a result, the particle velocity [5]. Particle movement and erosion are mostly determined by particle size. Centrifugal force is created by the tangential component of absolute velocity for particles flowing in a curved channel or swirl flow, whereas drag force is caused by absolute velocity. The balance of these two forces determines the critical diameter of the particle that will rotate in orbit. The critical diameter is determined by the drag coefficient, the particle's specific gravity, the radius at which the particle is moving, and the ratio of particle velocity in the peripheral direction to the absolute velocity of water. Particles bigger than the critical diameter travel away from the flow path's centre and strike the wall, while smaller particles flow with the water [6].

The second largest Kaligandaki 'A' hydro-power plant has a sediment concentration varying from 20 parts per million (0.02 kg/m^3) in the dry season to 50,000 parts per million (50 kg/m^3) in the wet season from June to September. After the commissioning in 2002, five major turbine maintenance's have been carried out till 2014 [7]. Water sediment content can no longer be ignored at any stage of hydro-power project implementation. This comprises all phases such as inquiry, design, operation, maintenance, refurbishment, and upgrading. Due analysis of the problem at each stage would have an impact on economics on the one hand, and long-term remedies would emerge on the other.However, increasing the size of the turbine, which increases the hydraulic radius of curvature and thus decreases accelerations, is one approach to reducing sediment erosion. Furthermore, while a Francis turbine can be designed to be more resistant to silt erosion, this may have an undesirable effect on other features of the turbine. Every

hydraulic turbine is, to some extent, a compromise between many requirements [8]. The study of the effects of these particles on Francis turbine and optimization strategies for minimizing erosion can be found in the literature. These studies showed that the erosion in the turbine's runner blade can be reduced by changing the blade angle distribution [9], and [10]. The highest proportion of quartz, which has a greater hardness value than any of the turbine materials, was a primary cause of erosion damage to turbine components [11]. Recent studies have shown that the problem of sediment erosion in runner blades is not only affected by its design, but also by the guide vanes (GVs) upstream of the runner [12], [13], and [14]. Secondary flow can expedite devastation in high sediment-laden rivers by producing irregular wear patterns and lowering the thickness of the vanes. In the bladed portions of Francis turbines, several types of erosion exist, depending on the types of flow behavior in that zone, such as leakage flow erosion, horseshoe vortex erosion, acceleration erosion, and turbulence erosion. These phenomena are predicted using computational and experimental methodologies [13]. Due to a pressure difference between the two sides of the GV, water tends to flow into the gap from the high-pressure side to the low-pressure side with high acceleration. Consequently, the primary flow in the low pressure or suction side distorts, adding to the losses in the turbine. Flow instability manifests itself as leaks through the clearance gap, a horseshoe vortex, rotor-stator contact, and turbulence fueled by high velocity and acceleration. Erosion, on the other hand, deteriorates the surface shape and exacerbates the flow [15]. GVs are present in Francis turbines to regulate the flow and maintain the turbine's operating conditions. To enable the opening and closing of GV, a small clearance gap is present between the GV and facing plates on both sides. However, due to the continuous impact of the sediment particles, the size of the clearance gap increases. The clearance gap in Kaligandaki 'A' (144 MW) power plant in Nepal was reported to have increased by 2.5 mm towards the leading edge and 4.2 mm towards the trailing edge on average after 16500 hours of operation [16].
The repair and maintenance impose a heavy loss of capital along with the premature failure of turbines compared to their estimated life expectancy. In order to eliminate the investor's reluctance to develop hydro-power in the country, the challenge of sediment erosion in turbine components needs to be addressed with a sustainable solution. This study focuses on an in-depth case study of one of the power plants in Nepal containing high head Francis turbines and affected severely by sediment erosion. A numerical study is performed on the GVs and runner fluid domains. Various flow behaviors inside this domain are analyzed, and the potential causes of the erosion due to the secondary flows are inferred. Hydraulic machinery erosion is affected by eroding particles, such as their size, shape, and hardness; substrates, such as their chemistry, elastic properties, surface hardness, and surface morphology; and working circumstances, such as velocity,

impingement angle, and concentration. The shape, size, and mineral composition of sediment vary based on the distance traversed by particles, the gradient of the river, and the geological formation of the river course and catchment areas [17].

In the case of Francis turbines, due to several secondary flow phenomena occurring inside the turbine, the erosion process is even more challenging to predict. Some numerical techniques have recently been developed to predict the amount of erosion caused by any particle travelling with the flow. However, validations of such results are problematic because of the difficulty in developing an erosion model through experiments that control all the above parameters [18]. Prior literature has shown that correlations for erosion rates can be developed experimentally by using simplified test apparatuses, such as a pot-tester [19], or a jet rig [20], where the characteristics of the sediments and the base material can be varied together with some geometrical and flow factors, such as impingement angle and velocity. Another type of test rig includes test specimens, which are mounted onto a disc or an arm and are rotated with the help of a high-speed motor [21].

The rotating disc apparatus (RDA) was later modified and submerged into a mixture of erodent and fluid medium to test the effect of sand erosion in actual blade profiles of Francis runner, rather than the flat surface only, and results showed good accordance with the results predicted by computational fluid dynamics (CFD) simulation in terms of the regions in the blade where erosion takes place [22]. The rig is constantly being used to carry out both qualitative and quantitative measurements of the erosion and erosion potential in rotating components of the turbines [23]. It has been mostly useful in making a comparative study between the two designs or analyzing the erosion patterns of the blades without any quantitative assurance. Moreover, the credibility of the apparatus for providing a flow field similar to that of the real turbine is questionable, especially in the cases where the blades are included. This study focuses on analyzing the credibility of RDA for estimating the erosion of guide vanes of Francis turbines. A numerical model for the apparatus was developed, which contains a mixture of sediment and water.

The flow behavior inside RDA was compared with the results of the actual turbine, using past research papers. In this Ph.D. work, several experiments were conducted to investigate the properties of the suspended sediment samples impacting the GVs and runner blades of hydro-power plants of Nepal. The suspended sediment concentration, particle size distribution, and mineral content tests have been thoroughly scrutinized. Data were collected from the desilting basin start, desilting basin end, and cooling tank. The 3D-scanned deteriorated GVs were measured using relative data, and the results were compared to CFD simulation analysis. The four scaled-down colour coating guide vanes were tested in the RDA and compared with the CFD simulation ANSYS-CFX.

This experimental test is used to learn about erosion at GVs and compare it to the actual situation in the power plant.

1.2 Statement of the Problem

This research demonstrates the importance of knowing the interaction between the two phenomena: secondary flow and sediment erosion, and it provides ways for predicting and mitigating the combined effect. In the case of guiding vanes' clearance gaps, the combined impact is prevalent. The surface of the guide vanes and facing plates is constantly degraded due to corner vortices around the clearance gaps. This erosion worsens the flow and promotes more erosion in downstream turbine components. As a result, the simultaneous effect can be reduced by managing one of the two events. The problems of sediment erosion are major challenge from an operation and maintenance perspective in Nepal with Francis turbines and is likely to worsen for the following reasons [12].

1. High concentrations of hard minerals like Quartz, Feldspar and Mica cause Wear in turbines.

2. The clearance gap, and pressure differences between pressure side, and suction side, of GV's enforce leakage flow creating vortex filaments.

3. The vortex filaments ultimately hit the runner towards the inlet, causing a loss in efficiency of the runner as well as erosion.

Various sorts of solutions may be implemented in the design, operation, and maintenance of hydro-power plants to decrease hydro-abrasive erosion [24].

1. High-resistance materials and coatings are utilized to prevent erosion. Improvements to turbine design and a more accurate maintenance plan.

2. Building and operating facilities for sediment settlement before entering the turbine (storage reservoirs, gravel and sand traps, etc.)

3. In situations of high erosion potential, temporarily blocking intakes and suspending turbine operation (Hydro-power plant shutdowns).

The first measure enhances erosion resistance while the final two minimize the "weight" of the silt on the sections of the machine. No hydro-abrasive erosion in medium and

high head hydro-power plants with heavy sediment loads can be completely averted despite the great breakthroughs in material science. Moreover, the turbine water cannot be excluded completely from fine sediments, and maintenance of civil structures and electro-mechanical equipment is therefore frequently implemented.

1.3 Research Questions

Three research questions (RQ) were designed to address the main problem outlined in this research. These are:

RQ1: What are the existing scenarios of hydro-power plants in Nepal in terms of sediment erosion, typically in the regions of GVs and runners?

RQ2: What are the various flow patterns that cause erosion of GVs and runner blades?

RQ3: How are the flow and sediment erosion in GVs predicted using simplified experimental investigations with SEM analyses?

1.4 Scopes and Limitations

The goal of this research is not only to improve GVs operating in sediment-laden water that is prone to sediment erosion but also to identify regions where special surface treatment is required to increase the lifetime of components for new hydro-power projects that face sediment erosion risks. This is accomplished by meeting the objectives outlined in Section 1.5. This study investigates the role of sediment properties in GVs and runner blades. The sediment erosion research on Francis turbines in general and GVs in particular aims to contribute knowledge to:

1. Operation strategy of GVs and runner blades

2. RDA experiment of scale down GVs

3. Erosion pattern in different locations of GVs using the experiment and Scanning Electron Microscope (SEM) analyses

As a result, only the technical aspect has been thoroughly investigated in the current work. It is anticipated that if a GVs designer combines hydraulic design and coating of the GVs and runner blades, a large reduction in erosion can be accomplished; however, detailed investigation of this aspect is limited by the scope of this research. This

thesis uses numerical and experimental criteria to investigate the flow behavior around GVs and Francis turbine runner. The GVs and runner blades belong to the Jhimruk hydro-power plant of Nepal. Numerical study is performed using CFD in ANSYS CFX 18.1. Experimental work includes four scale down symmetric GVs (NACA0012) at RDA were studied with pressure distribution around GVs, tip leakage vortex, stream line flow behavior, velocity along the length of the chord and erosion pattern and also compared those results with the real turbine case from past studies.
The GVs contain a uniform clearance gap of 1 mm on one side. The gap represents an eroded surface, which is non-uniform in the case of a real turbine. The sand particles poured inside RDA chamber were 150 to 200 micrometer in diameter. The RDA was made with proper dimensions in the TTL at KU, having 14 baffles, one shaft connecting with a rotating disc of 300 mm inner diameter with 4 bucket holding chambers, sand and water pouring valve as well as temperature and pressure sensor valve and also with inlet and outlet cooling valve [21]. Meshing of the fluid domain was done using integrated computer engineering and manufacturing (ICEM) with CFD and graphical user interface (GUI) technique [25] was used to carry out the mesh sensitivity study.
The experiment was done for single phase flow only; therefore cavitation model was not used. The effect of the vortices developed from the mixing of leakage flow with streamline flow was concluded from the pressure, velocity and vorticity contours. Scaling effect has basic connection between the prototype model and real model, though 4 scales down symmetric GVs have been used in this RDA experiment that represent the Jhimruk hydro-power plant, however this experiment hasnot considered scaling effect while conducting the experiment and analysis, which might have different results if researchers in future conduct scaling analysis.

1.5 Aim and Objectives

The research aims to carry out field-based, experimental and numerical investigations of Francis turbines exposed to sediment-laden rivers and to extend the knowledge of the causes and consequences of sediment-induced erosion on guide vanes and runner blades.

OB1: To find out the status of hydro-power plants of Nepal in terms of sediment characteristics and sediment erosion of turbines.

OB2: To conduct flow phenomena in GVs and runner of Francis turbines and their potential consequences on erosion in sediment-laden projects.

OB3: To perform an estimation of the erosion in GVs of Francis turbines using a simplified apparatus and study the erosion pattern using the Scanning Electron Microscopic technique.

1.6 Scientific Contributions

The published archival journal article stated in Table 1.1 and conference presentations listed in Table 1.2 are the contributions of this research. During this research, one journal publication was published, and two conference papers were delivered. As part of this research, the concepts, analysis, figures, and charts, among other things, were published in several recognized worldwide publications [26], [27] and [28] as part of the research's publication contributions. The published materials from this research are primarily incorporated in this structured thesis with permission from the copyrighted article publishers.

Table 1.1: Peer-reviewed archival journal papers

Author	Title	Publisher
Aryal et al., 2020	A case study of Wear in a High Head Francis Turbine Due to Suspended Sediment and Secondary Flow in a Hydro-power Plant of Nepal	International Journal of Fluid Machinery and Systems, 13(4), pp.692-703 Tokyo Japan

Table 1.2: Peer reviewed conference papers

Author	Title	Publisher
Aryal et al., 2022	Credibility of Rotating Disc Apparatus for investigating sediment erosion in guide vanes of Francis turbines	Earth and Environmental Science Vol. 1037, No. 1, p. 012034 Bristol, UK
Aryal et al., 2022	Coating technology in hydroturbines for sediment affected power plants: A review	Earth and Environmental Science Vol. 1037, No. 1, p. 012021 Bristol, UK

1.7 Dissertation Organizations

The thesis is organized into five chapters. The chapter-wise structuring of the contents is summarized here.

- **Chapter 1** introduces the research background, problem statement, research question, Scopes and limitations, aim and objective, list of scientific contributions and dissertation organization.

- **Chapter 2** provides a review of the literature on wear theory, erosion model, repair and maintenance, past studies, and state-of-the-art research in sediment erosion of Francis turbines, as well as the research gap and the proposed approach.

- **Chapter 3** presents case studies of erosion in Nepal's hydro-power plants.

- **Chapter 4** describes the methods, methodology adopted, and methodology used in research and experiment. Similarly, the investigation of sediment erosion includes suspended sediment concentration; parts per million, particle size distribution, and mineral content are presented. Numerical investigation of sediment erosion in turbine components, erosion in GVs of Francis turbine at Jhimruk hydro-power plant, steady-state approach with Navier-Stokes equations and turbulence models with shear stress transport theorem are analyzed. Numerical setup of RDA and experimental investigation of RDA and SEM are discussed.

- **Chapter 5** discusses the results and findings, analyses of experimental works and the necessary interpretations, including the Jhimruk hydro-power plant, Kaligandaki 'A' hydro-power plant, Middle Marsyangdi hydro-power plant, and Lower Marsyangdi hydro-power plant, flow around GVs of Francis turbine including runner blades, validation of the flow pattern around RDA compared to the actual turbine and SEM done with leading edge, trailing edge and mid-stream of scale down GVs and also the weight loss calculations and erosion rates.

- **Chapter 6** presents conclusions and recommendations for future works.

- **Appendices** A, B, C and D presents all published and accepted papers.

1.8 Chapter Summary

The study aims to conduct field-based, experimental, and numerical investigations of Francis turbines exposed to sediment-laden rivers to learn more about the causes and effects of sediment-induced erosion on guide vanes and runner blades. The flow phenomena in GVs and the runners of Francis turbine and their possible effects on erosion in sediment-laden projects, are analyzed experimentally and numerically. An

RDA is used to estimate erosion in the GVs of Francis turbines with post processing using SEM.

Chapter 2

Literature Review

The word "wear" is used to describe a variety of items. Wear can be categorized and defined in multiple ways. Erosion is one of many types of wear on a water turbine caused by sediment. This chapter deals with types of wear, factors affecting wear, erosion model, general erosion model, erosion models for hydraulic machinery, basic erosion model, Tabakoff erosion model, Finnie erosion model, repair and maintenance, past studies and state-of-the-art sediment erosion of Francis turbines, research gap and the proposed approach

2.1 Wear Theory

The definition of wear deals primarily with the gradual loss or degradation of material due to the mechanical contact of components. It is defined as "damage induced by relative motion between a solid surface and a contacting substance on a solid surface, frequently comprising slow material loss" American Society for Testing and Materials (ASTM G40-88). Wear is directly proportional to $velocity^n$, where n represents the exponent value between 3 and 4 given by equation 2.1.

$$w \propto v^n \tag{2.1}$$

Similarly, wear is related to the product of the main flow acceleration, coefficient of friction, particle layer thickness, solid-liquid density difference, and fluid viscosity. As a result of this, the following equation is obtained 2.2.

$$Wear \propto \frac{U^3 \cdot (P - \rho) \cdot d^3 \cdot p \cdot k}{D} \tag{2.2}$$

Where U represents the characteristic velocity of the liquid, ρ represents the density of the liquid, D is the characteristic size of the machine, p is the number of particle

count per unit surface area, and K is the experimental coefficient based on the abrasive nature of the particle, according to Bergeron [29]. A single solid particle reacting on the surface of a material generating erosion is represented by E', and E' is proportional to the kinetic energy produced by the particle's moment, according to Duan [30], which is given by equation 2.3.

$$E' = \alpha \cdot \frac{(m \cdot c^2)}{2} \tag{2.3}$$

Where the mass of particles is marked by m, the average particle velocity of translation is marked by C, and a coefficient dependent on flow conditions, particles, and materials is marked by α. The following equation is used to compute the number N of the abrasive particles containing with the plate surface at the time interval t defined by the equation 2.4.

$$N = \beta \cdot \epsilon \cdot v \cdot t \tag{2.4}$$

Where a coefficient influenced by the flow conditions around the plate and the flow's carrying capabilities is denoted by β, the mean velocity of the flow is marked by v, and the particle concentration is represented by ϵ. The plate erosion E at the interval of time 't' is given below 2.5.

$$E = E' \cdot N = \alpha \cdot \beta \cdot \frac{(m \cdot c^2)}{2} \cdot \epsilon \cdot v \cdot t \tag{2.5}$$

The average velocity c of the suspended solid particles in the flows is directly proportional to the flow speed v, i.e. $c = \gamma \cdot v$ 2.6.

$$E = \alpha \cdot \beta \cdot \gamma^2 \cdot \frac{(m \cdot \epsilon \cdot v^3)}{2} \cdot t \tag{2.6}$$

$$E = K \cdot m \cdot \epsilon \cdot v^3 \cdot t \tag{2.7}$$

The preceding equation 2.7 indicates that the abrasive erosion of stationary components passed by liquid flow containing solid particles is proportional to the mass of the particles, volumetric concentration, third power of the flow velocity and duration of the flows.

2.2 Types of Wear

2.2.1 Abrasive Wear Mechanism

Abrasive wear is caused by the clash of the hard and soft surfaces of various components. American Society for Testing and Materials defines abrasive wear as material loss caused by hard particles colliding with a solid surface. As demonstrated in Figure

2.1, [31] the particles or grains can be removed via micro-cutting, micro-fracturing, individual grain pulls, or repeated fatigue.

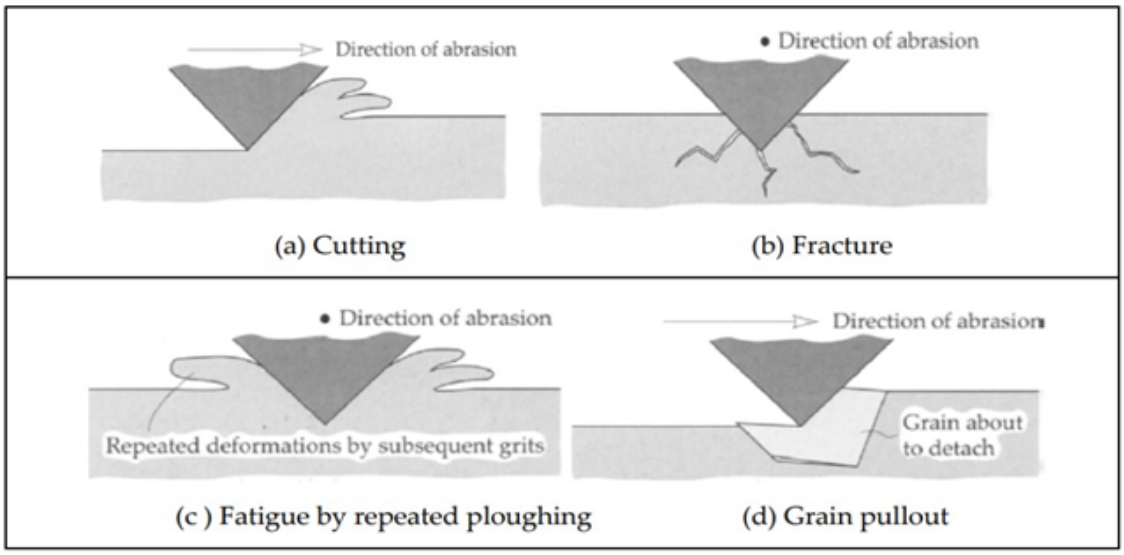

Figure 2.1: Mechanisms of abrasive wear

2.2.2 Erosive Wear Mechanism

Erosive wear is defined as a sliding movement that takes place over a short period; when solid or liquid particles collide with the surface of the components. Figure 2.2, [31] show that particles can be removed via cutting, fatigue, plastic deformation, or brittle fracture.

2.2.3 Adhesive Wear Mechanism

The major source of adhesive wear is frictional contact between two or more surfaces. There is a complicated particle attachment from one material's surface to another. The relative motion of the two components causes wear debris, and materials from one are transferred to the surfaces of the other, resulting in adhesive wear. Sufficient distances are provided between the two surfaces of the components, even though the two surfaces come into contact due to cohesive adhesive forces.

2.2.4 Surface Fatigue

Cyclic stress causes micro-cracks from where the materials of the surfaces are removed, also known as fatigue wear.

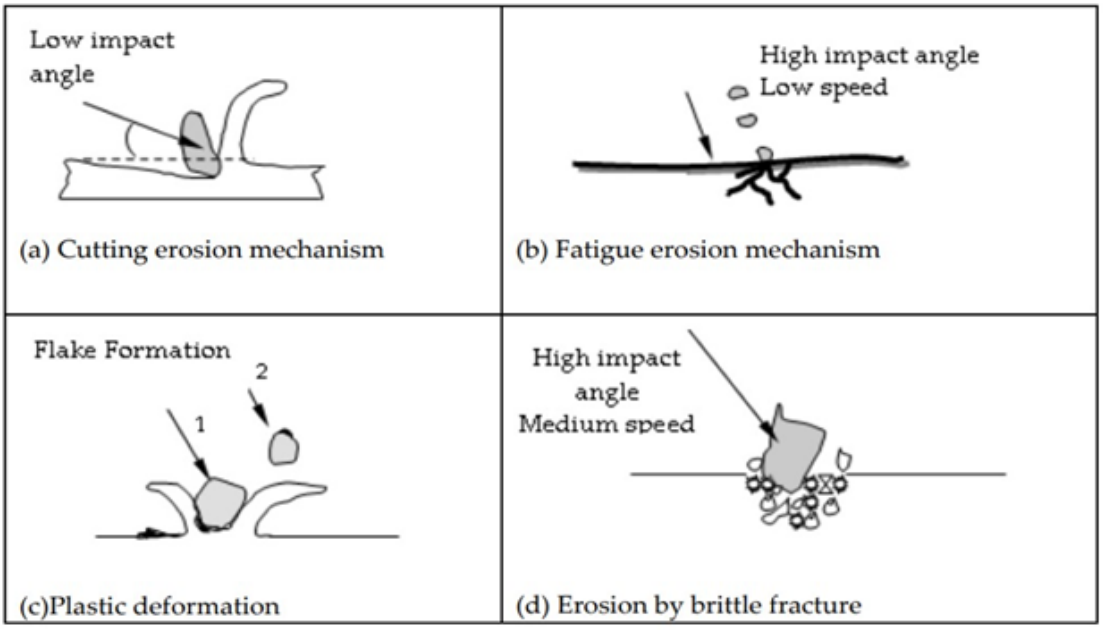

Figure 2.2: Mechanisms of erosive wear

2.2.5 Fretting Wear

The surfaces of constituents come into contact with constant cyclical motion, which causes material loss from the surfaces, known as fretting wear. Bearing wear is the finest illustration of this type of wear.

2.2.6 Corrosion and Oxidation Wear

Corrosion and oxidation are two of the most common causes of wear. Wear is caused by the contact of components, whether wet or dry. The chemical interactions between the worn material and the corroding media are the primary culprits for wear. Before 1950, the most common types of wear were adhesive, abrasive, surface fatigue, and corrosion [32]. Burwell discovered that erosion occurs as a result of contact between solid components and droplets [32]. Bhushan has identified six basic wear mechanisms with one feature in common: the removal of solid material from rubbing surfaces [33]. Table 2.1, [34] shows the wear mechanisms with its short definition [34].

2.2.7 Methods of Separating Materials from Wear

1. Mechanical activity: Ductile and brittle breakdowns are examples of mechanical activity. Tiredness is classified into two types: elastic fatigue (high cycle) and plastic fatigue (low cycle).

Table 2.1: Wear Mechanisms

Wear mechanisms	Short definition
Erosion	Particulate cutting, fatigue and melting.
Corrosive wear	The material is lost unless new substances are formed.
Abrasive wear	Cutting, weariness failure.
Diffusive wear	Transfer from one object to another of individual atoms.
Adhesive wear	System cannot be maintained to remove all debris from the surface.
Cutting wear	Sharp object indentation, followed by material breakage.
Deformation wear	Involves material breakage.
Fatigue wear	Cyclically stressed material failure.
Sliding wear	Intended to separate out erosion but not corrosion.
Cavitation	Fatigue failure due to collapse of liquid bubbles.
Impact wear	Failure due to fatigue and loss of oxide.
Thermal wear	Melting or chemical activity might be affected.
Chemical wear	Formation of new substances are more readily removed than substrate.
Oxidation wear	Similar to chemical wear, only oxides form
Fretting	Oxide and substrate fatigue failure.
Scuffing	A disastrous surface shape for sliding lubricating elements.

2. Chemical activities: Losses caused by chemical dissolution and trimming of substrate components, which can be easily eliminated by sliding.

3. Thermal activities: As the temperature rises during work, materials melt and alter their nature, allowing them to be worn.

2.2.8 Wear Rate

Diverse types of wear have different mechanisms, means, locations, and magnitudes of damage. As a result, the wear process is commonly defined in terms of wear rate, but due to the aforementioned variances, it is extremely difficult to define wear rate consistently. The depth or volume of material removed per unit of sliding or rolling distance is the usual means of defining the wear rate of a surface [33]. The rate of material removal or dimensional changes due to wear per unit of exposure parameter, for example, the quantity of material removed (mass, volume, thickness) in the unit of sliding distance or unit of time, according to the American Society for Testing Material G40-88 standard. As the majority of wear rate data is derived through friction and wear, such information is dependent on the material pair, which is usually expressed as a dimensionless wear coefficient. The relative magnitude of the wear statistics reported in the literature is more relevant than their absolute values [33]. As a result, it's difficult to apply those facts to the erosion rate of hydraulic machines, because the nature and

rate of material removal varies. Erosion rate is the rate at which material is removed owing to erosion.

2.3 Factors Affecting Wear

The following are the primary factors that influence hydraulic machine wear:

1. Impact angle and flow rate are the operating conditions.

2. Hardness, structures, and compositions of materials

3. Relative density, concentration, hardness, sharpness, and size of solid particles

2.3.1 Effect of Flowing Solid Particles

Clay, silt, and gravel are present in the sediments, which have a specific gravity of 2.6, based on sediment movement; sediment particles are known as bed load or suspended load in river hydraulics. These particles move considerably slower than flowing water that has settled on the bed. The velocity of the particles flowing with water is almost the same as the velocity of the flowing water. A portion of the suspended load settles in settling basins or reservoirs, while the remainder passes through turbines, causing part erosion [35].

2.3.2 Effect of Hardness

Wear occurs as a result of increased particle hardness compared to the contact metal. The wear rate decreases as abrasive hardness increases and, after the discovery of 13% Cr, cast steel outperformed unalloyed steel in terms of wear resistance [36], and [37]. Quartz was the principal erodent agent for material that develops erosion in experiments with multiple grades of fine sand (200 μm) under dry circumstances [38].

2.3.3 Effect of Grain Size and Shape

The absolute wear rate is related to grain size and sharpness. Wear is proportional to the size of the sliding scrap. At a certain grain size, the scrap erosion rate remains constant (about 50-100 μm depending on velocity). The mass and length of a particle are used to calculate its size. According to the theory of kinetic energy, the energy of the particle and the mass of a curved particle are directly proportional to its mass and its radius simultaneously [36], [38], [39], [40], and [41]. As particle size increased

from tiny to large, there was a transition from ductile to brittle mode of erosion. In the experiment with tiny and bigger particles, the total erosion rate varied from 30° to 80° impact angle. Smaller particles are more effective at cutting, but bigger particles strain materials through elastic deformation and fatigue. Hardness determines the erosion rate rating for tiny particles, while material toughness determines the erosion rate rating for big particles [31].
The shape of the particle predicts the erosion process. The erosion accelerates with an irregular shape and sharp edges particles and slows down with an uneven shape and softer edges [42]. Poudel demonstrate how the shape of the sediment affects the turbine system's overall performance. For the quantitative study, silt samples in 21 different forms were collected from four distinct rivers. Sediments can have many different forms, such as being well-rounded with high sphericity, rounded with low sphericity, rounded angular with high sphericity, high angular with low sphericity, high elongation, moderate square, high triangular (irregular), e.t.c [43].

2.3.4 Effect of Concentration

The mass of a particle in a unit mass of fluid is defined as concentration. Parts per million concentration is measured in mg/liter or kilogram of particles per 1000 m^3 of water. This is especially essential in the case of river sedimentation (1000 parts per million is equivalent to 0.1%). Wear formulations based on the density difference between solids and liquids are included by both directly altering whether other variables remain constant or as a more sophisticated function, according to Bergeron and Bovet [29] and [44].

2.3.5 Effect of Temperature

The process and the rate of erosion are affected by temperature, Shida identified a tight relationship between the rate of erosion and the mechanical characteristics of the material. The effects of temperature on erosion are negligible [45].

2.3.6 Effect of Media

Fluids transport the sediment particles. The carrying media's characteristics have a significant influence on the rate of erosion.

1. Density and viscosity of fluids

2. Flow type (laminar or turbulent)

3. Characteristics of micro structure: corrosives, lubrication, and cooling

The eroding particles are pulled by the viscous fluid, which changes the impingement angle and hence the erosion rate. Its collision efficiency measures the effects of an erosive medium. Collision efficiency is defined as the ratio of particles reaching the eroded surface with the medium to particles striking the eroded surface. The flow medium has influenced the particle trajectory according to Hojo [46].

2.3.7 Effect of Material Properties

Only stainless steel based on Mn has been proven to be abrasion resistant. When the base metal is appropriately prepared, the hard Cr-plate offers good resistance to both cavitation and abrasive erosion. Shchelkanov has researched water-turbine steel testing, with its microstructure and work hardness as an important wear strength phenomenon.
Austenitic and martensitic steels are far superior to ferritic steels. Therefore, low and medium Cr-alloy, which hardens stains (3.5-10.5%), was suggested because of good abrasion and cavitation resistance. Stauffer proposed a stainless steel alloy with 12-14% Cr and 2.5% Ni for hydraulic turbines [37]. Similarly, Bovet proposed a stainless steel alloy of 1.5% Mn with 25 Ni/0.7% Mn and, at the same time, stainless steel with 13% Cr [44]. Leith determined that Al had a poor tolerance for sediment erosion but was extremely excellent at avoiding cavitation, and performed a comparative investigation of cavitation and abrasive erosion [47].

2.3.8 Effect of Flow

Bergeron found that the difference in velocity between a fluid and a particle produces similar phenomena[29]. The velocity exponent has a broad range of values, according to Duan, such as n = 2.5-3.0 for revolving disc, n = 1.8-2.7 for disc stands, and n = 2.0-2.2 for water jet. It is difficult to calculate and estimate erosion rates [30]. Goodwin found wear is proportional to (velocity)$^{2\cdot3}$ for metals and polymers with particle sizes higher than 125 μm [38]. According to Shida, wear is proportional to (velocity)^3 and also directly proportional to (total head)$^{1\cdot5}$ [45]. Bitter has defined wear as the quantity of cutting erosion [48]. According to Wood, the continuity equation is employed to compute particle velocity, which is wrong because particle velocity is always lower than fluid velocity [49]. Zahavi discovered that particle velocity was one-third that of fluid velocity in a jet type erosion test rigs [50].

2.3.9 Effect of Impact Angle

Bergeron's theory covered only pure sliding (friction) wear, whereas the more sophisticated theory handled the broader issue of oblique effects [29]. Stachowiak discovered the rate of degradation was about 10% of the maximum [31]. According to Bhushan, brittle material has a higher erosion rate than ductile material and no erosion at low impingement angles [33].
Bajracharya has discovered the jet angle, commonly referred to as the particle impingement angle in practice; however this is not the actual impact angle. Even if particle flow in a straight pipe or parallel plates is at impingement angle 0, erosion might occur. When the flow is turbulent, the particles in the boundary layer oscillate in the direction of the flow, resulting in an effective impingement angle close to 90 [35]. According to the Bovet hypothesis, the tangential aspect of particle velocity dictates wear, and wear is reduced as the impact angle rises [44]. According to Bitter, total wear was based on both normal and tangential velocity components [48]. Matsumura discovered that ductile materials erode faster at zero-degree impingement [51].

2.3.10 Effect of Performance

Bezinge and Duan illustrate the effect of worn labyrinth seal clearances on storage pump capacity. A loss of turbine performance was 10% in 1 year of operation at one of the Trans-Caucasus powerhouses were used to assess the rate of erosion. Such a severe decline in performance can be attributed to a malfunction in the device's runner and labyrinth seals [30], and [52]. The empirical turbine equation was established at Best Efficiency Point (BEP), in which efficiency drops into a straight diagonal line as particle concentration increases. The efficiency ratio for pure water mixing is given by equation 2.8 below [35].

$$\frac{\eta_m}{\eta_w} = -0 \cdot 085 C_w + 1.0 \tag{2.8}$$

C_w is the solid weight that reflects the weight of the mixture divided by the weight of clean water, η is the efficiency, and the subscripts m and w signify the mixture and clean water respectively. Direct-induced erosion reduces overall turbine performance more than altering sediment levels in the fluid.

2.4 Erosion Model

According to Truscott, the most often used term for erosion is proportional to velocity^n [53]. Humphrey describes an extensive study has been conducted to build a wear model in terms of the material characteristics involved, but little attention has been paid to the

impact of fluid motion, particularly in turbulent flow regimes [54]. Many models have been presented over the years for a variety of scenarios. Unfortunately, most models are system-specific since they are correlated in nature. They are only effective for the specific material pair, contact geometry, operating condition, and range, as well as the specific environment and lubricant. Because they are so complicated, few designers can confidently use any of the existing equations to forecast product life. The fundamental causes of this problem are the complexity of wear and the enormous number of variables that influence the result. While reviewing the available literature, multiple fundamental studies of erosion behavior under various situations were discovered. However, only the general erosion model and specific erosion models built for hydraulic equipment applications are described here.

2.4.1 General Erosion Model

The exact process of erosive wear has yet to be discovered. As a result, no simple, trustworthy, and generic erosion model has been devised for engineering purposes. The most frequent expression of erosive wear is based on experimental experience, and it's usually represented as a function of the things that cause it. The easiest method to write the erosion equation is, Erosion = f (operating condition, properties of particles, and properties of base material). This equation is usually expressed as a function of velocity, material hardness, particle size, and concentration. The most general formula 2.9 for pure erosion is as follows, according to Bardal [55].

$$W = K_mat \cdot K_{evn} \cdot c \cdot V^n \cdot f(\alpha) \tag{2.9}$$

W is the erosion rate (material loss) in mm/year, K_{mat} is the material constant, K_{env} is the constant based on the environment, c is particle concentration, and $f(\alpha)$ is the Impingement angle function α. The particle's velocity is V, and the exponent of velocity is n.

2.4.2 Erosion Models for Hydraulic Machinery

Bergeron gave equation 2.10, to forecast the erosion rate of a pump [29].

$$W \propto \frac{V^2}{D} \cdot (\rho_p - \rho) \cdot d^3 \cdot p \cdot K \tag{2.10}$$

Where V is the typical liquid velocity, D is the machine's characteristic size, ρ_p is particle density, d is particle diameter, p is the number of particles per unit surface area, ρ is liquid density, and K is the experimental coefficient, dependent on the type

of the abrasive particles. This equation is based on an experimental coefficient that is affected by the abrasiveness of the particles. Duan developed a surface erosion equation based on the impact effect of particles and the kinetic energy of a single particle. They predicted that non-homogeneous particles, changing concentration, constant modification and pulsation of velocities and pressure, non-uniform flow distribution, and other uncertainties would cause erosion to deviate from the equation [30].
Bitters' model, for example, was established for dry conditions. A small number of researchers have given models for hydraulic machinery. With reduced assumptions such as pure sliding of spherical particles over the surface [53]. On the other hand, Tsuguo used 8 years of erosion data from 18 hydro-power facilities to establish a link between elements affecting turbine erosion, and the turbine repair cycle is calculated using the turbine erosion equation 2.11, which yields the erosion rate in terms of thickness loss per unit time (W) [56].

$$W = \lambda \cdot c^x \cdot a^y \cdot k_1 \cdot k_2 \cdot k_3 \cdot V_{char}^z \tag{2.11}$$

Where λ represents the turbine coefficient at the eroded section, "c" represents the suspended sediment concentration, and "V" represents the typical velocity. The word "a" refers to the average grain size coefficient based on a unit value of 0.05 mm grain size. The words k_1 and k_2 refer to sand particles' form and hardness coefficients, respectively, and k_3 refers to the material's abrasion resistance coefficient. The exponent values for concentration, size coefficient, and velocity are x, y, and z, respectively. The values of x and y are close to unity, and the plot of wear versus parameter determines any divergence from this linear proportionality. Based on the relationship between relative velocity and erosion, z values for various turbine components are provided. For the Pelton bucket, the minimum value of n is 1.5, and the maximum value is 3.0 for the Francis turbine runner. This number is also suggested as 2.5 for the Francis turbine guiding vanes and the Pelton turbine needle.
To explain how several essential aspects affect the particle abrasion rate in the turbine, International Electrotechnica Commission (IEC) 2008 recommends the following theoretical model of abrasion rate, $\frac{ds}{dt}$ = f (particle velocity, concentration, physical parameters of particles, flow pattern, turbine material qualities, and other variables). Since this formula is rarely used, various simplifications are made. The first simplification is to consider the various variables as independent, as follows: $\frac{ds}{dt}$ = f (particle velocity) f (particle concentration) f (particle physical properties, turbine material properties) f (particle physical properties) f (flow pattern) f (turbine material properties) f (other factors). This simplification has not been validated. Nonetheless, justified hydraulic

machinery based on literature studies and experience. Finally, the IEC proposed equation 2.12 below, which includes more simplifications and a new variable.

$$S = W^3 \cdot PL \cdot K_m \cdot K_f \tag{2.12}$$

Where S is the abrasive depth in millimeters, W is the typical velocity, PL is the particle load calculated by integrating particle concentration over time, K_m is the material factor, and K_f is the flow factor.

2.4.3 Basic Erosion Model

Finnie and Tabakoff are the two erosion models included in ANSYS CFX. The decision to use one model over another is mostly based on simulation results. With its higher number of input parameters, the Tabakoff model often allows for more customization. The erosion model may be customized for any boundary or area. When the domain is activated, the domain settings will apply to any borders that do not have erosion model settings applied to them directly.

2.4.4 Tabakoff Erosion Model

With its higher input parameters, the Tabakoff model often allows for more customization. The decision to use one model over another is mostly based on simulation results. The erosion model may be customized for any boundary or area. When the domain is activated, the domain settings will apply to any borders that do not have erosion model settings applied to them directly. Five parameters must be specified in the Tabakoff model. All of the parameters, including the k_{12} constant, three reference velocities, and the maximum erosion angle of γ_0, must be given. The erosion rate E is calculated using the following formulas 2.13, 2.14, 2.15, 2.16, and 2.17.

$$E = K_1 \cdot f(\gamma) \cdot V_p^2 Cos^2\gamma \cdot \left[1 - R_T^2\right] + f(V_{PN}) \tag{2.13}$$

$$f(\gamma) = \left[1 + k_2 \cdot k_{12} \cdot sin\gamma \cdot \left(\frac{\frac{\pi}{2}}{\gamma_0}\right)\right]^2 \tag{2.14}$$

$$R_T = 1 - k_4 \cdot V_p \cdot sin\gamma \tag{2.15}$$

$$f(V_{PN}) = k_3 \cdot (V_P \cdot sin\gamma)^4 \tag{2.16}$$

$$K_2 = \begin{cases} 1.0, & \text{if } \gamma \leq 2\gamma_0, \\ 0.0, & \text{if } \gamma \geq 2\gamma_0. \end{cases} \tag{2.17}$$

The dimensionless mass E is equal to the mass of the eroded wall material divided by the mass of the particle. The particle impact velocity is V_p. γ is the radian impact angle between the oncoming particle track and the wall, with γ_0 being the greatest erosion angle. The model constants k_1 to k_4, k_{12}, and γ_0 are dependent on the particle, and wall material combination. The following equation 2.18 is used to calculate the total erosion rate of a wall due to a particle:

$$E = E \cdot \dot{\mathrm{N}} \cdot m_p \tag{2.18}$$

The mass of the particle is m_p, and the number rate is $\dot{\mathrm{N}}$. The total amount of erosion on the wall is then calculated as the sum of all particles. This results in a kg/s erosion rate and a $kg/s/m^2$ erosion rate density variable in the res file and post-processor. Furthermore, until specific values for the model constants are available, this erosion rate is simply a qualitative pointer to erosion.

2.4.5 Finnie Erosion Model

The erosive effect of particle impacts on a wall's wear is a complicated function of particle impact, particle, and wall parameters. According to the relationship, erosion is observed to change with impact angle and velocity for virtually all metals (Source: ANSYS, 2018.1) 2.19.

$$E = k \cdot V_p^n \cdot f(\gamma) \tag{2.19}$$

Where E is a dimensionless mass, V_p is the particle impact velocity, and $f(\gamma)$ is a dimensionless impact angle function. The impact angle between the oncoming particle track and the wall is measured in radians. For metals, the exponent, n, is typically in the range of 2.3 to 2.5. Finnie's erosive wear model, which uses n = 2, connects the rate of wear to the kinetic energy rate of particles impacting on the surface 2.20 and 2.21.

$$E = k \cdot V_p^3 \cdot f(\gamma) \tag{2.20}$$

$$f\left(\gamma\right) = \begin{cases} \frac{1}{3} \cdot Cos^2\gamma, & \text{if } tan\gamma > \frac{1}{3}, \\ \sin 2\gamma - 3 \cdot Sin^2\gamma\ , & \text{if } tan\gamma < \frac{1}{3}. \end{cases} \tag{2.21}$$

2.4.6 Bitter's Model

Bitter's model is based on observations of cast iron particles striking a silver plate at various angles. Bitter described two types of erosion based on the visible appearance

of the surface of a silver plate. Deformation wear (W_D) is deformation caused by repetitive contact of particles that are normal to the object. Cutting wear (W_C) is caused by free-moving particulates hitting a surface at an acute angle [48].

2.4.7 Sundararajan's Model

Sundararajan model is founded on the assumption that the erosion rate is regulated by deformation rather than fracture and that the properties of the plastic zone (size, shape, stress, and strain) determine the amount of energy lost through plastic deformation [57]. Sundararajan suggested calculating the degradation rate (E) using the following expression 2.22:

$$E = L^3 \left(\frac{\Delta \varepsilon_p}{\varepsilon_c} \right)^x \tag{2.22}$$

Where, L is the plastic zone size and $\Delta\varepsilon_p$ and ε_c are average strain per impact and failure strain.

2.5 Repair and Maintenance

It was reported that the efficiency of the turbines in Jhimruk reduces to around 5% after erosion in the wet season [58]. Out of the total loss, the ones contributed by the leakage due to erosion of labyrinth seals were found to be between 2-4%. However, the turbines undergo repair and maintenance in the dry season so plant's loss is retained. The change in the efficiency of the turbines after each repair has not been reported yet, but since the hydraulic profile of the blades are maintained with high-quality machining, the change in the efficiency of the runner for each successive repaired turbines can be considered marginal. Repair and maintenance of the electro-mechanical components are the part of the annual routine of the power plant. The normal repairing period for the runner, GVs, and upper and lower rings is 150 to 180 days. Various processes involved in the repairing and maintaining of these components are shown in Figure 2.3. In the case of GVs, the repair work includes welding, machining and grinding. The base material of the guide vane, i.e. 13.4Ni5Cr is used as the weld material. After filling the eroded sections, the GVs are machined according to the reference design, with 97 mm span height and 180 mm chord length. Final finishing is done by grinding, which brings the GVs into their original shape. Repairing of the runner involves similar processes. However, the outlet eroded section undergoes cutting of a V-shaped section as shown in Figure 2.3 (d) before welding. According to the reference design, this cut-out section is replaced with a new section. The eroded area at the runner's inlet is repaired using the same technique as the GV but with the base material of 16Cr5Ni.

Figure 2.3: Different processes of repairing eroded GVs (a, b, c) and runner (d, e, f)

2.6 Past Studies and State-of-the-Art in Sediment Erosion of Francis Turbines

The size, shape, and concentration of silt influence erosion on Francis turbine blades. The reduction of erosion is linked not only to the reduction of particle velocity but also to the reduction of flow separation, which is dependent on the properties of the sediment. If a numerical forecast is adopted, a considerable reduction in erosion rate can be accomplished [5]. Chitrakar analyzed the optimum designs with fluid-structure-interaction (FSI). In experimental examinations under various sediment loads, Rajkarnikar verified the optimal design of the runner blade. The decrease in the response ratio is also shown to raise the absolute speed around the GVs and hence to further enhance the erosion within the GVs. The conclusion was that research into merging the runner's design optimization issue with the GVs was required in order to achieve minimum erosion in both components [5], [9], and [22].

The tungsten-carbide based coating was applied to the Francis runner blades and GVs of the Cahua hydro-power plant, which dramatically improved performance as compared to the un-coated runners and GVs during the same period, [5], [59], [60], and [61]. A series of research activities have been carried out the design of the GVs for

Francis turbines operating under high sediment loads. These studies were aimed at developing experimental methods for assessing the performance of the Francis turbine in the presence of GV erosion. Earlier research revealed the presence of sediment-loaded turbines as well as the unfavorable effects of GV erosion. Some investigations were carried out to investigate the leakage flow through the clearance gap and its effect on GVs and runner blades [7], and [23].

The pressure difference between the GVs' pressure side and suction side is proportional to the secondary flows that enter the GVs and runner blades through the clearance gap. The thickness of the guide vanes has been reduced in highly sediment Rivers due to leakage flow, which generates turbulence and forms an uneven wear pattern. The flow behavior is responsible for secondary flow erosion, horseshoe vortex erosion, acceleration erosion, and turbulence erosion in the turbine's various components. The hydrofoils' forms significantly impact have a significant impact on the pressure velocity field, leakage flows, and vortex filament properties. These are mainly owing to their direct impact on erosion and turbine efficiency [9], [13], and [18]. Secondary flow can expedite devastation in high sediment-laden rivers by producing irregular wear patterns and lowering the thickness of the vanes. In the bladed portions of Francis turbines, several types of erosion exist, depending on the types of flow behavior in that zone, such as leakage flow erosion, horseshoe vortex erosion, acceleration erosion, and turbulence erosion. These phenomena are predicted using computational and experimental methodologies [12].

Recent research has concentrated on the study of erosion in GVs of Francis turbines, because the flow in this location has the highest acceleration. It has been claimed that there is a simultaneous impact on secondary flow and turbine erosion. When flow-containing silts are passed through the clearance gaps of the GVs, the gap expands due to erosion and disturbs the flow of the GVs on the suction side, reducing turbine performance and causing runner blade degradation [18]. Due to their form, dimension and concentration, the sediment particles were described by CFD to analyze erosion in various components. The density of erosion rate ($kg/m^2/s$) was used to measure erosion in the turbines using CFD. After all, confirmation of the simulated erosion results by experiment is a challenge due to various sand particles and non-uniform eroded components. RDA was developed to test the loss of materials as well as the removal of color from the runner blades attached to a rotating disk, submerged inside a sand and water cylindrical chamber [21].

The developed RDA was successful carried out sediment erosion experiments because the findings were equivalent to be equivalent to the erosion circumstances at the actual hydro-power site. The wear pattern observed throughout the experiment is also pretty comparable to the pattern predicted by the CFD analysis performed in previous

research. The results also demonstrate that the impacts of sediment erosion are rather considerable in the test specimens. It can also be stated that turbines developed using standard design methodologies are very vulnerable to damage caused by sediment erosion [21]. After 350 minutes of operation, the average rate of erosion in the reference design was 0.28 mg/gm/min. The optimized design's, the erosion rate was just 0.24 mg/gm/min. It was also discovered that if the optimized design was employed instead of the reference design for the duration of the trial, it may reduce sediment erosion by 14.4% [22]. Numerical methods for estimating silt erosion on Francis' turbine elements have successfully been implemented in Neopane's doctoral trial. Mette has prepared her Ph.D. thesis on techniques and numerical research for Francis sediment management optimum hydraulic design.

Several authors believe the wear rate is a function of velocity, material hardness, grain size, and solid concentration. As a result, wear is proportional to the n power of velocity ($w \propto v^n$), where 'n' varies depending on the material and other circumstances [36], [37], [38], [40], [53], and [62]. Finnie published an extensive paper on surface erosion using solid particles in 1960. Finne and Truscott carried out a thorough investigation of abrasive wear in general in hydraulic machines [53], and [63]. The size of a particle is inversely proportional to its velocity, and it was discovered that spherically formed particles had higher settling velocities than other shapes. Non-spherical particles, on the other hand, will have lower settling velocities since both decreases in spheroid and increases in angularity tend to decrease velocities [64].

Sediment erosion of hydraulic turbines is reported to have been going on for more than 100 years. The difficulties with Nepalese hydro-power plants have been examined during the last 50 years. The main mineral component of Nepal's rivers is quartz, which has a hardness rating of 7 on the Moh's scale. The turbulent flow of quartz degraded components of both the Pelton and Francis turbines. The architecture of the Francis turbines typically includes a dry clearance space between the guide vanes and the cover plates. The clearance distance increases by multiples of its design value due to cover plate movement and component erosion. The pressure differential between the guidance vane sides causes a leakage flow due to the larger clearance distance. A comprehensive analysis of the leakage flow features and their impacts on the flow conditions inside the Francis turbine distributor has yet to be published. These studies are required for the design optimization of turbine components as well as the planning of effective upkeep plans for fixing eroded turbine parts [65].

The primary goal of this research is to investigate the impacts of sediment erosion in water turbines, with a particular emphasis on the flow around the guidance vanes of a low-specific-speed Francis turbine. This research has emphasized experimental studies of the features of leakage flow from the increased clearance space between eroded

guidance vanes and cover plates [65]. The relative velocity at the runner inlet increases up to three times locally for the crucial magnitude of the clearance gap. The source of excessive erosion at the runner's intake at the hub has been recognized as a local increase in relative velocity. This study discovered the formation of a corner vortex between the guide vane and the walls, even when there was no clearance space. In the case of flow with a clearance gap, a leakage vortex with greater strength than the corner vortex was found. Both the corner vortex and the leakage vortex originate from the suction side of the guide vane at about 75% of the chord, close to the wall. The leaking vortex is attracted towards the mid-span as the flow moves downstream of the guide vane [65].

The clearance gap of up to 0.5 mm has no noticeable impact on the flow characteristics and can thus be taken as the upper limit. The leakage flow, with a clearance gap greater than 1 mm, is observed to substantially alter the velocity components at the runner inlet. A clearance gap of 2 mm has the greatest impact on flow velocities and is deemed the crucial dimension. The overall crosswise leakage flow recorded from the crucial clearance gap is greater than 1% of the primary flow. As a result of the leakage flow, the relative velocity at the runner intake increases up to three times from its intended value. In sediment-laden projects, this local rise in IV relative velocity is recognized as the source of severe erosion at the runner hub. The leakage flow also alters the pressure pattern around the guide vane, increasing tension on the guide vane shaft by up to 28% [65]. Detailed analyses of the management and maintenance of hydraulic turbine sediment erosion for sediment-laden turbines have been created. Various types of turbine sediment erosion were tested in various Himalayan basins with various coatings [66].

It has been discovered that a clearance gap of up to 0.5 mm has no noticeable effect on the flow characteristics. At the runner inlet, leakage flow with a clearance gap greater than 1 mm are found to modify the velocity components and the blade loading in both the circumferential and span-wise directions. The case with a clearance gap of 2 mm has the greatest effect on flow velocities and is regarded as the crucial size that must be avoided as much as possible [67]. An experimental setup is being built at the best efficiency point to explore flow around the distributor of a Francis turbine under flow conditions similar to those of a prototype low specific speed Francis turbine. The amount and consequences of leakage flow from different sizes of GV clearance gaps are estimated using pressure and velocity measurements. The results reveal that the pressure difference between neighboring surfaces is induced by the GV of a Francis turbine with symmetric NACA profiles. At roughly 75% of the GV chord, the maximum pressure difference between the GV surfaces occurs, which is comparable to 20% of the net hydraulic head pushing on the turbine. A differential pressure of this magnitude

is sufficient to push leakage flow through the clearance gap between the GV and cover plates [67]
Four distinct GVs with varying Camber percentages were compared using the experimental method of RDA and the computational tool of ANSYS. NACA4412 exhibited comparatively greater performance in water packed with sediment due to its decreased erosion and pressure difference between the Pressure side and suction side. NACA4412 lost less weight in the experiment than the other two. It was also discovered that the operational and performance parameters matched the minimal change for the instance under consideration. This work was done near the selection of guide vane profiles for Francis turbines running in sediment-laden water. To establish an appropriate profile, a computational analysis of the turbine flow passage and experimental research using the rotating disc apparatus was done. Unsymmetrical profiles were shown to be better at controlling erosion while retaining turbine performance constancy [68].

2.7 Research Gap and the Proposed Approach

The literature review shows that different types of wear on GVs and runner blades are caused by sediment erosion. GVs and runner blades are two inter-related vital components of Francis turbine. Therefore GVs and runner blades bridge the turbine system's overall performance according to the action of sediment erosion on them. The clearance gap between the upper and lower facing plates and GVs increases during the operation, due to the pressure difference between pressure side, developing secondary flow along with vortex filaments, which are responsible for the further degradation of the surface morphology of GVs and runner blades.

1: The study of the flow behavior and its consequent impact on erosion patterns in Francis turbines using 3D scanned geometries and CFD.

2: Use of RDA for GVs of Francis turbines and credibility analysis of such an experimental setup.

3: Use of RDA for determining erosion patterns and erosion rates of GVs with Scanning Electron Microscope (SEM) analysis.

This thesis is expected to add knowledge on the behavior of the flow through the clearance gap of GVs and its impact on the sediment erosion of turbines. Similarly, specimen GVs have been used in RDA and SEM experimental setups to understand the erosion pattern as well as the credibility of using such setups for hydro turbines.

2.8 Chapter Summary

A detailed literature review on sediment erosion's cause and effects on turbine components has been carried out. Sediment erosion challenges are identified and proposed basic turbulence model as well as an erosion model. Flow phenomenon with primary and secondary flow as well as leakage flow and vortex filament and its cause and effect on the GVs and runner inlet and outlet are recognized. The investigation of flow behavior and its influence on erosion patterns in Francis turbines using 3D-scanned geometry and CFD. RDA is used to calculate the erosion pattern and rates in GVs of Francis turbines and to assess the plausibility of such an experimental setup.

Chapter 3

Case Study of Hydro-power Plants of Nepal

The chapter deals with the basic phenomenon of Nepal's medium and large generation hydro-power plant.

3.1 Case Study of Erosion in Hydro-power Plants of Nepal

3.1.1 Jhimruk Hydro-power Plant

In this study, the case of Jhimruk hydro-power plants was considered. The general specification of the power plant are provided in Table 3.1. It consists of a 205 m long and a 3 m high concrete dam with gates and intake structures, a 1045 m long headrace tunnel, surge chamber with a 380 m shaft, three units of horizontal Francis turbines with 4 MW capacity each, and $3 \cdot 5$ MVA generators. The head-works were designed for a flood discharge of 2000 m^3/s (1 in 100-year flood) and the desilting basin can trap sediments of size larger than 0.2 mm.

The power plant is continuously facing the challenges of repair and maintenance due to sediment erosion in turbine components. It was studied that more than 60% of the constituents of sand in this river contain Quartz, which has the hardness value of 7 in Moh's scale [17]. The turbines that come in contact with water are made with stainless steel containing chromium (Cr) and nickel (Ni). The turbine sealing rings contain nickel, aluminum, and bronze. After a few hours of operation of the turbines, the gap between the turbines sealing rings and the runner was reported to have increased from 0.35 and 0.7 to over 1 mm [69].

Table 3.1: Specification of Jhimruk hydropower plant

Project	Jhimruk HPP
Location	Pyuthan District
River	Jhimruk Khola
Project Type	RoR Type
Head	205 m
Speed	1000 rpm
Discharge	7 m^3/s in total
Machine Type	Horizontal Francis
Capacity	3*4 MW Francis

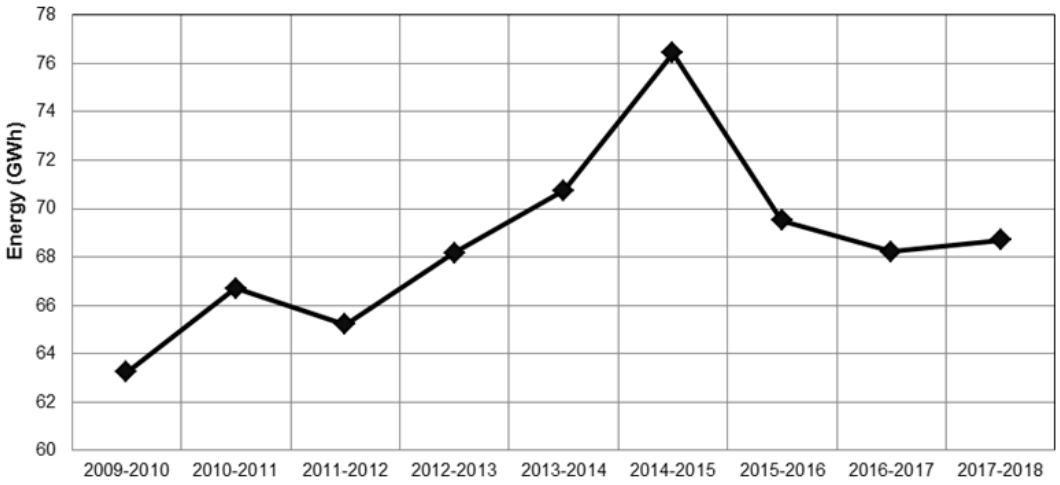

Figure 3.1: Yearly generation in Jhimruk hydro-power plant from 2009-2018

During the first year of operation, the plant generated about 45.1 GWh of energy, with a plant factor of 43% [69]. It was studied that the high sediment load in the water was one of the major obstacles to the downtime of the power plant. The generations of the plan in the last 9 years are shown in Figure 3.1. Although the plant factor has improved in some years compared to the first year, the generation has not reached the designed value.After five months of operation of the turbines when Unit 3 was dismantled, it was seen that the turbine components, runner sealing rings, turbine covers, and guide vanes were severely eroded. Similar effects were found in the turbines of other Units. The wear thickness on the blade was up to 1.5 mm, with grooves at the edges of the inlet and outlet [69].

When these minerals impact the turbine at high velocity, erosion occurs on the surface, further aggravated by cavitation. Several studies have been carried out in the past

to know the erosion phenomena in the turbines of the Jhimruk and possible design and coating strategies for better sediment handling. This study presents the daily averaged discharge, generation and sediment concentration data from the year 2017-2018. Sediment samples were collected from two locations desilting plan and cooling tank basin. Particle size distribution and mineral content analysis were performed on the collected samples. The erosion on the turbine components was studied from visual inspection as well as from the 3-D scanned models of the eroded regions. A CFD analysis was performed on the available geometry of the turbine, such that the flow behavior inside the turbine can be correlated with erosion. Figure 3.2 shows the aerial view of the catchment and dam area of the Jhimruk hydro-power plant. Similarly, Figure 3.3 shows the severe eroded runner blades and guide vane of Jhimruk hydro-power plant.

Figure 3.2: Aerial view of the catchment and dam area of Jhimruk hydropower plant

3.1.2 Kaligandaki 'A' Hydro-power Plant

The project is located in the Syangja district of Nepal's western development area. It is a 144 MW, 842 GWh run-of-the-river hydroelectric plants near the towns of Mirmi and Beltari, which are 6-kilometers away on land. The Kaligandaki River runs in a U-loop for 50 kilometers with elevation change in this stretch of the river of approximately 124-meters. At Mirmi, right after the junction of the Andhi-Khola and Kaligandaki Rivers, a 44-meter-high dam is built to redirect a portion of the river's flow into a 5.9-kilometer tunnel which transports water to Beltari, which houses a 144 MW power station. The dam coveres a 5.3-kilometer-long reservoir with a total size of 65 hectares. A 132-kilovolt transmission line is also be built from the power facility to substations in Pokhara and Butwal. Power to the dam site and rural electrification is provided through a modest 12-Kilovolt connection. The power plant is situated a 28.5 kilometer

(a) (b)

Figure 3.3: (a) Eroded runner blades (b) Eroded GV of Jhimruk hydro-power plant

from the Sidhartha highway, access road leads to the dam and reservoir source, with a side road leading to a power plant site. Figure 3.4 shows the dam, intake (bottom), spillway (top) and the Kaligandaki 'A' hydro-power plant.

Figure 3.4: The dam, intake (bottom), spillway (top), Kaligandaki 'A' hydro-power plant

The planned dam location has a catchment area of 7618 square meter for the Kaligandaki 'A' hydro-power plant. The flow diverges significantly, as is typical for a monsoon basin. Based on hydrological data gathered since 1964, the estimated average flow is around 288 m^3/sec. Though, daily flows during the dry season are around 40 m^3/sec, daily monsoon floods range from 1,000 m^3/sec to 4,500 m^3/sec. The Kaligandaki 'A' River has a high sediment transport capacity, which is typical of Himalayan Rivers.

Monsoon runoff transports the majority (90-96)% of the bed load and suspended sediments at the dam site, which are expected to total 40-47 million tons per year. Large landslides are common during the monsoon season producing major changes in the flow-sediment interaction. Following a landslide, the highest point recorded concentration was around 48,000 parts per million (collected on 20 August 1993).
By its nature the Kaligandaki 'A' River flows through the Himalayas and carries a lot of silt generating a suspended sediment load of 43 Mt/yr, with sand accounting for around 25% of it. This sand contains a high concentration of angular quartz, which is very abrasive. The monsoon provides approximately 95% of this suspended sediment load, which is sufficient to fill the reservoir in a single monsoon season, which lasts from late May to late September. When the concentration of suspended sand increases in the river and fed to the turbines rapidly in early June the reservoir level is reduced on these days, allowing sand to be moved. As the reservoir level increases to the impounding level, the sand concentration falls, decreasing flow velocity and sand transport rate. Sluicing has substantially stabilized reservoir capacity, resulting in reservoir sediment balance. Figure 3.5 shows the eroded runner and GVs of Kaligandaki 'A' hydro-power plant.

(a) (b)

Figure 3.5: (a) Eroded runner blades (b) Eroded GV of Kaligandaki 'A' hydro-power plant

3.1.3 Soft Coating at Kaligandaki 'A' Hydro-power Plant

The examination of suitable coating technologies applicable to hydro turbines, within the context of hydro power plants exposed to sediment particles. The review has shown numerous materials and approaches of applying the coating, their performance evaluation using experiments and important findings. Figure 3.6 shows the eroded

runner blades of Kaligandaki 'A' hydro-power plant, the metaline series 685 was used to the runner with brushing and with hands, three coats simultaneously were provided and the result was obtained after the use of 2318 hours. This result show that the coating is not as satisfactory as the authority expected.

(a) (b)

Figure 3.6: (a) and (b) Soft coated eroded runner blades of Kaligandaki 'A', hydro-power plant

Similarly, Figure 3.7 shows the eroded GVs of the same plant, the metaline series s-700 was used to the GVs with cartridge spray system, three coats simultaneously were provided. The evaluation conducted after 2318 hours of use revealed that the coating applied to the GVs exhivited a higher level of satisfaction compared to the coating applied to the runners.

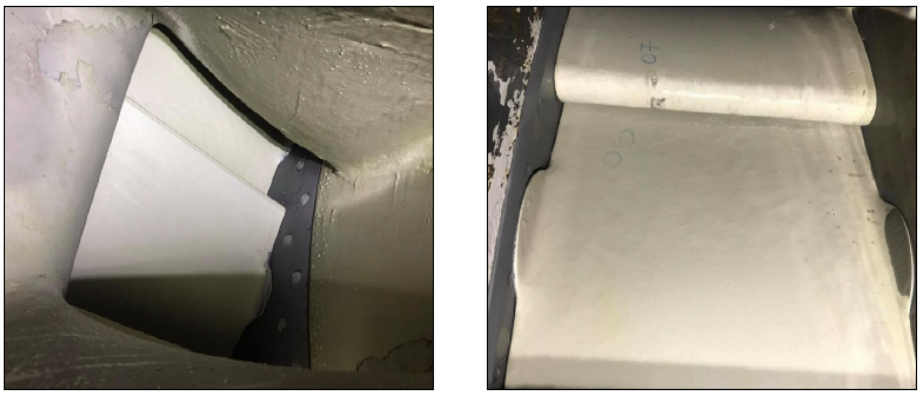

(a) (b)

Figure 3.7: (a) and (b) Soft coated eroded GVs of Kaligandaki 'A' hydro-power plant

3.1.4 Middle Marsyangdi Hydro-power Plant

The Middle Marsyangdi hydro-power plant located in Siundibar, Lamjung, boasts a capacity of 70 MW. THis facility operates as a peaking run-of-river project characterized by a five-hour daily pondage and an annual design generation of 398 GWh. It was commissioned on December 14, 2008, and it employs the most advanced technology of any NEA power plant. The station's cumulative generation reached 1574.84 GWh as of 2011/12, with a high generation of 425.34 GWh in the same year, above the planned generation of 397.59 GWh and goal generation of 39.9.31 GWh. It has provided 10.18% of integrated Nepal power system's total energy contribution.
The catchment area is 2729 square kilometers, with a maximum net head of 98 m and a maximum gross head of 110 m. The dam's live storage volume is 1.65 million m^3, and the average yearly flow is 99.5 m^3/s. This facility employs two vertical shaft turbines with rated discharges of 40 m^3/s and rated outputs of 35.9 MW are employed. Figure 3.8 shows the Middle Marsyangdi hydro-power plant dam site. The 72 MW hydroelectric power plants are constructed with two vertical Francis turbines and a gross head of about 108 m with the expectation of around 400 GWh average annual productions.

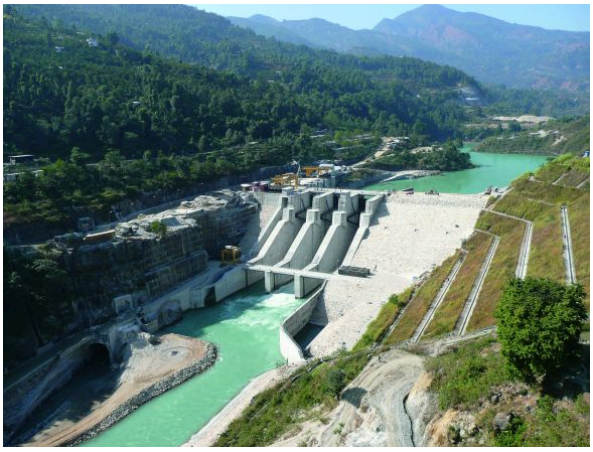

Figure 3.8: Middle Marsyangdi hydro-power plant dam-site, Udipur Lamjung

Since 1990, comprehensive measurements of suspended sediment concentrations have been carried out for the existing Middle Marsyangdi hydro-power plant, yielding a mean total suspended load of 15 mt/a. The annual sediment yield corresponds to 3850 $t/km^2/a$. When concentration measurements began in February 1997 at the Middle Marsyangdi, dam site the data at the start of the monsoon season suggests that the yield may be lower. Table 3.2 shows the bed load transport capacities at Middle Marsyangdi hydro-power plant.
Similarly, Table 3.3 shows the bed load transport rates at Middle Marsyangdi hydro-power plant. However, the current data is insufficient for a definitive assessment of

the yield. As a result, the same yield was conservatively used for Middle Marsyangdi hydro-power plant. The annual suspended sediment load for the 2729 squaremeter catchment area at Middle Marsyangdi, dam site is 10.5 mt/a. The Meyer-Peter and Muller formula, or the Einstein technique is used to calculate bed load transfer capacity. The resultant transport capacity for 1997 is shown in the table below.

Table 3.2: Bed load transport capacities at Middle Marsyangdi hydro-power plant

Months	Discharge in m^3/s	Depth in m	Velocity in m/s	M-P-M tons/day	Einstein tons/day	VAW tons/day
June	162.5	1.98	2.24	0	2118	2778
July	373.5	3.24	3.00	30511	28901	24647
August	412.3	3.43	3.10	39785	34893	28883
September	280.4	2.74	2.72	10550	13937	14659
October	127.8	1.72	2.05	0	562	0

Table 3.3: Bed load transport rates at Middle Marsyangdi, dam site

Discharge in m^3/s	132	150	200	250	300	400	500
Bed load Rate in tons/day	0.0	1166	4628	8292	12079	19880	27845

3.1.5 Lower Marsyangdi Hydro-power Plant

The Lower Marsyangdi hydro-power plant, owned by the Nepal Electricity Authority (NEA), is located in Aanbukhaireni, Tanahu and has an installed capacity of 69 MW with an annual design generation of 462.5 GWh. It was completed in 1989 AD with the combined funding from the international development association, credit for construction, the Asian Development Bank (ADB), and the government of Nepal (GON) at a total cost of USD 22 million. The power plant's net head is 90.5 meters, with a rated discharge 30.5 m^3/s. The head-race tunnel is 7199 meters long, 6.4 m in diameter, and concrete-lined, with a pressure shaft is 75 m long and 5 m in diameter that connects to a surge tank 20.5 m in diameter and a concrete throttle shaft 56 m high. Three sets of vertical Francis turbines, each with a capacity of 26 MW and a rotational speed of 300 rpm, have been erected. The planned yearly generation is 462.5 GWh with a catchment area of 3850 squaremeter. Figure 3.9 shows Lower Marsyangdi hydro-power plant, and dam site.

The erosion mainly depends on sediment characteristics like size, concentration, mineral composition and shape of the sediments. Sediment samples were collected and analyzed from three different locations of Lower Marsyangdi hydro-power plant i.e. head-work, intake and tailrace. Mineral analyses were carried out by a physical method called particle count method in Stereo Zoom Microscope and revealed that Quartz is the most

abundant mineral and common particle size distribution of sediment varies at different locations of plant. Furthermore, erosion tests were also carried out in RDA and found that erosion rate is directly proportional to the sediment size and quartz content [26].

Figure 3.9: Lower Marsyangdi, hydro-power plant dam site, Aanbukhaireni

Quartz is the most common mineral in river sediments with Moh's hardness of 7 that can easily cause erosion of turbine. Other minerals that are harder than turbine materials include feldspar, garnet, tourmaline, etc. whereas mica is softer than turbine material found in river sediments of Nepal. Erosive wear involves wear mechanisms, which are largely controlled by the particle material, the angle of impingement, the impact velocity and the particle size.

If the particle is hard and solid, it will be possible that a process similar to abrasive wear will occur, Lower Marsyangdi hydro-power plant head works samples were taken and sieve size varied as 125-200 μm, 200-300 μm and 300-600 μm. After the test observation, the weights were noted and erosion rate were calculated. From analysis, it is observed that the erosion rate varies with size of the sediments. The erosion rate increases with the increase in the size of the sediments keeping all other parameters constant. The higher the particle size, the higher the sediment erosion occurs. Erosion tests were performed keeping the size constant as 125-200 μm for all three samples. From analysis of Lower Marsyangdi hydro-power plant, it is found that erosion rate decreases in going from head works to tail-race keeping size 125-200 μm. The erosion is reduced while going from head-works to tail race [70]. Figure 3.10 shows the eroded runner blades of Lower Marsyangdi hydro-power plant.

(a) (b)

Figure 3.10: (a) and (b) Eroded runner blades of Lower Marsyangdi, hydro-power plant

3.2 Chapter Summary

A thorough case study on Nepal's medium and large hydro-power plants was conducted and analysed. The Jhimruk, Kaligandaki 'A', Middle Marsyangdi, and Lower Marsyangdi hydro-power plants' specifications were examined. The soft coating mitigation techniques debate at Kaligandaki 'A' was summarised.

Chapter 4

Methodology

This chapter focuses on the challenges of sediment erosion in GVs and runner blades. It finds suitable methods for experimental and numerical investigations of Francis turbines exposed to sediment-laden river and extends the knowledge on the causes and consequences of sediment induced erosion on GVs and runner blades. It discusses the overall research design including conceptual frameworks of research studies, experimental tools and techniques use, data collection, and assumptions made for simulation and analyses.

4.1 Description of Methods

Analytical methods, physical model testing with reduced size, field measurement with prototype scale, and numerical simulations are commonly used for the research of physical phenomena, notably hydro-mechanical and electro-mechanical engineering. But this study employs the methods of measurement at prototype scale, i.e. at an existent medium-head hydro-power plant of a Francis turbine as well as CFD in this work for the following reasons;

1. The issues cannot be solved solely analytically, and certain fundamental factors must be identified in order to solve them.

2. Because large-scale model experiments are expensive and impractical, scale effects may impact model testing on hydro-abrasive erosion.

3. Due to a lack of data for model calibration, validation, as well as a lack of appropriate mathematical models, all important processes cannot be numerically reproduced.

The following approach structured in three tasks of methodology was adopted according to the three specific objectives (Figure: 4.1)

1. Task A, investigation of concentration, particle size distribution and mineral content test and analysis

2. Task B, monitoring of 3D-scanned eroded GVs and runner blades and comparison with CFD analysis

3. Task C, evaluation of erosion of GVs tested at RDA and SEM analysis

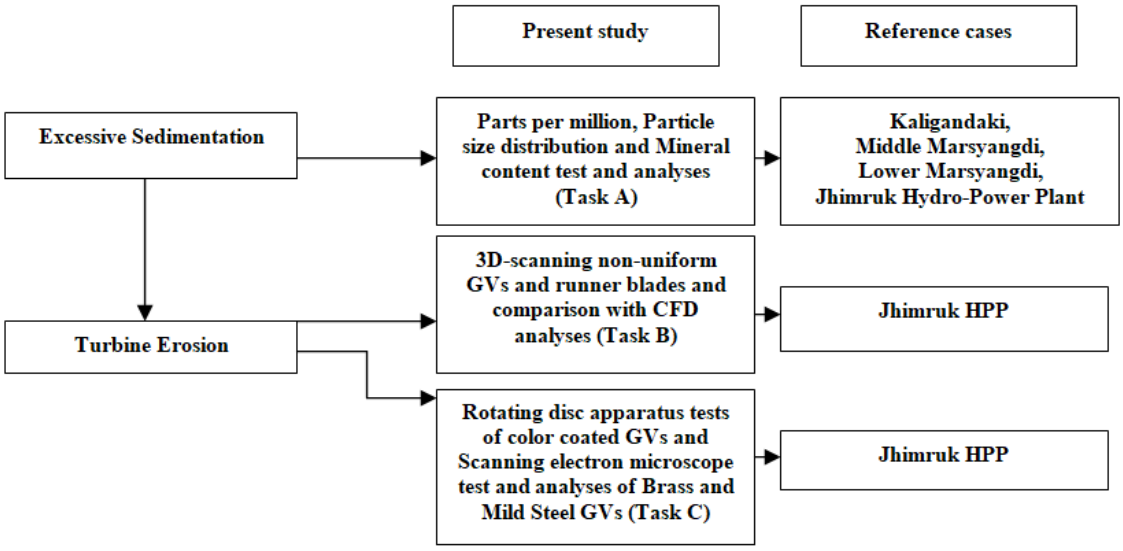

Figure 4.1: Methodology adopted in this study

4.2 Methodology Adopted

4.2.1 Jhimruk Hydro-power Plant

The author gathered secondary and source material by viewing Jhimruk hydro-power plant site. Sand and water samples were collected from various sites in the Jhimruk river, including the catchment area, desilting basin start, desilting basin end, and colling tank. These samples were properly sieved. Suspended sediment concentration, particle size distribution, and mineral content analyses were performed at the Turbine Testing Lab (TTL), Kathmandu University (KU) and Hydro Lab Nepal (HLN), Lalitpur. Staff and experts were questioned to determine the potential reasons for GVs and runner blade erosion. At Nepal Hydro Electric, Butwal, eroded as well as regular GVs and runner blades were inspected. Wear, fissures, and surface structure were investigated using a 3D scanning camera and vernier callipers to measure wear depth and

surface roughness. Wear and grooves from leading edge to trailing edge of GVs and runner blades were analyzed with loading curve, velocities diagram, vortices diagram and CFD.
An extensive literature review was conducted to examine the impact of sand erosion on Francis turbines, as well as field analysis of functioning plants and an experimental inquiry. Experimental and numerical study of the impact of sand erosion on the GVs and runner blades of a Francis turbine was carried out using 3D scanner, EISCAN PRO PLUS 2x (White Light 3D-Scanning) technology, 2D camera, physical measuring scale, digital Vernier Caliper and CFD. The impacts of sand erosion on the scale-down GVs were investigated experimentally and numerically using RDA and CFD. Finally, data were generated and analyzed.

4.2.2 Lower Marsyangdi, Middle Marsyangdi, and Kaligandaki 'A', Hydro-power Plant

The researcher gathered secondary and source material by viewing the hydro-power plant site. Sediment samples were collected from various sites in hydro-power plants, including the catchment area, desilting basin start, desilting basin end, and cooling tank. These samples were properly sieved. Suspended sediment concentration, particle size distribution, and mineral content analysis were performed at the TTL, KU and Hydro Lab Nepal, Lalitpur.

4.2.3 Suspended Sediment Concentration

The concentration of suspended sediment particles in each water sample collected from various places was evaluated by laboratory analysis. An automated calibration mechanism was included with the balance. It was not necessary to compensate for fluctuations in air pressure. The observed weight was shown in grams on the balance. In the laboratory, all weight readings and calculations were done in grams. The balance measured the weight of the combination of water and sediment in the sample via and the weight of the suspended sediments collected on filter papers. Which has a capacity of 2100 g and a count of 0.1 g. The thermostat-controlled oven was used to dry the filter papers that had been saturated with damp sediments. The filters were put in special dishes and were serially numbered. A marker was used to number the dishes. The dried filter papers and plates were removed from the oven and allowed to cool for about 10 minutes at room temperature. The filter paper dish was then placed on a disc of balance to weigh. The balanced cabinet door was closed to wait about 15 seconds for the balance to settle. The measuring disc on the balance was cleaned and dried. Before filtration

begins, a sufficient supply of clean (distilled) water must be provided in the filtration lab. It was ensured that all of the wash bottles were filled with clean water.
To prevent leakage, samples were transferred from the collection location to the Sediment Lab in a dedicated container under tight observation. Each bottle was branded in accordance with the Tab supplied by Hydro Lab. The oven's temperature was set at 95°C. To confirm that no water has seeped out during transit, the water level in the bottle was measured and compared to the water level seen at the location. The appropriate filter paper was placed on top of the filter funnel's screen, and the filter tunnel and container were clamped together. The vacuum pump was started, pouring the upper layer of clean water from the sample container into the filtering unit without jostling it. The filter device was filled with the water sample. The sample bottle and the upper half of the filtering unit were flushed with distilled water. The vacuum pump was turned off and the filter unit's upper section (container) was removed. The filter was placed in the appropriate dish with care. The dish was put in the oven separately. The sink was filled with the water from the filter flask. The distilled water was used. The filter flask and filtration machine was cleaned. After cleaning and drying, the sample vials were placed in the designated containers. Another bottle was chosen and the procedure was repeated until the oven was full or all samples collected from the location have been evaluated (Source: hydro lab Nepal). Figure 4.2 shows the process of sediment concentration analysis.

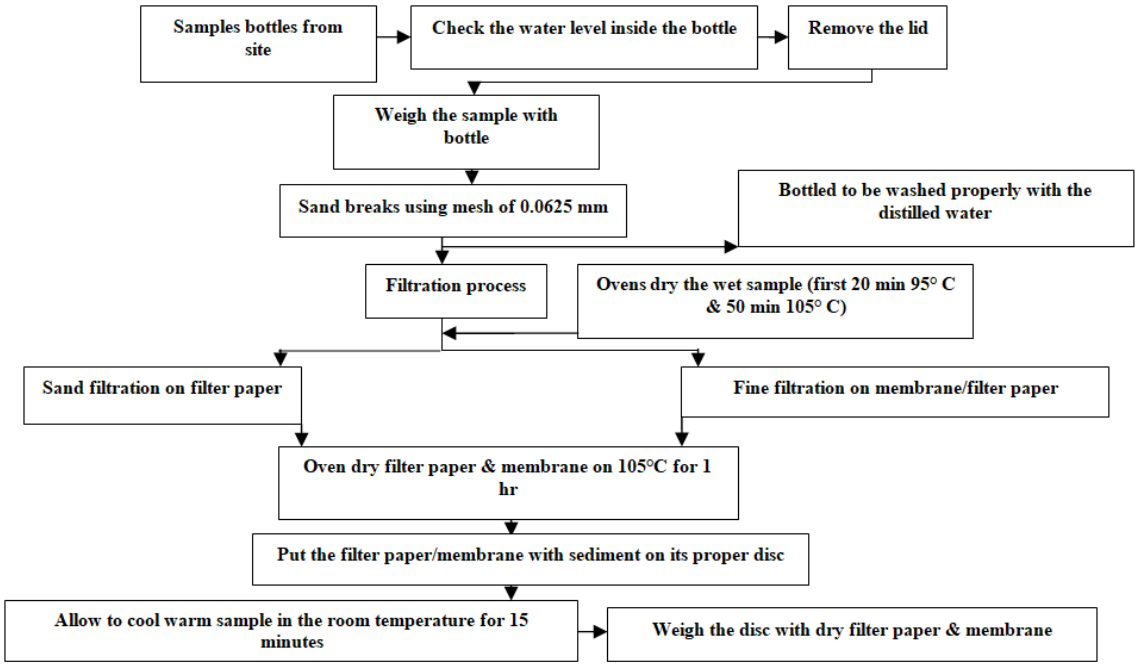

Figure 4.2: Process of sediment concentration analysis (source: hydro lab Nepal)

4.2.4 Particle Size Distribution

Particle size distribution studies were performed using the Beckman Coulter Particle Size Analyzer. This apparatus use the laser diffraction technique to evaluate particle sizes ranging from 0.4 micron to 2,000 micron. Table 4.1 shows a detailed description of the laser diffraction technique of LS 13 320.

Table 4.1: Description of LS 13 320

Instruments	Model No.	Quantity
Optical Bench	Al 38598	1
ALM sample cell W/PIDS	ALM S.C. – Al 38049	1
Aqueous Liquid module	ALM-AL 31032	1
Sonicator	CV 181- 7606	1

4.2.5 A Diffraction System

Figure 4.3 shows the working principle of the laser diffraction system. The suspended sediment concentration was then analyzed using a Laser diffraction particle size analyzer ranging in size from $10^{-}4$ to 10 mm to determine the particle size distribution. The test was carried out by adding up to 8% to a maximum of 18% of the sample each time.

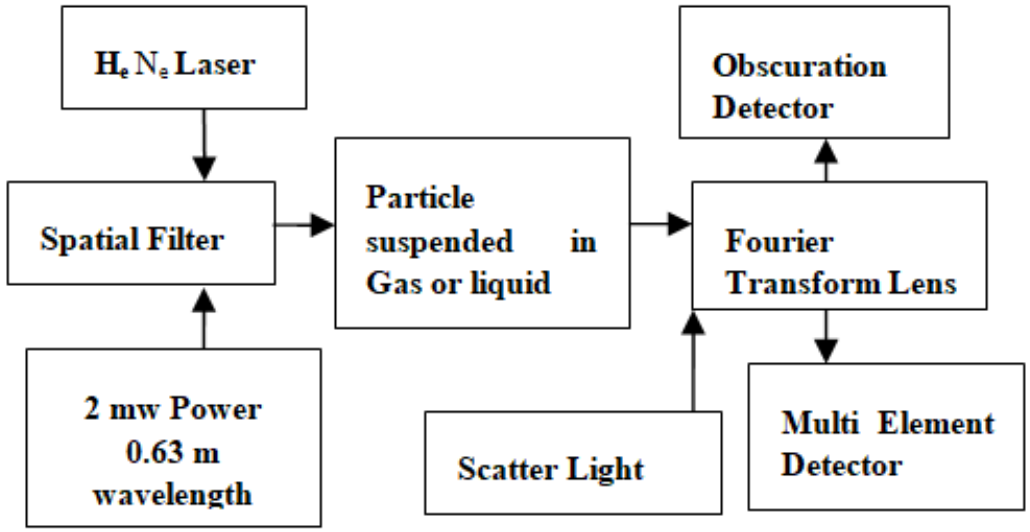

Figure 4.3: Working principle of laser diffraction system (source: hydro lab Nepal)

1. Particles traveled through a laser beam, were dispersed by light, and were collected at various angles in the forward direction.

2. The angle of diffraction is the simplest situation in which the particle size is inversely linked.

3. The particles have passed through an enlarged and collimated laser beam in front of a lens with a photosensitive detector comprised of rings in its focal plane.

4. The computer has processed the scattered intensity distribution to produce the particle size distribution.

4.2.6 Mineral Content Analyses

The minerals were identified using a Zoom Stereo microscope. Minerals were identified using the visual identification approach. The acid approach was used to assess the amount of carbonate present. Representative samples from the sampling period were chosen, and mineral content studies were performed. Each sample was separated into three groups and examined independently. Finally, the findings of each set were averaged to get the best mineral representation.
These samples were properly sieved and suspended sediment concentration, particle size distribution, and mineral content were analyzed and performed at the turbine testing lab, KU and hydro lab Nepal, Lalitpur. Finally, data were generated and analyzed.

4.3 Numerical Investigation

4.3.1 Numerical Setup for Guide Vanes and Runner Blades

A CFD analysis for the designed condition was performed in this study using ANSYS CFX including the GVs and runner blades to relate the erosion inside the turbine with various flow phenomena. The full model of the turbine consists of 24 GVs and 17 runner blades, whose geometry was made available from past studies in the form of co-ordinates. These co-ordinates were used to prepare the mesh in Turbo-grid, as shown in Figure 4.4. The GV consisted of a clearance gap of 1 mm on both sides, such that the effect of the increase in the clearance gaps on the flow can be inferred. The mesh sensitivity study for the same geometry was performed in the previous study using the grid convergence index (GCI) technique [25], this technique is found to be effective in predicting the numerical uncertainties for the case of Francis turbines [71], which showed the uncertainty of 0.14% for the total mesh count of 1.03 M in the one runner blade passage. The average y^+ value of 30 was maintained in the near-wall regions.
The mass flow rate of 2350 kg/s at the inlet of the GV and the atmospheric pressure was defined at the outlet. The inlet velocity vectors in cylindrical co-ordinate system

were provided based on the stay vane's opening angle at its outlet, i.e. tangential and radial components of 0.97 and 0.22 respectively, with 0 values for the axial component, assuming no change in the velocity in this direction. Considering the flow development at the inlet of the GV in the numerical model compared to the real turbine, a turbulence intensity of 5% was added at the inlet of the passage. The change in the velocity distribution due to the wakes from the stay vanes was not considered in this study, as the major region of damage was due to the interaction of the GV and the runner and the flow disturbances inside the runner. In the chosen mesh, the clearance gap of 1 mm contained 20 layers of mesh to resolve the leakage flow through the gap. The simulations used Reynolds's average Navier-Stokes based shear stress transport turbulence model. The convergence criteria were set based on the residual target of $10^{-}5$ Root Mean Square (RMS). A frozen rotor interface model was selected between the stationary and rotating domains in the steady simulation. However, to resolve the localized vortices originated from the leakage flow, a transient simulation was performed taking the initialization of the steady solution and the time step of 1° rotation. In this study the complete numerical model consisted of 11 GVs and 8 runner blade passages, such that the interface pitch ratio close to 1 could be maintained. For the transient simulation, the interface was modeled with Transient Rotor-Stator, such that the vortices could be resolved.

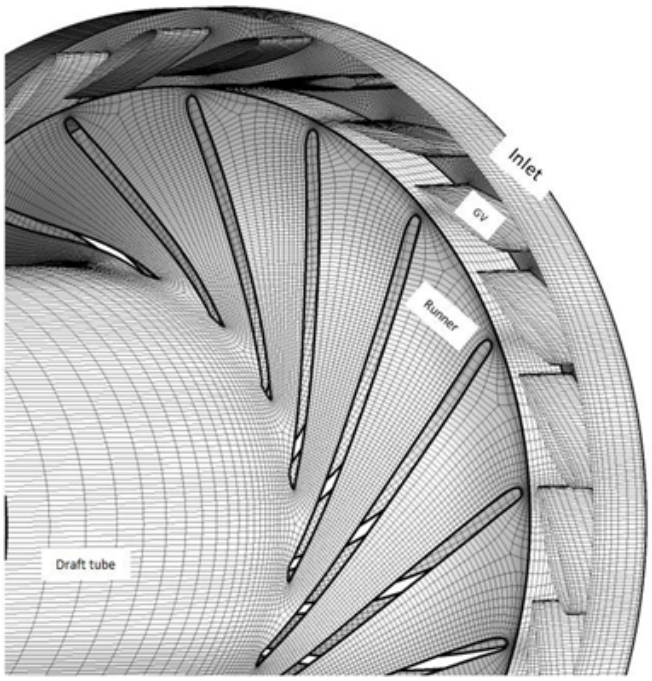

Figure 4.4: Mesh in the GV and runner domain

4.3.2 Numerical Setup of Rotating Disc Apparatus

The numerical model consists of a stationary domain with the 14 baffles and a stationary domain with the 4 GVs as shown in Figure 4.5. CFD was carried out using a commercial code, ANSYS CFX 18.1 using a steady-state Eulerian-Lagrangian approach, where water was modeled as a continuous fluid and sediment as particles carried by the fluid. The domains were discretized in integrated computer engineering and manufacturing, which consisted of 1.5 million hexahedral structured meshes. The size of the mesh was chosen based on a mesh independent study, which resulted in a deviation of <1% in average erosion rate density of GVs. Taking the reference of the experiment, the speed of the rotating domain was set at 600 rpm. Two outlets were present in the stationary domain during the experiment to compensate the leakage losses and measure the static pressure. In the numerical study, these outlets were kept closed by defining the wall in end surfaces. The size of the sediment particles were 0.25 mm, which was controlled in the experiment by sieving the sand. Erosion in the surfaces of GVs was modeled using Tabakoff and Grant erosion model.

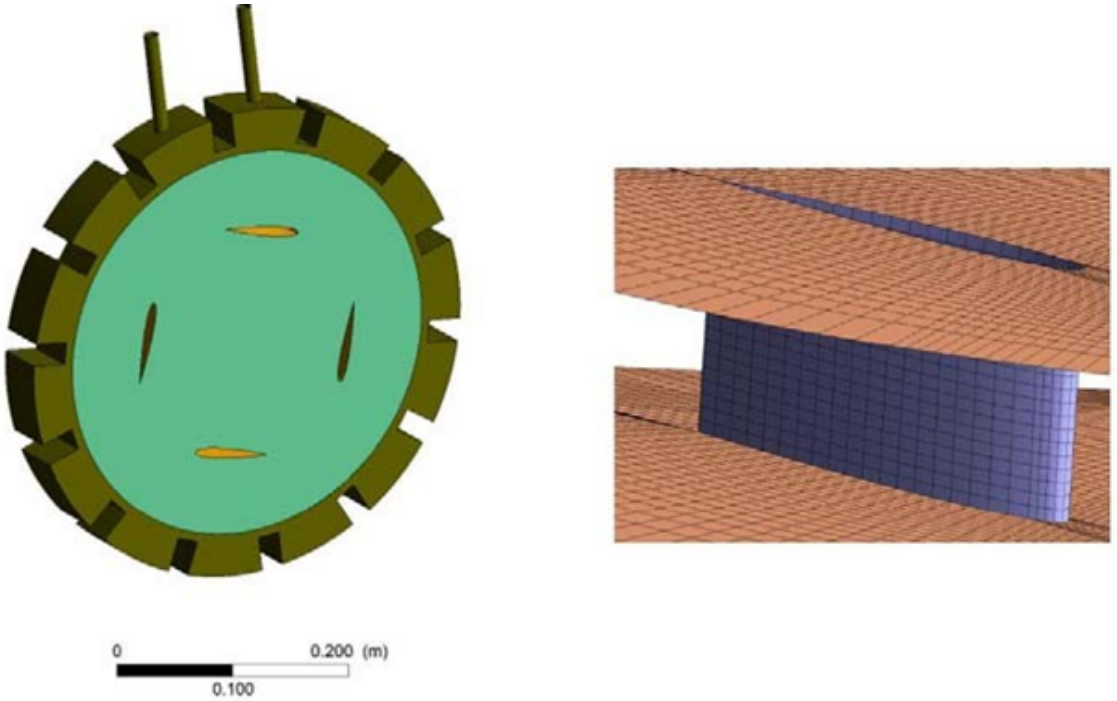

Figure 4.5: Fluid domains for CFD and mesh around GV

4.3.3 Navier-Stokes Equations and Turbulence Models

The Navier-Stokes equations, created in 1822 by Claude-Louis Navier and George Gabriel Stokes, may be used to calculate the velocity field that applies to a fluid given

some initial circumstances. The Navier-Stokes equations are derived from the fundamental concepts of mass, momentum, and energy continuity. It is occasionally essential to consider a finite arbitrary volume, referred to as a control volume, across which these concepts can be applied. The Navier-Stokes equations are the basic equations that control the motion of an incompressible viscous fluid. In general, the Navier-Stokes equations are nonlinear partial differential equations that persist in practically every real-world scenario. Many times, the equations may be reduced to linear equations. The Navier-Stokes equations are a set of differential equations that explain how the speed of a fluid's flow changes as a result of internal forces such as pressure, viscosity and external forces such as gravity acting on the fluid.
The momentum balance equation in vector form, velocity field u (x,t) and pressure field p (x,t), similarly the convective term $((u\cdot\ \nabla)u)$ as well as diffusive term $(\nu\nabla^2 u)$ is defined by the equations 4.1, 4.2, 4.3, 4.4, and 4.5 below.

$$u_t + (u\cdot\nabla)u = -\frac{1}{\rho}\nabla p + \nu\nabla^2 u + f \tag{4.1}$$

or

$$\rho\frac{Du}{dt} + \rho(u\cdot\nabla)u = -\nabla p + \mu\nabla^2 u + \rho f \tag{4.2}$$

where,

$$\nabla^2 = \frac{\delta^2}{\delta x^2} + \frac{\delta^2}{\delta y^2} + \frac{\delta^2}{\delta z^2} \tag{4.3}$$

Mass balance equation is as below

$$\nabla\cdot u = 0 \tag{4.4}$$

$$\nabla\cdot u = \frac{\partial u}{\partial x} + \frac{\partial v}{\partial y} + \frac{\partial w}{\partial z} = 0 \tag{4.5}$$

After convective term is very small the equation 4.2 become 4.6.

$$\rho\frac{Du}{dt} = -\nabla p + \mu\nabla^2 u + \rho f \tag{4.6}$$

Newton second law, force 4.7.

$$\rho\frac{Du}{dt} \rightarrow \frac{mass}{volume} \times Acceletation \tag{4.7}$$

Unsteady plus convective acceleration 4.8.

$$\rho\frac{Du}{dt} = \frac{\partial u}{\partial t} + u\cdot\nabla u \tag{4.8}$$

Internal forces including pressure force and viscous force 4.9.

$$-\nabla p + \mu \nabla^2 u + \rho f \tag{4.9}$$

external forces or body forces is ρf
The above equations 4.2 and 4.6 are known as Navier-Stokes equations for an incompressible fluid motion. The parameters ν is the kinematic viscosity, ∇ is defined as the navla operator, body forces like Coriolis and centrifugal forces is denoted by f. The Navier-Stokes equations are to be solved in a spatial domain omega (Ω) at time interval t. The mathematical derivation of the N-S equations follows the Newton's second law of motion 4.10.

$$\rho \frac{Du}{dt} = \nabla \cdot \sigma + \rho f \tag{4.10}$$

The material derivative is $\frac{Du}{dt}$ and the stress tensor is denoted by σ. Acceleration term from the above equation is as follows 4.11.

$$\frac{Du}{dt} = u_t + (u \cdot \nabla)u \tag{4.11}$$

From equation 4.10, and 4.11, $\rho \frac{Du}{dt}$ is density $\times$ acceleration, density is mass per unit volume, defined force in left hand side and is balanced by force in right hand side induced with fluid velocity motion u, stresses σ and external body forces f. The other basic fundamental equation for the fluid in motion is the continuity equation of mass conservation 4.12.

$$\rho_t + \nabla \cdot (\rho u) = 0 \tag{4.12}$$

Also in the form 4.13,

$$\nabla \cdot u = \frac{1}{\rho} \frac{D_\rho}{dt} \tag{4.13}$$

Incompressible fluid motion describes the constant density of the fluid during motion, that is $\frac{D\rho}{dt} = 0$. And hence the continuity equation of Navier-Stokes equation $\nabla \cdot u = 0$. The second equation of equations (4.12 and 4.13) is partial differential equation most use for incompressible flow with the unknown motion of velocity field u.
Unknown motion of velocity field u has different relations with different fluids and also the internal stress σ has different relations with different fluids. A Newtonian fluid has linear and an isotropic relation between σ and u 4.14.

$$\sigma = -pI + \mu(\nabla u + (\nabla u)^T) \tag{4.14}$$

The identity tensor is denoted by I, and dynamic viscosity is denoted by $\mu(\mu = \rho\nu)$. The equation 4.14 is the incompressible flow equation. Now, imply equation 4.14

into equation 4.10 to get equation 4.1 or 4.2, after dividing by ρ,$\nabla\cdot(pI)$= ∇p, again calculating $\nabla \cdot (\nabla u + (\nabla u)^T)$ as $\nabla^2 u + \nabla(\nabla \cdot u) = \nabla^2 u$. The vector operations are with the ∇ operator by the use of index also known as dyadic notation. After the numerical methods apply $\nabla \cdot \sigma = -\nabla p + \nabla \cdot (\nabla u + (\nabla u)^T)$ in equation 4.1 or 4.2, they become equation 4.15 or 4.16 as follows.

$$u_t + (u \cdot \nabla)u = \frac{1}{\rho}\nabla \cdot \sigma + f \tag{4.15}$$

or

$$u_t + (u \cdot \nabla)u = -\frac{1}{\rho}\nabla p + \nu\nabla \cdot (\nabla u + (\nabla u)^T) + f \tag{4.16}$$

4.3.4 Reynolds-Averaged Navier-Stokes Equations

Reynolds-averaged Time-averaged Navier-Stokes equations are time-averaged fluid flow equations. The equations are based on Osborne Reynolds' theory of Reynolds decomposition, which divides an instantaneous variable into time-averaged and fluctuating values. The Reynolds-averaged Navier-Stokes equations are a simplified version of the general Navier-Stokes equations. The steady-state solution in the Reynolds-averaged Navier-Stokes equations is decoupled from the system's time-varying fluctuations, which account for turbulence in different flow regimes. The average turbulent flow field for the incompressible fluid motion is derived by the time-averaging of the Navier-Stokes equations and the continuity equation. The above Navier-Stokes equations have four unknowns, three velocities components of u and pressure p. This is a highly non-linear partial derivative equation, which can be solved with a computational approach. These studies need Reynolds-averaged Navier-Stokes method to solve the fluid problems. For the time-average value, the momentary value is decomposed into fluctuating value $\tilde{u_i}$ and mean value $\overline{\mathrm{u_i}}$. The substitution of these new terms in the original transport equation gives 4.17 and 4.18.

$$\frac{\delta \overline{\mathrm{u_i}}}{\delta x_i} = 0 \tag{4.17}$$

$$\frac{\delta \overline{\mathrm{u_i}}}{\delta_t} + \overline{\mathrm{u_j}}\frac{\delta \overline{\mathrm{u_i}}}{\delta x_j} = -\frac{1}{\rho}\frac{\delta \overline{\mathrm{p}}}{\delta x_i} + \frac{\delta}{\delta x_j}(\nu\frac{\delta \overline{\mathrm{u_i}}}{\delta x_j} - \overline{\tilde{\mathrm{u}}_\mathrm{i}\tilde{\mathrm{u}}_\mathrm{j}}) \tag{4.18}$$

Where, $\overline{\mathrm{u_i}}$ = mean velocity or time-averaged velocity components, $\overline{\mathrm{p}}$ = time-averaged pressure, ρ = fluid density, ν = kinematic viscosity of fluid, $\tilde{u_i}$ = fluctuating velocity components, and t = time. The continuity equation cannot be changed with the Reynolds-averaged Navier-Stokes, but the additional stress term acting on the mean flow will come as a result due to the fluctuating velocity, are called Reynolds's stress

and it is written as

$$\tau_{ij} = -\overline{\tilde{u}_i \tilde{u}_j} \tag{4.19}$$

Equation 4.19 arises from the non-linear convective term in the un-averaged equations and represents the effect of the turbulence on the mean flow. Now the Reynolds-averaged Navier-Stokes equation has 6 unknowns which are solved by using different turbulence models. The Reynolds-averaged Navier-Stokes equation turbulence models are divided into

1. eddy-viscosity models and

2. Reynolds stress model.

The eddy viscosity model assumes that the Reynolds stress is related with the mean velocity gradients and eddy (turbulent) viscosity by the gradient diffusion (Boussinesq) hypothesis, given by the equation 4.20 below.

$$\tau_{ij} = -\overline{u_i u_j} = \nu_t \left(\frac{\delta \overline{u_i}}{\delta x_j} + \frac{\delta \overline{u_j}}{\delta x_i}\right) - \frac{2}{3}\left(k + \nu_t \frac{\delta \overline{u_k}}{\delta x_k}\right)\delta_{ij} \tag{4.20}$$

Where, turbulent kinetic energy (k) is represented by $\frac{1}{2}\overline{\tilde{u}_i \tilde{u}_j}$. kronecker delta is given by δ_{ij}. Turbulent or edda viscosity is noted by ν_t. In two-equation eddy-viscosity turbulence models, the velocity and turbulent length scale are solved using two separate transport equations, one for kinetic energy (k) and another turbulent dissipation rate (ϵ) or the specific dissipation rate (ω). In $k - \epsilon$ model, the turbulence viscosity or eddy viscosity (ν_t), is related to the turbulence kinetic energy (k) and the dissipation rate (ϵ) by the given relation 4.21 below.

$$\nu_t = C_\mu \frac{k^2}{\epsilon} \tag{4.21}$$

Where, C_μ is a constant [72].

4.3.5 Shear Stress Transport (SST) Theorem

Menter's shear stress transport turbulence model, is a popular and reliable two-equation eddy-viscosity turbulence model for CFD studies. The sensitive study of the turbulence models shears stress transport, baseline two equation model and Ω Reynolds Stress with respect this test rig was performed earlier, which showed that shear stress transport turbulence model is suited for the CFD of this test rig [18]. The shear stress transport $k - \omega$ turbulence model is a two-equation eddy-viscosity model that is widely used in aerodynamics. It's a hybrid model that combines the Wilcox $k - \omega$ and $k - \epsilon$

models. The $k-\omega$ model is active near the wall flow region, where adverse pressure gradient is developed, whereas the $k-\epsilon$ model is active in the free stream flow region [73].

4.4 Experimental Investigations of Rotating Disc Apparatus

The RDA used in this study is shown in figure 4.6. It is a rotating type test rig, which consists of a fixed diameter disc rotating at a provided speed along with sediment slurry. The disc and/or specimen for the test can be made with the same material as that of the turbine, or any other softer materials, so that experiments can be conducted in accelerated test mode where the effect of sediment can be seen in laboratory operating time. Since this research focuses on studying the erosion pattern on GVs, both the disc and the test specimens were fabricated using mild steel. In this study, a reference case of Jhimruk hydro-power plant was taken, which consisted of 3 units of Francis turbines at 4.1 MW installed capacity each [26].

The GVs were modeled with a scale factor of 1:4 compared to the original size. The GVs were shaped as NACA0012 symmetrical hydrofoil. These specimens were coated with spray color (Aerosol lacquer) which had a maximum sustained temperature of 40°C. The apparatus was maintained below 35°C during the experiment by introducing cooling water in regular interval to avoid color melting. Several color coating layers were applied over the GVs, such that the vulnerability of particular regions of the specimen could be inferred from the eroded color pattern. The volume of the water inside the casing was 7.88 liters mixed with 500 gm concentration of sand. The first eroded pattern was observed after every 10 minutes of operation. In order to check the repeatability of the patterns, the experiment was conducted twice with the duration of 210 and 180 minutes each. To conduct erosion tests, four GVs, each with identical geometries but different materials were fabricated. Two of them were Computer Numerical controlled (CNC) machined from Mild Steel, while two GVs were cast from Brass. Before subjecting the GVs to erosion test, the complete sample was meticulously spray painted. Before beginning the erosion testing, several measurements, including weight measurements, were taken to gather preliminary data.

Table 4.2 explains about the experimental parameters of RDA and Table 4.3 explains the properties of Brass and Mild Steel.

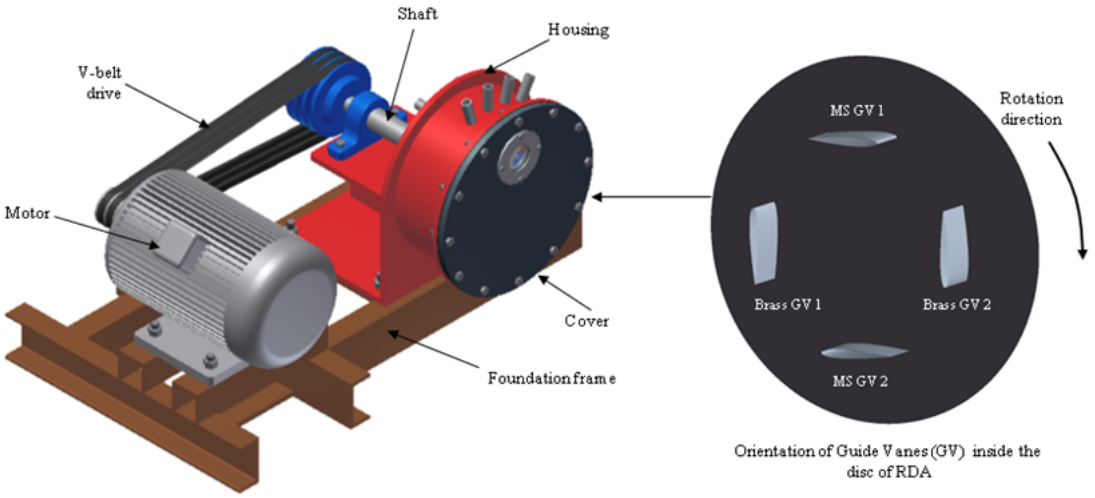

Figure 4.6: 3D of Rotating Disc Apparatus (RDA) with the dimensions of the disc and positions of the 4 GVs

Table 4.2: Experimental parameters of Rotating Disc Apparatus

Parameters	Description
Speed of rotation of motor	2900 RPM
Speed of rotation of disc	1450 RPM
Direction of rotation of disc	Clockwise as viewed from front
Diameter of disc	350 mm
Outer Diameter of mounting of specimen	300 mm
Volume of water in casing	9.17 Liters
Specimens used	Guide Vanes of Francis turbine of Jhimruk NACA0012
Materials specification	Mild Steel and Brass GVs
Operating time	15 min (Color coating test), 390 min (Weight loss test)
Sediment concentration and amount of sand	60,000 PPM which require 500 gm sand in single run
Sediment used	Sieve sand sample of desilting basin end from Jhimruk hydro-power plant
Sediment particle size	Size ranging from 0.15 to 0.2 mm
Thermometer	Digital ranging from 0-100 degree (Each test 90 min, has temperature ranging from 9-50 degree)

Table 4.3: Properties of Brass and Mild Steel

SN	Material	Density g/cm^3	Alloy Present	Alloy Percentage	Brinell Hardness	Ultimate Tensile Strength Mpa	Yield Strength Mpa
1	Brass GV	8.4-8.73	Copper, Zinc, Lead, Arsenic	55-65, 34-45, 1.7-2.8 and 0.02-0.15	37-155	338-469	124-310
2	Mild Steel GV	8.73	Chromium, Low Carbon and Manganese, Silicon, Copper	0.5-1.25, 0.15, 0.2-0.5, 0.25-0.55	95-146	340-680	285-355

4.5 Scanning Electron Microscope

The JSM-IT100 $InTouchScope^{TM}$ scanning electron microscope was used to analyze surface morphology of GVs at different locations, i.e. leading edge, trailing edge and mid-stream. Computer numerical control machine and lathe machine were used to give proper shapes and sizes to those GVs. The leading edges and trailing edges of Brass and Mild Steel GVs were cut with 10 mm height and 8 to 10 mm diameter and 5 mm height and 8 to 10 mm diameter respectively. The mid streams of both GVs were cut with 10 mm height and 31 mm diameter. These specimens were then microscopically examined to determine the erosive wear mechanism.

4.6 Chapter Summary

Methodology adopted and the methods used to analyze and generate data are the main focus of this chapter. The conceptual design, numerical and experimental setup has also played vital role to generate data in right direction.

Chapter 5

Analysis, Results, and Discussion

Research concepts and problem formulations were discussed in chapter 1. Literature review were largely studied in chapter 2 and 3, while the conceptual research frameworks based on the objectives defined with adopted methodology were presented in chapter 4. This chapter discusses the outcome of the characteristics of sediment erosion in GVs and runner blades, experimental outputs, and empirical/numerical analysis with findings and contributions.

5.1 Characteristics of Sand Particles

5.1.1 Kaligandaki 'A' Hydro-power Plant

The highest and lowest sediment concentrations were observed throughout the kaligandaki 'A', hydro-power plant sample period at desilting basin end from the 1^{st} to 31^{st} of August 2019 at different time tables, as shown in the graph at Figure 5.1. The part per million concentration is displayed vertically on the graph, while the date and time are displayed horizontally. As seen in the graph, the highest part per million concentration is around 3900 on 9^{th} August and the lowest concentration is around 800 on 30^{th} August 2019.

August 2019, particle size distribution was conducted on a near-daily basis. Particle size distribution was measured at the Kaligandaki 'A' hydro-power plant's desilting basin end. The diameter in mm is used to depict the graph's horizontal sections, while the percent finer is used to depict the graph's vertical sections. According to particle size distribution in Figure 5.2, the majority of the particles have diameters from 0.01029 to 0.16887 mm.

Figure 5.3 illustrate the mineral content in desilting basin end, of Kaligandaki 'A'

hydro-power plant. Graph shows a comparison of Quartz 64%, Feldspar 6%, Mica 13%, Carbonate and Clay 16% and Tourmaline and Garnet 1% of the August 2019.

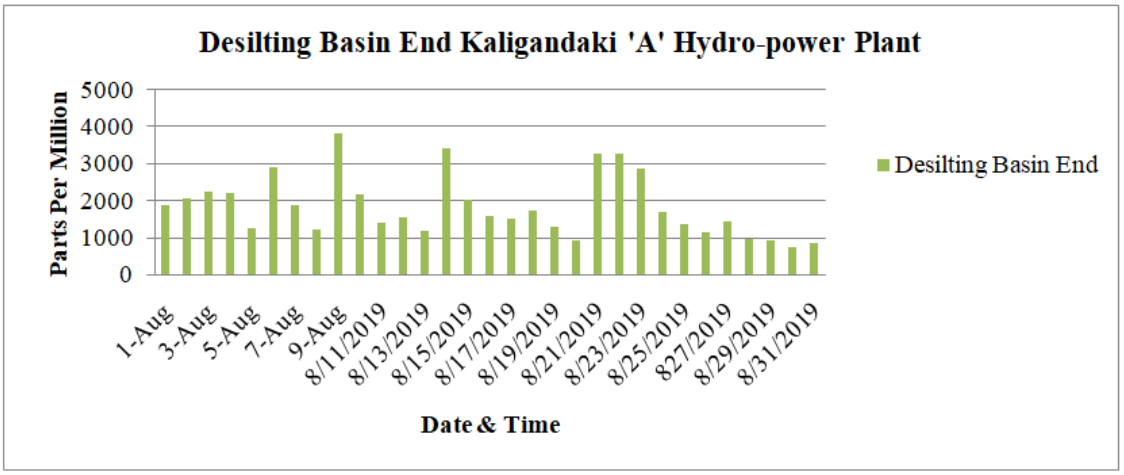

Figure 5.1: Parts per million analysis, Kaligandaki 'A' hydro-power plant

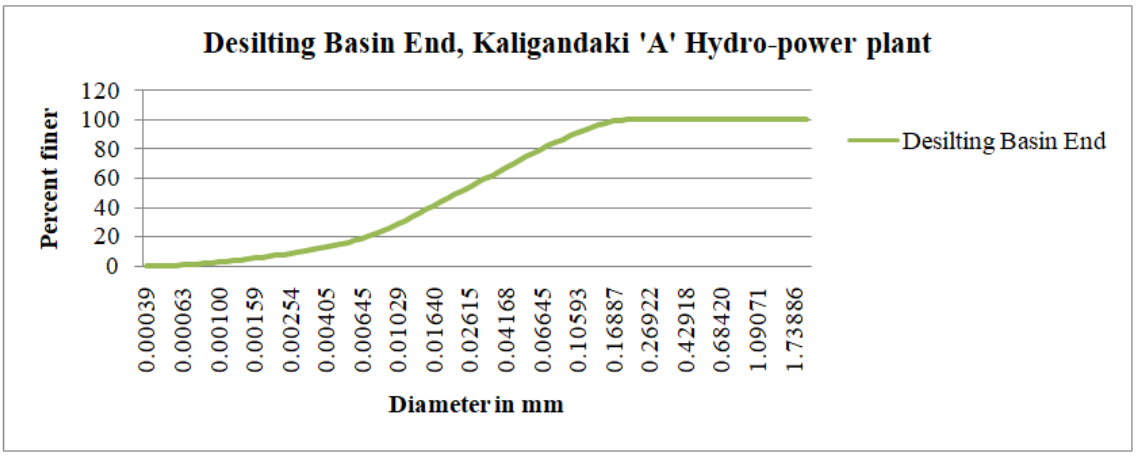

Figure 5.2: Particle Size Distribution, Kaligandaki 'A' hydro-power plant

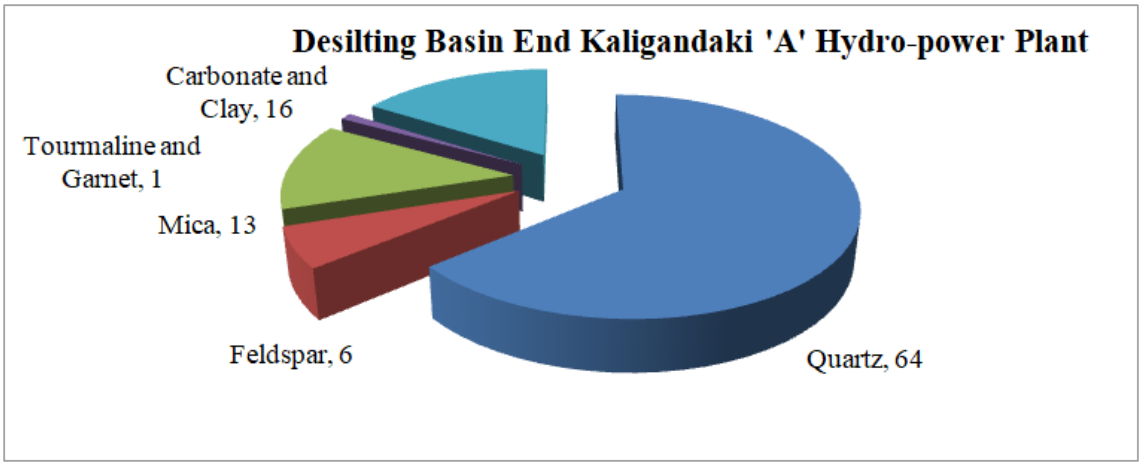

Figure 5.3: Mineral content analysis, Kaligandaki 'A' hydro-power plant

5.1.2 Middle Marsyangdi Hydro-power Plant

The highest and lowest sediment concentrations were observed throughout the Middle Marsyangdi hydro-power plant sample period at desilting basin end from the 1st to 31st of August 2019 at different time tables, as shown in the graph at Figure 5.4. The part per million concentration is displayed vertically on the graph, while the date and time are displayed horizontally. As seen in the graph, the highest part per million concentration is around 8000 on 27^{th} and 29^{th} August and the lowest concentration is around 500 on 12^{th} August 2019.

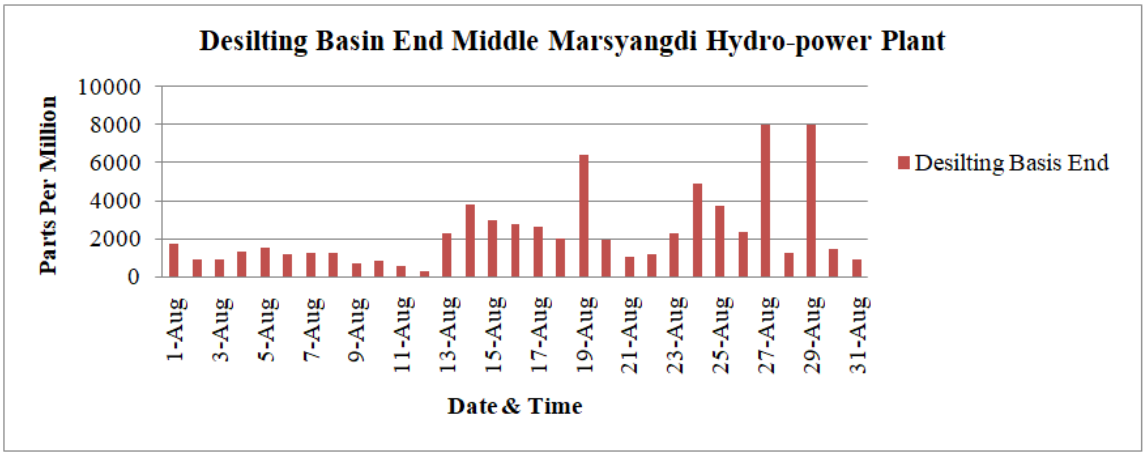

Figure 5.4: Parts per million analysis, Middle Marsyangdi hydro-power plant

August 2019, particle size distribution was conducted on a near-daily basis. Particle size distribution of desilting basin end was measured at the Middle Marsyangdi, hydro-power plant. The diameter in mm is used to depict the graph's horizontal sections, while the percent finer is used to depict the graph's vertical sections. According to the particle size distribution in Figure 5.5, the majority of the particles have diameters from 0.01640 to 0.22340 mm.

The mineral content at desilting basin end, as well as a comparison of quartz, feldspar, and mica percentages, is shown in Figure 5.6, August 2019. Desilting basin end has a Quartz content of 65%, Mica 10%, Feldspar 5%, Carbonate and Clay 19% and Tourmaline and Garnet 1%.

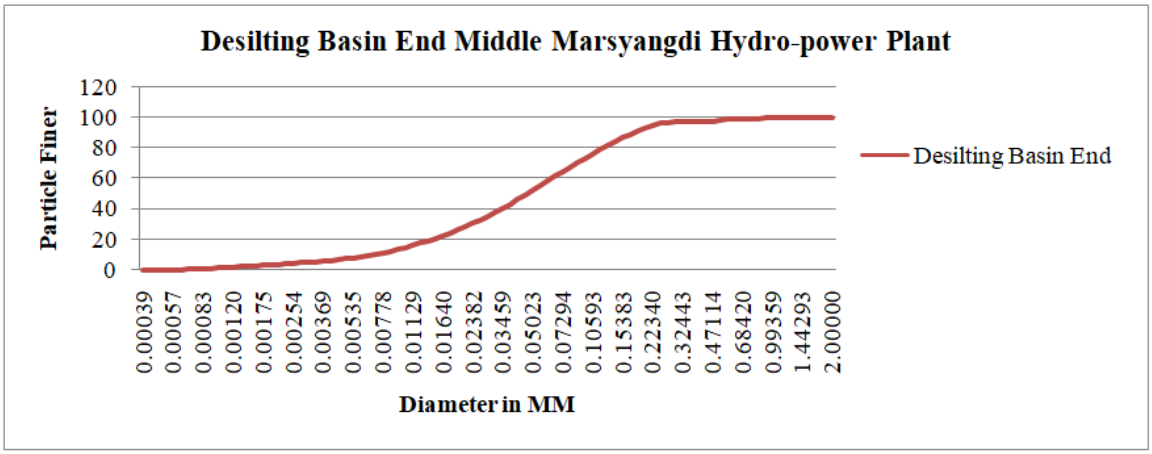

Figure 5.5: Particle size distribution, Middle Marsyangdi hydro-power plant

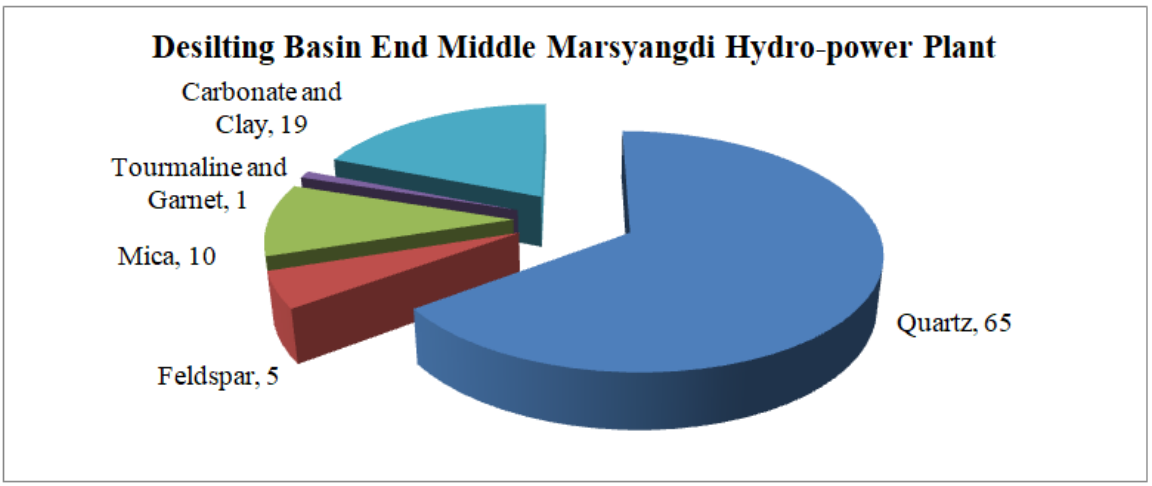

Figure 5.6: Mineral content analysis, Middle Marsyangdi hydro-power plant

5.1.3 Lower Marsyangdi Hydro-power Plant

The highest and lowest sediment concentrations were detected throughout the sample period of Lower Marsyangdi, hydro-power plant at desilting basin end on August 2019 at different time periods, as shown in the graph in Figure 5.7. The parts per million concentration are displayed vertically on the graph, while the date and time are displayed horizontally. As seen in the graph below, the highest concentration is on 1^{st} August 2019 and the lowest concentration is on 21^{st} August 2019 as shown in figure. August 2019, Particle size distribution was done on a near-daily basis. Particle size distribution was taken at the Lower Marsyangdi, hydro-power plant's desilting basin end. The graph's horizontal portion is represented by the diameter in mm, while the vertical sections are represented by the percentage finer. According to particle size

distribution in Figure 5.8, the bulk of the particles sizes have ranged from 0.01129 to 0.68420 mm.

Figure 5.9, shows the mineral compositions of desilting basin end on August 2019. Desilting basin end has a Quartz content of 63%, Mica 13%, Feldspar 4%, Carbonate and Clay 19% and Tourmaline and Garnet 1%.

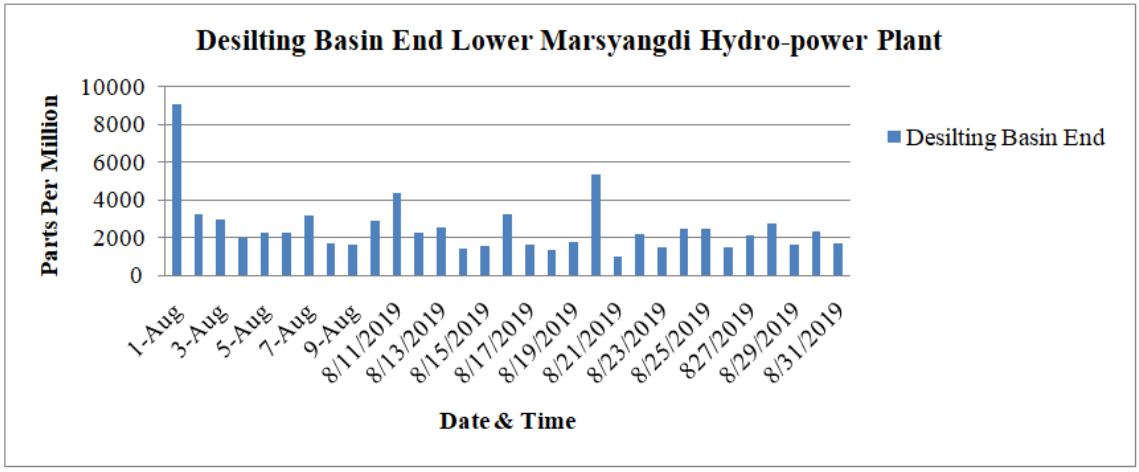

Figure 5.7: Parts per million analysis, Lower Marsyangdi hydro-power plant

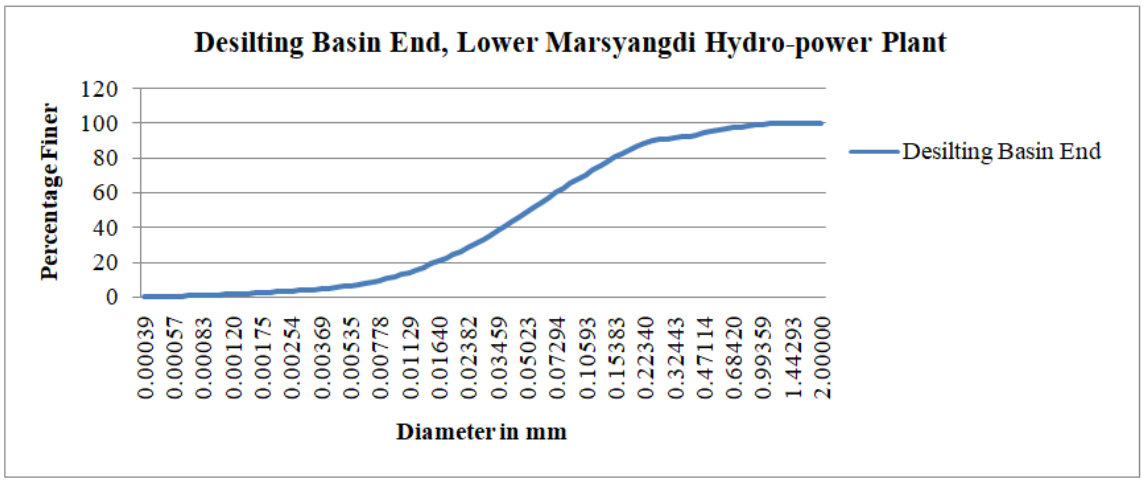

Figure 5.8: Particle size distribution, Lower Marsyangdi hydro-power plant

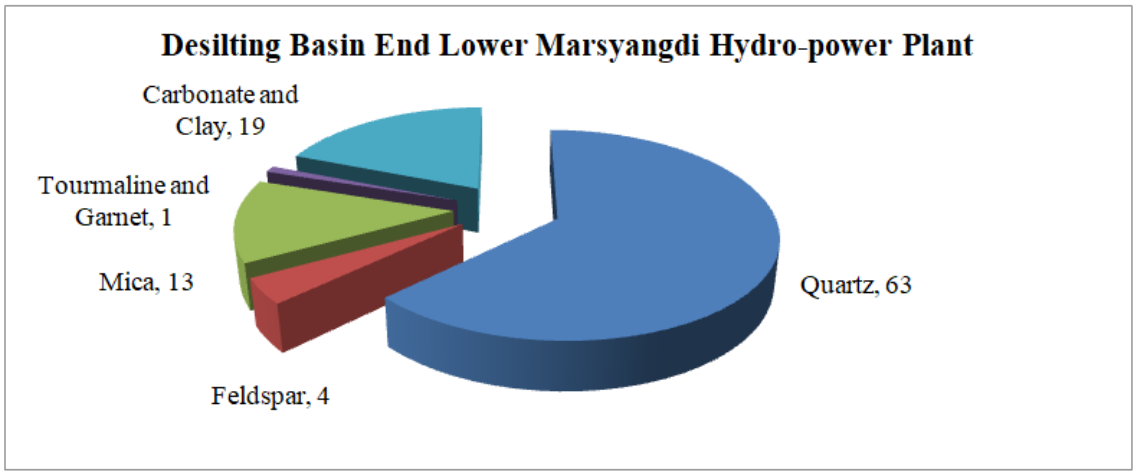

Figure 5.9: Mineral content analysis, Lower Marsyangdi hydro-power plant

5.1.4 Jhimruk Hydro-power Plant

The average daily discharge of Jhimruk for the year 2017-2018 is shown in Figure 5.10. It can be seen from the figure that there is a significant difference in the maximum and minimum discharge in the river. During the wet season, the river is usually flooded with heavy rain, which makes the discharge reach higher than 160 m^3/s at one point, and with the values over 20 m^3/s for almost 100 days a year. During the dry season, the lowest average discharge is 1.11 m^3/s and the values less than 7 m^3/s is for more than 200 days. With the designed discharge of 7 m^3/s (for the three units), this data implies that the power plant is running mostly at the off-design conditions.
Figure 5.11 shows the sediment concentration data in the power plant for the same period. It can be seen that the sediment concentration in parts per million increases with the increased discharge. The water is mostly clean in the dry season, with the sediment concentration of less than 10 parts per million for the period of around 200 days. However, during the wet season, the concentration is about 1000 parts per million in average and the maximum value is over 10000 parts per million. The maximum value of sediment concentration is on the same day as the maximum average discharge. Figure 5.12 shows the average generation of the plant in the studied period. The maximum generation from the plant is between September-November, when the discharge and sediment concentration is optimum. The plant reaches the designed discharge of 12 MW or more for the period of 72 days, whereas at other times, the part-load operation or shut-down of some units is dominant. It can be seen that although the discharge is above the designed discharge during the wet season, the generation is ceased because of the operation strategy implemented by the power plant to shut-down the turbines simultaneously at high parts per million. The energy generation for this period was

calculated to be 67.44 GWh. With the planned generation of 72 GWh annually, there is a gap of around 5 GWh of energy, which implies the loss of around 0.45 million USD every year considering the energy price of 0.1 USD per unit.

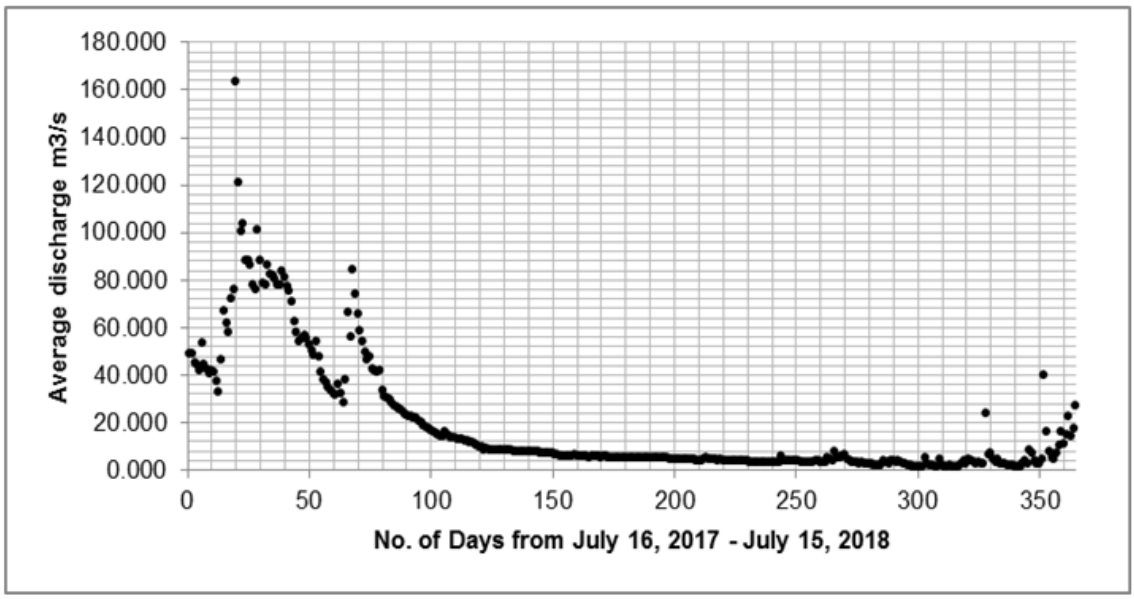

Figure 5.10: One year discharge data at Jhimruk hydropower plant averaged daily

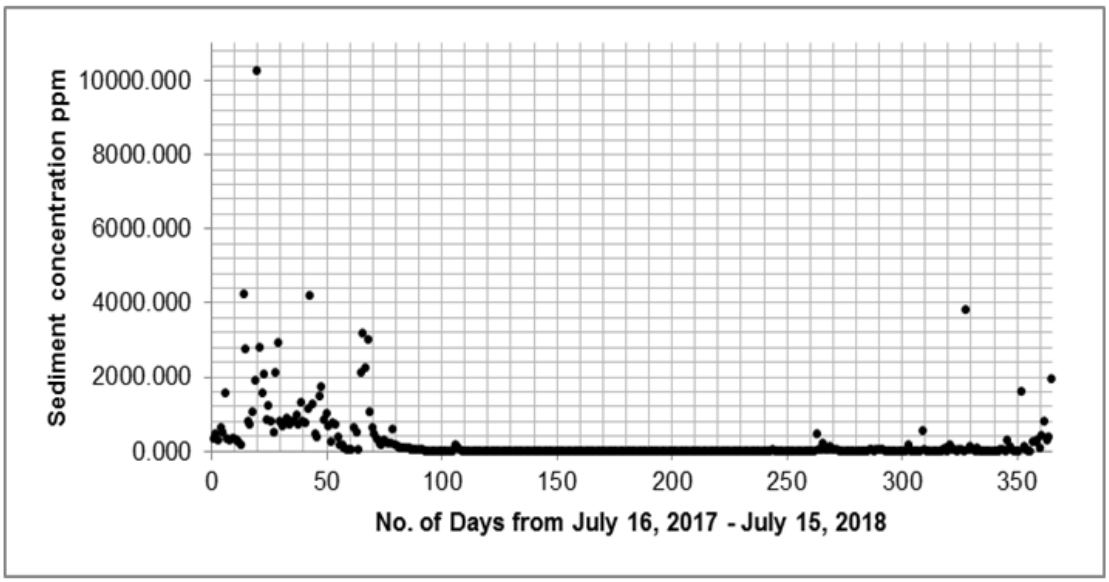

Figure 5.11: One year Sediment concentration at Jhimruk hydro-power plant

Figure 5.13 shows the particle size distribution analysis of the sediment samples collected from the start and end of the desilting basins and the cooling tank. It shows

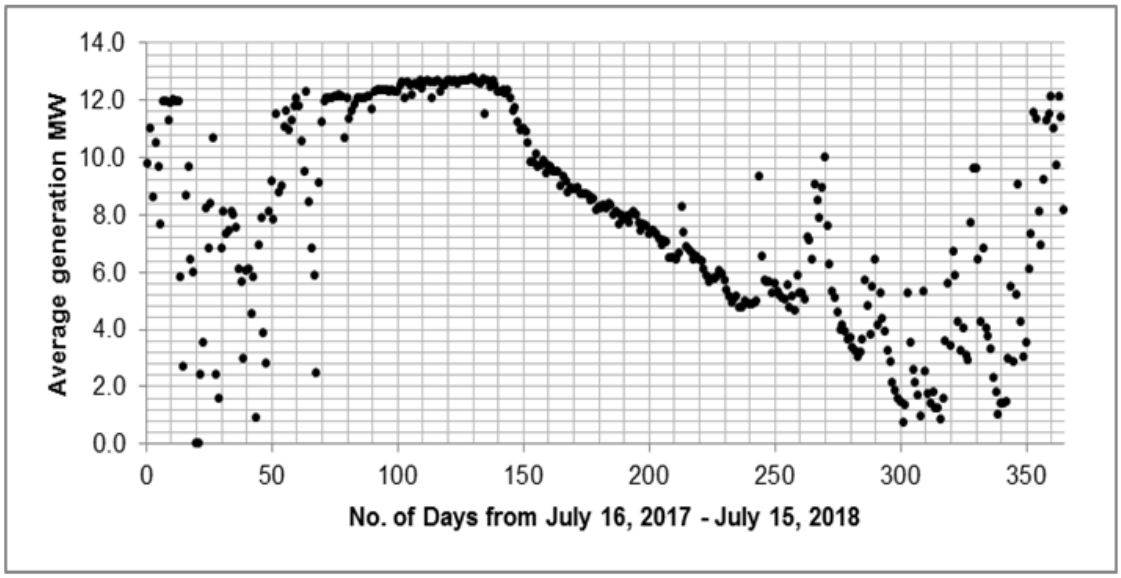

Figure 5.12: One year generation data at Jhimruk hydro-power plant averaged daily

that the particles are mostly within the range of 0.01 mm to 0.2 mm. The desilting basins are designed to trap the sediment particles larger than 0.2 mm. However, since most of the particles are less than this size, most of the particles remain suspended in water leaving the basin. As a result, these particles are carried into the penstock and finally, into the turbines.

Figure 5.14 shows the mineral content analysis from the same samples collected as in Figure 4.4. It can be seen from the figure that Quartz is the major constituent in the sediments flowing into the power plant. As Quartz is the hardest mineral found in the sediments with the Moh's hardness of 7, these particles have the highest potential for causing wear in the turbine components. From the mineral content analysis of desilting basin end and cooling tank, it can be seen that out of all the sediments that are exposed to turbines, 73% of them contain Quartz. When the turbines are continuously operated at such high concentration of Quartz, erosion remains inevitable, especially during the full load operation in wet seasons.

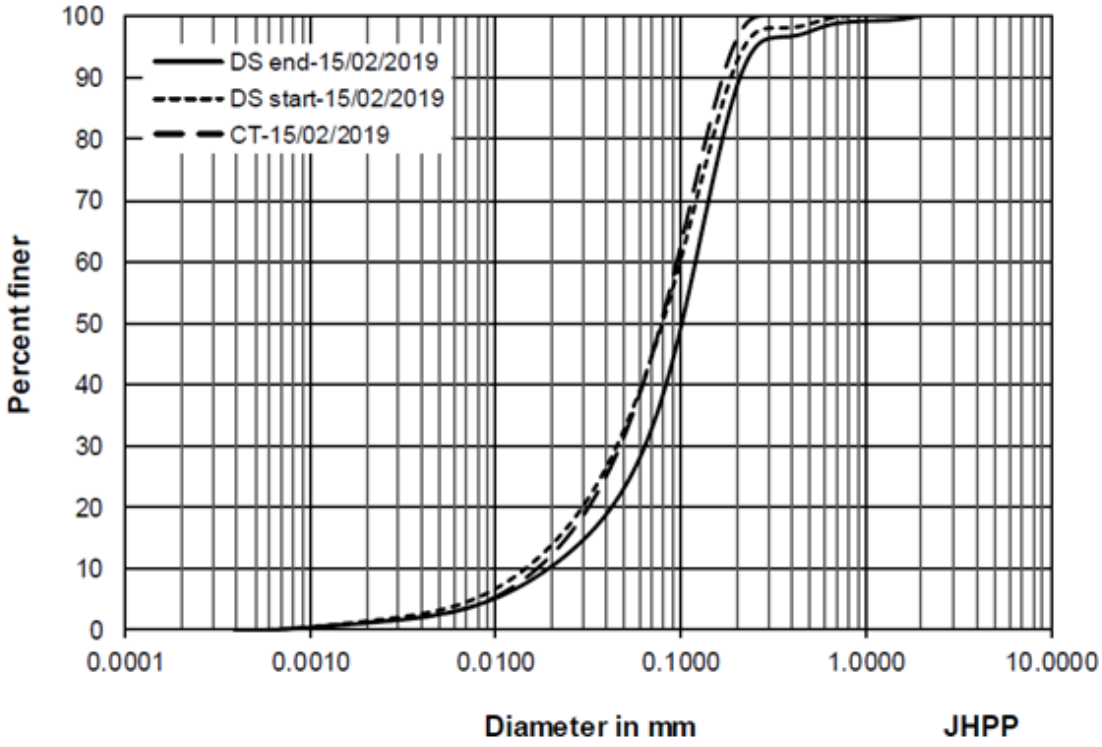

Figure 5.13: Particle size distribution analysis from desilting basin end, desilting basin start, and cooling tank at Jhimruk hydro-power plant

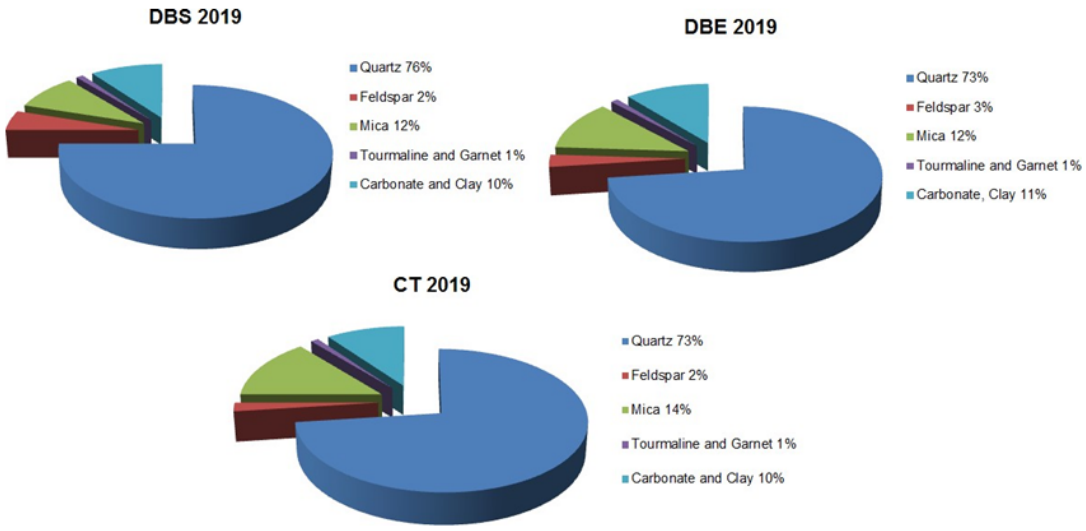

Figure 5.14: Mineral content analysis from desilting basin start, desilting basin end, and cooling tank at Jhimruk hydro-power plant

5.2 Flow Around Guide Vanes of Francis Turbine

The excessive concentration of hard minerals causes erosive and abrasive wear in the turbine components as shown in Figure 5.15. At the inlet of the runner, erosive grooves are found to have occurred near the edges. These grooves make certain angle from the edge and have similar patterns for all the blades. The erosion on the trailing edge of the blade is concentrated at the edge of the shroud. On the guide vanes, the ends of the vanes, or the space between the facing plate and the guide vane were found to be severely eroded.

Figure 5.15: Erosion in the runner and guide vanes of the plant

5.2.1 Classification of Erosion in GVs

The eroded GVs in the turbine consisted of similar patterns. Of all the GVs, one GV was 3D scanned in order to conduct in-depth analysis of the eroded parts. Figure 5.16 shows the actual eroded picture of the GV compared with the 3D scanned model. It can be seen that the eroded regions are precisely captured by the scanner. In the GV erosion was concentrated on the surfaces between the facing plates and the GV. The span length at the leading edge of the erosion GV was measured to be 97 mm, whereas the length was reduced to 91 mm at the trailing edge. Depending upon the location along the chord-wise direction of the GV and the various flow behaviors in those locations, the erosion on the side walls of the GV can be divided into four categories.

1. Leading edge to mid-chord: These locations are mainly accompanied by horse-shoe vortices near the edges followed by leakage flow within the clearance gap

from the high pressure side to the low pressure side. The formation of the grooves shows that the direction of the erosion is from the pressure side to the suction of the GV until the flow hits the GV's shaft.

2. Around the GV's shaft: The flow within the gap stagnates the shaft which tends to distribute around the shaft. However, due to the cylindrical geometry of the shaft, separation of the flow occurs at one point, which causes turbulence around the surfaces of the shaft, causing erosion.

3. Downstream of GV's shaft: The separation of the flow at the shaft causes further turbulence downstream of the shaft. The flow at this location is further aggravated by the leakage flow from the pressure side to the suction side of the GV.

4. Near trailing edge: The pressure difference between the two sides of the GV near the trailing edge is maximum. Hence, the intensity of the leakage flow increases in this region. Moreover, the leakage flow creates a greater angle with reference to the streamline flow, compared to the leading edge regions.

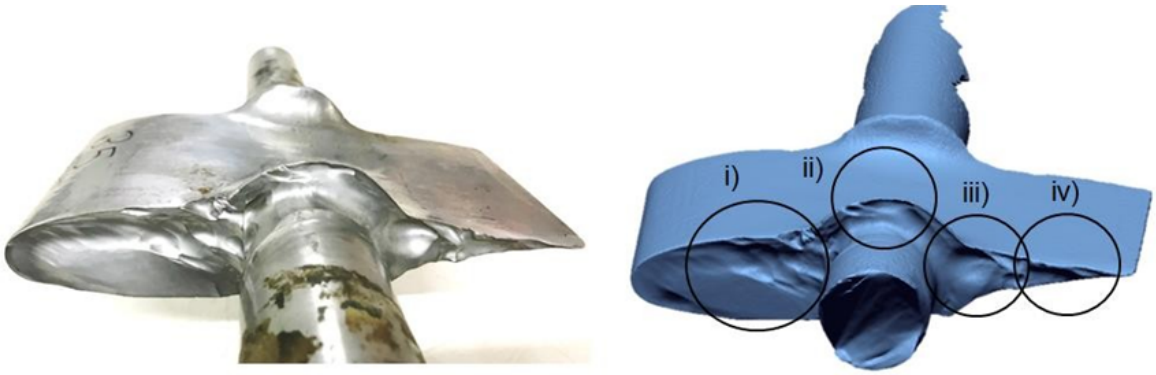

Figure 5.16: Actual eroded and 3D scanned GV with various types of erosion

The erosion on the side walls of the GV was further compared with the results from the CFD analysis as shown in Figure 5.17. In the fluid domain of the GV, a 1 mm uniform clearance gap was incorporated. However, in reality, the size of the clearance gap varies non-uniformly due to erosion. Because of the complexities of the eroded geometry and the high quality of the mesh required in those locations, average uniform clearance surfaces were chosen for this analysis. The streamlines within the clearance gap predicted by CFD are in agreement with the types of erosion discussed in Figure 5.16. Deviation of the mainstream flow originates from the leading edge with low intensity due to the low pressure difference between the two sides of the GV.

The illustration of the pressure difference between pressure and suction sides of the GV is shown in Figure 5.17, as a GV loading curve. The x-axis in the plot starts from the leading edge and ends at the trailing edge of the GV. In the y-axis, the pressure values are normalized with the maximum pressure. It can be inferred from the figure that the maximum pressure difference is towards the trailing edge of the GV. It can be seen that the erosion upstream of the shaft is mostly concentrated towards the pressure side because the flow enters the clearance gap from this side. The intensity of the leakage flow towards the trailing edge is high, which results in higher erosion and is aggravated by the separation of the flow at the cylindrical shaft.

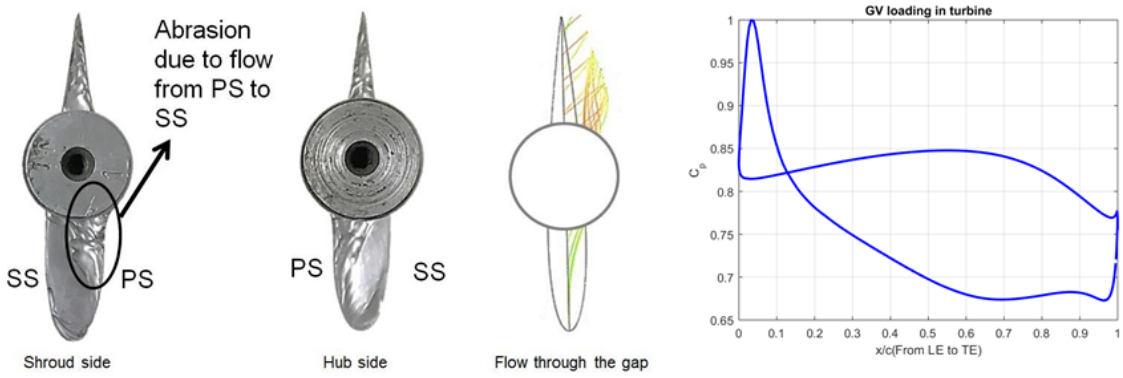

Figure 5.17: (a) Eroded side walls of the GV illustrated with the result of CFD (b) GV loading curve.

5.2.2 Classification of Erosion in The Runner

In the case of runner, erosion is mostly concentration at inlet and outlet of the runner blades. Three types of erosion were identified based on the observation of the eroded model shown in figure 5.18.

1. Leading edge erosion: In all the runner blades, the regions near hub and shroud were found to have eroded. The nature of the erosion is similar for all the blades, i.e. formation of the grooves, most likely due to vortices near the end walls. These vortices might have originated from the leakage flow through the clearance gap of the GVs.

2. Outlet holes: In the turbine, there are 30 runner blades, including 15 splitter blades and 24 GVs. The runner blades experience 24 GV passing frequencies at every revolution. As the leakage flow takes place from each GV, the frequency of the vortices hitting the runner blades is same as the Rotor Stator Interaction frequency. During the course of the revolution, some vortices enter into the

runner blades without hitting the inlet. As soon as the vortices hit any part of the blade, erosion might occur on the blade surface. As the thickness of the blade towards the outlet is less than towards the inlet, holes on the blades might be possible with few impacts.

3. Erosion at the shroud end of the trailing edge: Erosion in this region is due to high relative velocity of the flow. As erosion is directly proportional to the n^{th} order of the velocity, the high relative velocity in this region followed by small thickness of the runner blade could cause large erosion intensity.

The vortices originated from the leakage flow impacting the runner blades are further illustrated through the results of the CFD analysis in Figure 5.19. These vortices are captured as an iso-surface of the vortex core region having the frequency of 500 Hz. The locations of the vortices striking on the runner blades match with the eroded regions of the blades. This vortex originates through mixing of the mainstream flow with the leakage flow, which has certain angle compared to the direction of the ideal flow. This mixing of the flow results in the rotating component with an axis along the direction of the vortex path. The rotational energy contained in this vortex filaments are released partially at the inlet of the runner blades, and partially on any stream location of the blade surfaces.

An illustration of a vortex missing the runner inlet and hitting the surfaces towards the trailing edge is shown in Figure 5.20. It was analyzed from the scanned model that the erosion originated from the pressure side of the blade, as the impinged marks were clearly visible from this side.

Finally, illustration of the type iii) of the runner erosion is shown in Figure 5.21. Erosion at the outlet of the runner towards the region of the shroud is mainly governed by the high relative velocity of the flow. A meridional surface of the GV and the runner is shown from the CFD analysis. Velocity of the flow is plotted on this surface, which shows that the shroud region towards the outlet of the blade contains maximum velocity. The eroded regions in the actual runner match with the high velocity regions predicted by CFD. This figure shows the validity of the most often quoted expression for erosion [53], i.e. Erosion $\propto$ (Velocity)^n, where n is between 2 to 3 depending upon the types of the base material.

In the runner blade, this is also the region with minimum thickness, to avoid the trailing edge wake losses from the runner. In a recent numerical study conducted in Jhimruk hydro-power plant, it was shown that the interblade vortex predominant in off-design conditions is the main factor that induces severe erosion wear at the outlet of the blade [74]. These vortices were found to be generated by the flow separation at the

leading edge of the blades due to improper stagnation. Past studies [9] and [10] have focused on changing the blade angle distribution of the runner blades, such that the velocity profile inside the runner can be optimized for minimum erosion and minimum drop in the efficiency of the runner in doing so. Although these solutions have been investigated numerically, the experimental or field tests for the optimized runner have not been performed yet.

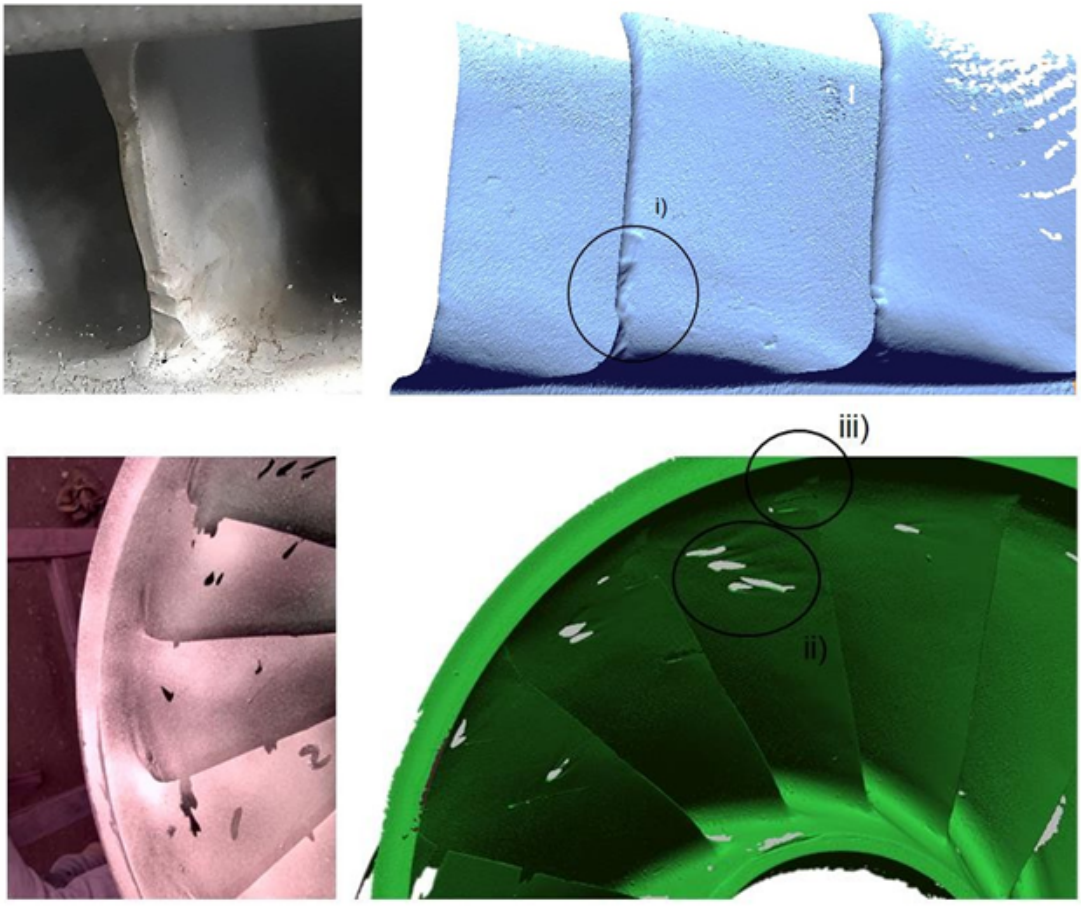

Figure 5.18: Actual eroded and 3D scanned runner with various types of erosion

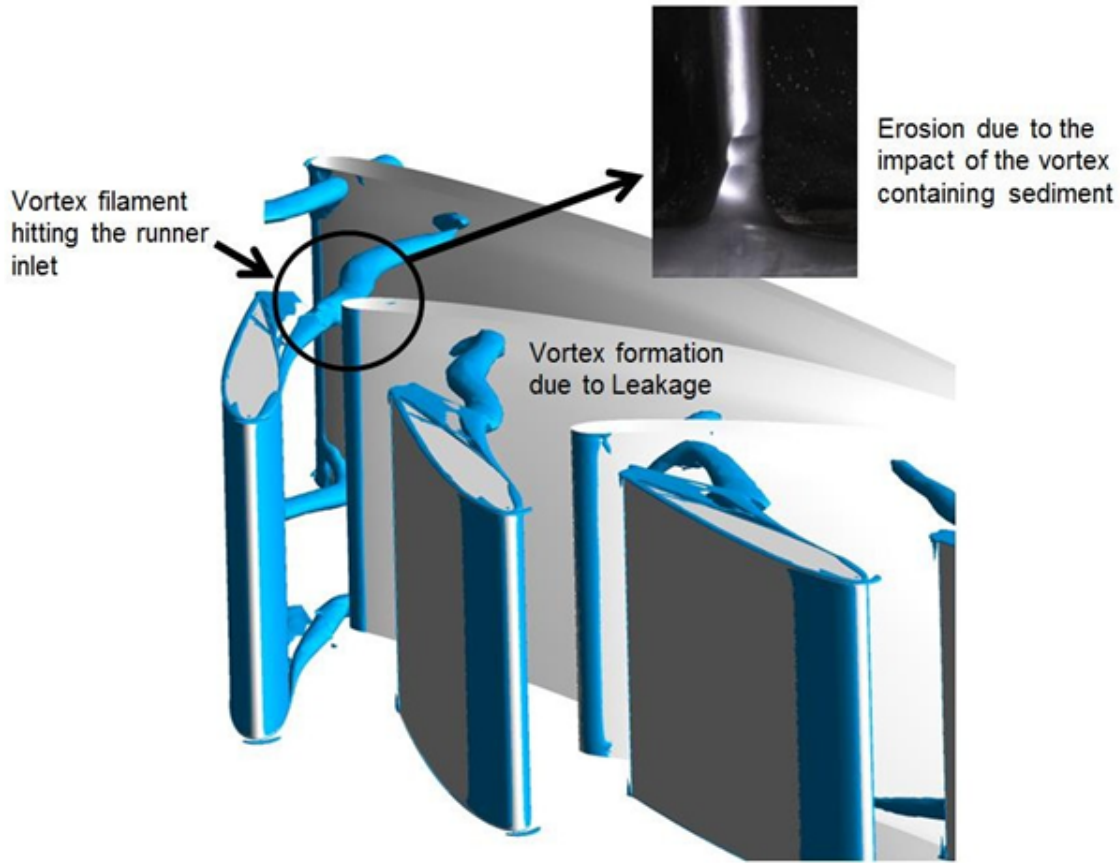

Figure 5.19: Illustration of the runner inlet erosion (type i) due to the vortex originating from the leakage flow

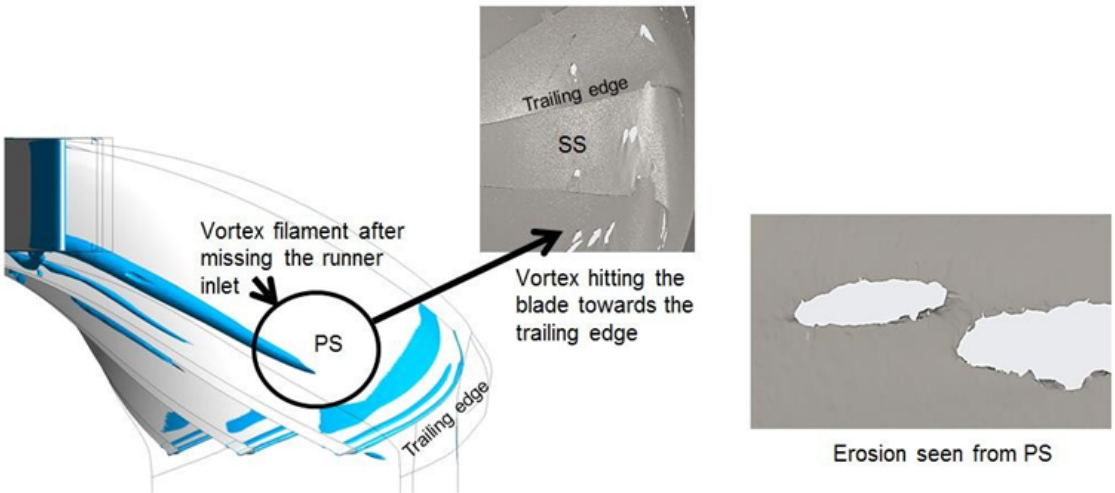

Figure 5.20: Illustration of the runner outlet erosion (type ii) due to the vortex filament

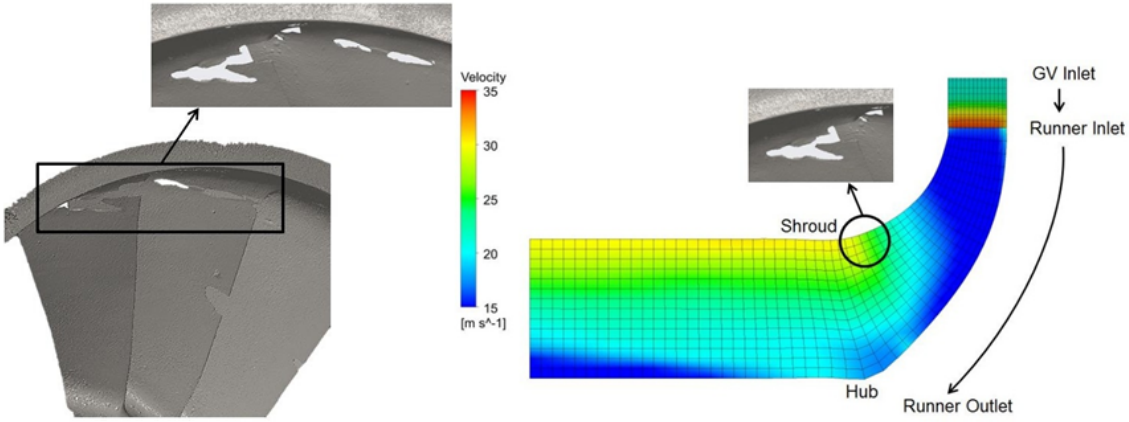

Figure 5.21: Illustration of the runner outlet erosion (type iii) due to high relative velocity

5.3 Validation of The Flow Pattern Around RDA Compared to The Actual Turbine

5.3.1 Pressure Distribution and GVs Loading Curve in RDA

Figure 5.22 shows the pressure distribution around the GVs in the apparatus. Maximum pressure was found to have developed at the leading edge, with high pressure side at the top surface. Due to the rotation of the disc, a low pressure region might have been formed towards the center of the chamber, which resulted the flow towards the circumference to be driven into the center. The distribution of the pressure and suction side around the surface of GV is comparable to that of the real turbine. To illustrate the pressure difference between the two sides of GV, a blade loading curve is plotted as shown in Figure 5.23. Towards the leading edge, the difference in pressure is negative, which is because of the incorrect stagnation point. Comparing to the real turbine scenario, such stagnation could be related to the higher load conditions, when the opening of the GV is higher than that of best efficiency point.

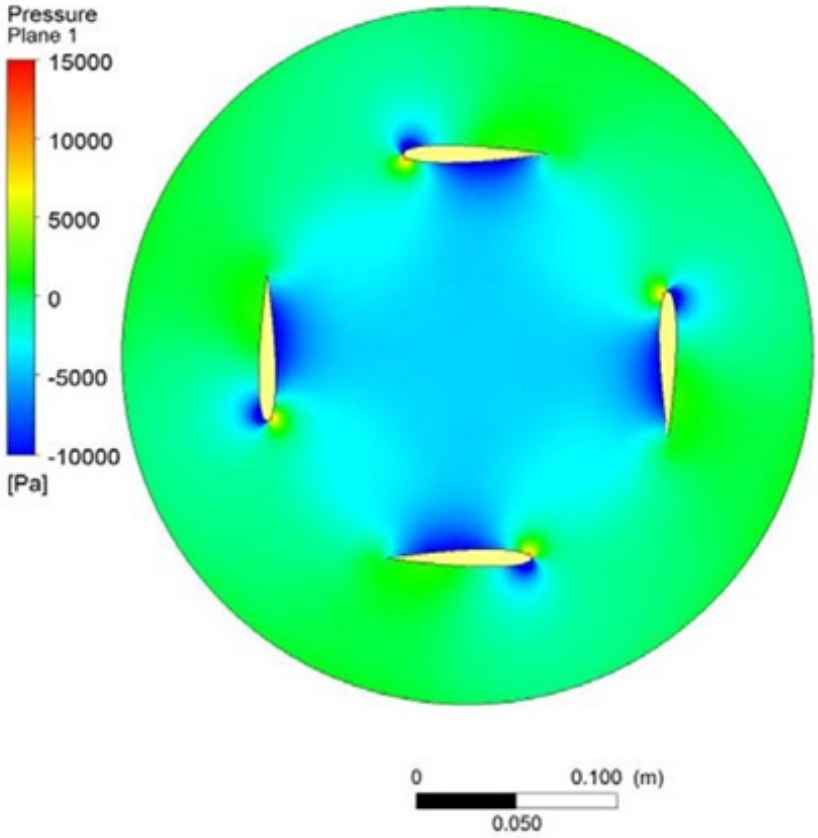

Figure 5.22: Pressure distribution around GVs in RDA

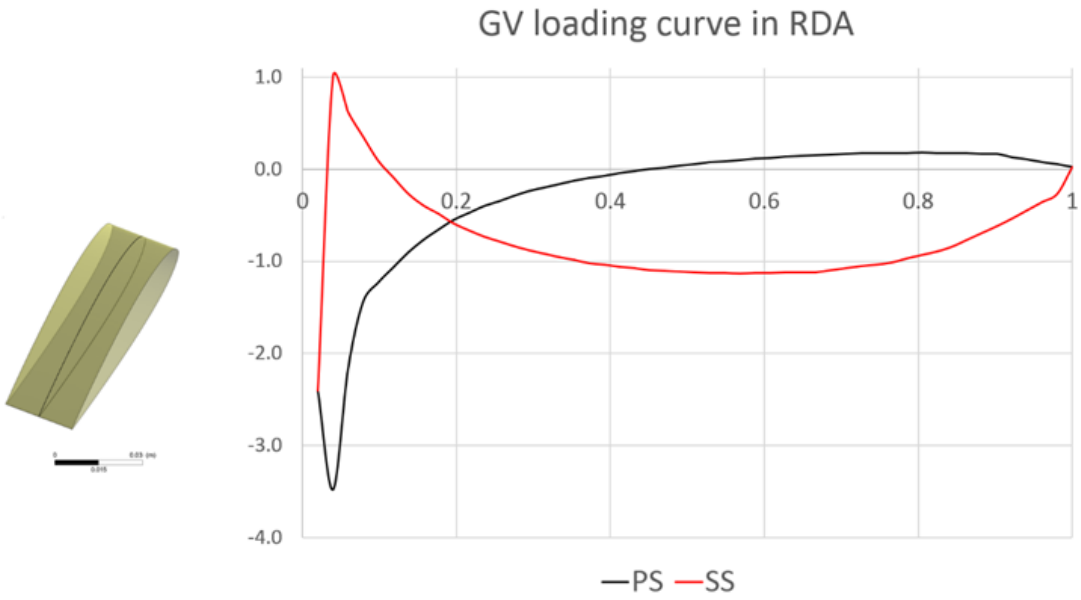

Figure 5.23: GV loading curve in RDA measured at the mid-span

5.3.2 Tip Leakage Vortex

In GVs of Francis turbines, a small clearance gap is present in order to make it possible to open and close based on different flow and load conditions. However, as the flow containing sediment particles strike these gaps, the erosion occurs inside the gap, which as a result increases the size of the gap [15]. Since flow is driven by a pressure difference, and because of the pressure difference between the two sides of the guide vanes, the flow passes through this gap which is termed as a leakage flow and the consequent vortex formed due to the interaction of this flow with the primary flow is called as a leakage vortex. Figure 5.24 [15] shows the leakage flow plotted along the chord of the GV in terms of velocity vectors 1 mm away from the tip for both RDA and the actual turbine. The velocity components perpendicular to the chord lengths signifies the intensity of the leakage flow. It can be seen through this comparison that RDA is able to produce the vector field in these regions with high degree of agreement from that of the actual turbine.

The leakage flow shown in Figure 5.24 produces a rotational component of the flow after mixing with the main flow and forms a vortex filament. These vortices eventually hit the runner blades towards inlet and cause more problems of erosion and efficiency loss of the runner. Figure 5.25 shows the streamlines from two points upstream of a GV observed during CFD and comparison with the streamlines from a GV cascade rig from a past study. The GV cascade rig was focused on investigating the flow field around GVs of Francis turbines using particle image velocimetry technique. The flow field in this cascade rig was found to be similar to that of the real turbine. Figure 5.25 (b) shows the comparison made between two hydrofoils. In the case of asymmetrical GV profiles like NACA4412, the pressure difference between the two sides of GV was found to be less than that of NACA0012, which helped to reduce the leakage flow and consequences of the vortex filament [75]. In RDA, it can be inferred from Figure 5.25 [13] that the tip leakage flow along with the resulting vortices can be predicted similar to that of the cascade rig [76].

Furthermore, Figure 5.26 [15] shows the plot of the velocity component normal to the chord of the GV obtained from RDA and compared to the previous studies conducted on the real turbine. In Figure 5.26 (b), the red dotted line indicates the symmetrical GV (NACA0012), which was also used for RDA. On comparing this curve with Figure 5.26 (a), the trend of the velocity component normal to the chord was found to be similar to that of the real GV. Hence, from these analyses, it can be determined that even for a much simplified apparatus like RDA, the flow conditions around GVs match closely with that of the real turbine. This could be because the water flows in turbines are compensated with the rotation of the GVs in RDA. Although the fluid remains

stationary initially in the apparatus, the rotation of the GVs fitted in the disc rotates the fluid, creating a particular flow structure inside the chamber. By orienting the GVs at a certain angle, it might also be possible to relate the flow behavior with some other operating conditions of the turbine.

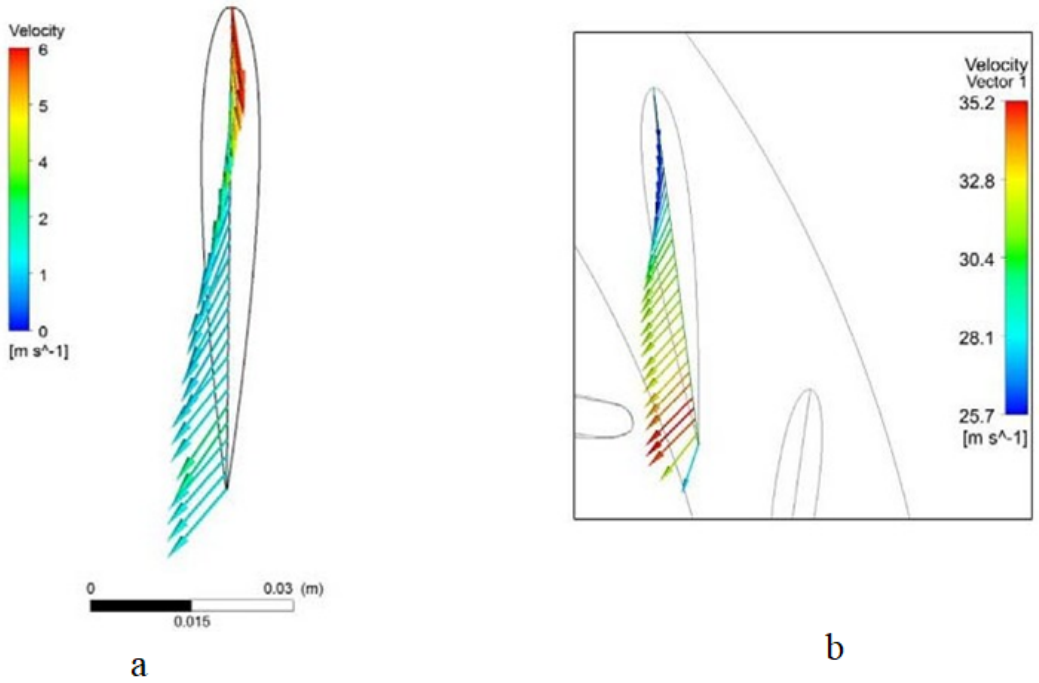

Figure 5.24: Leakage flow through the tip of the GV a) in RDA (from present study) and b) in actual turbine

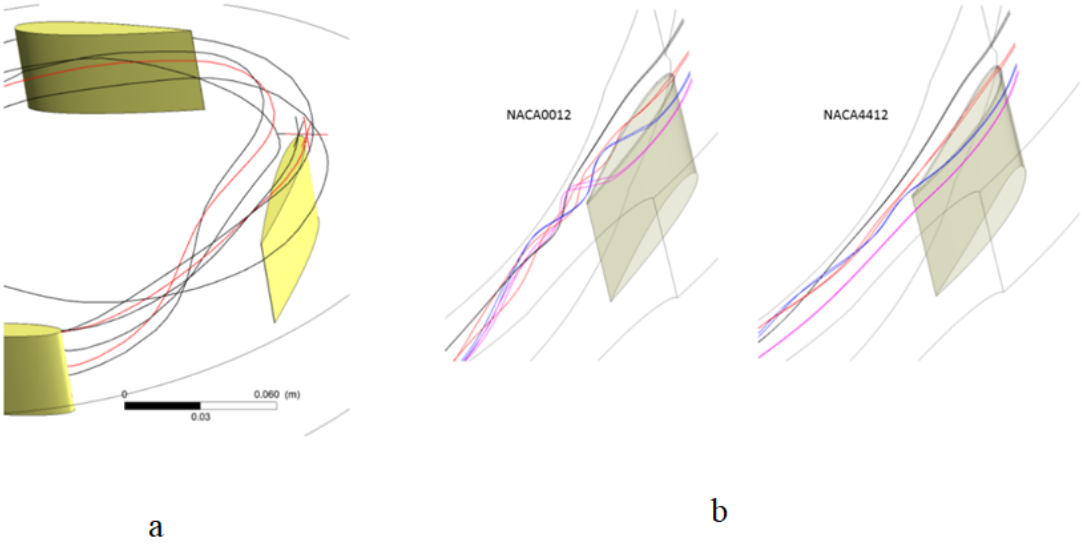

Figure 5.25: Streamlines starting from two points upstream of GV tip in a) RDA (from present study) compared to that of the b) GV cascade rig

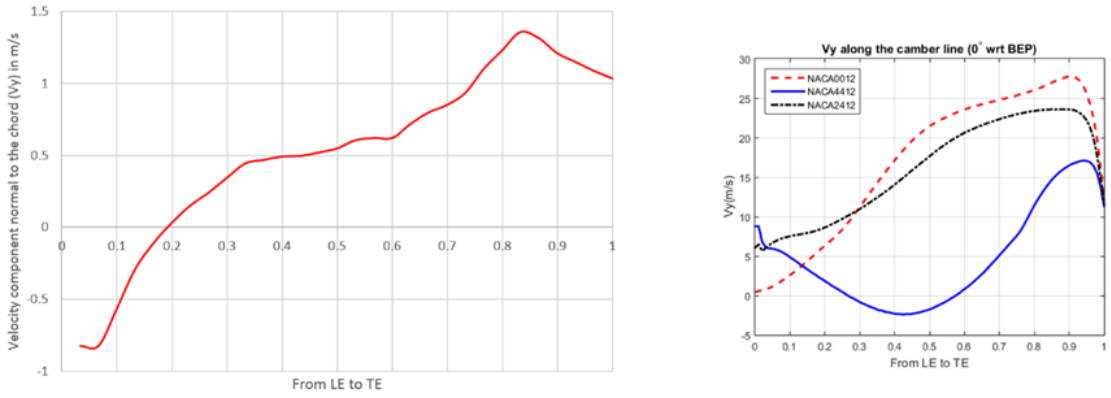

a b

Figure 5.26: Velocity component normal to the chord along the chord length in a) RDA (from present study) compared to that of the b) Real turbine's case

5.4 Rotating Disc Apparatus and Scanning Electron Microscope Tests and Analyses

The color coated GVs in the RDA consisted of similar erosion patterns. Out of four GVs two of them were made up of Brass with casting process and two of them were made up of Mild Steel with Computer Numeric Control (CNC) machining. Figure 5.27 (a) show the suction side of the Brass and Mild Steel GVs and Figure 5.27 (b) shows the pressure side respectively. At suction side at the trailing edge the pressure difference between the two sides of the GV is maximum, the intensity of the leakage flow increases in this region and greater angle with reference to the primary flow generates by the leakage flow, therefore color at those regions of both GVs are removed.
Similarly, at the pressure side of the both Brass and Mild Steel GVs, the color is removed near the leading edges and bottom parts of the mid-stream of GVs. Actually these are the regions seen with horse-shoe vortices near the edges followed by leakage flow within the clearance gap from the high pressure side to the low pressure side.
During the experiment, the amount of material lost was observed 2 times in a 210 minutes and 390 minutes of interval. Following each test, the weights of the test subjects were measured. Before beginning the experiment, the weights of specimens Brass GV1, Brass GV2, Mild Steel GV1, and Mild Steel GV2 were 249.44g, 241.27g, 283.89g and 276.78g respectively. The weights of all test specimens decrease after each run, which is due to the removal of material from the specimens caused by the action of silt erosion. After 210 minutes of operation, the weights were 246.60g, 238.13g, 282.04g and 275.61g and after 390 minutes, the weights were 244.5g, 236.0g, 280.9g, and 274.9g respectively

as shown in Figure 5.28. This demonstrates that the weight loss in specimen Brass GV2, which is 5.27g, is somewhat greater than the weight loss in specimens Brass GV1, Mild Steel GV1, and Mild Steel GV2, which is 4.94g, 2.99g, and 1.88g, respectively. The increased loss in Brass might be attributed to the hardness of the material.
Subsequently, in order to study the erosion patterns on the GVs, trailing edges with 5 mm height and 10 mm diameter, leading edges with 10 mm height and 10 mm diameter and mid streams with 10 mm height and 31 mm diameter specimens were extracted. These specimens were then subjected to microscopic investigations to analyze the erosive wear mechanism using SEM as shown in Figure 5.29.

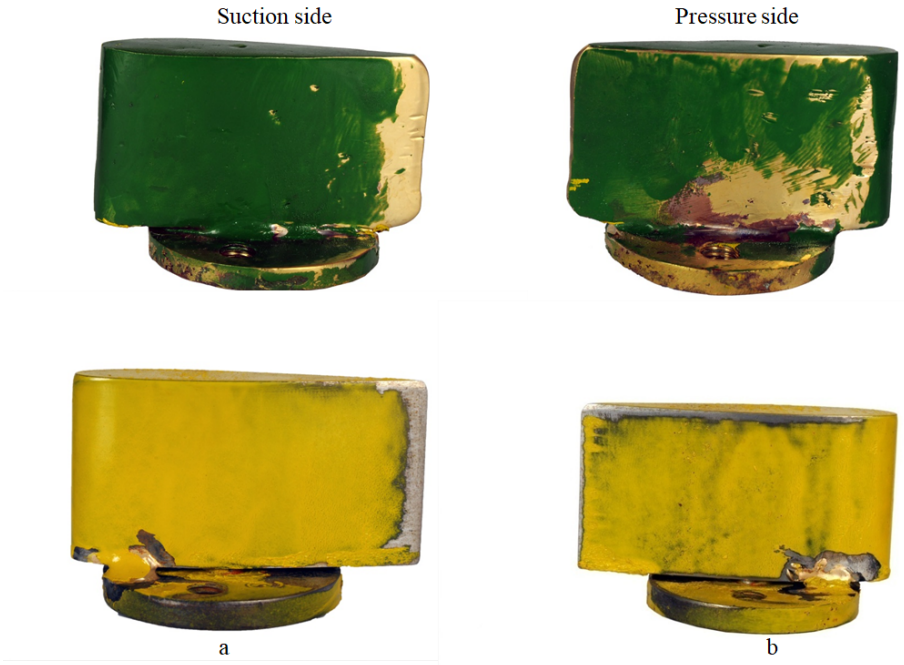

Figure 5.27: Erosion pattern of color coated Brass and Mild Steel GVs

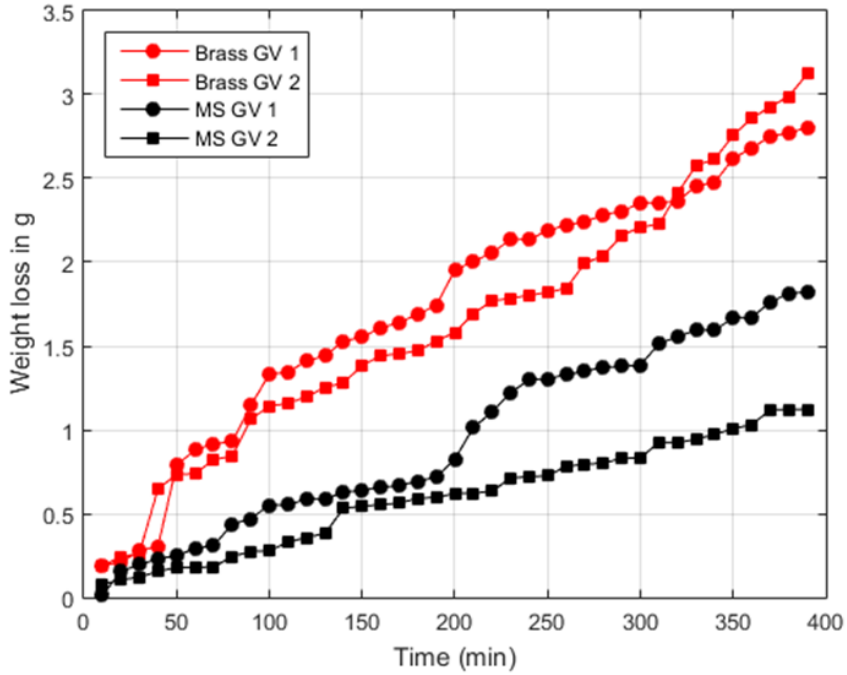

Figure 5.28: Trend of weight loss in GVs with increasing time

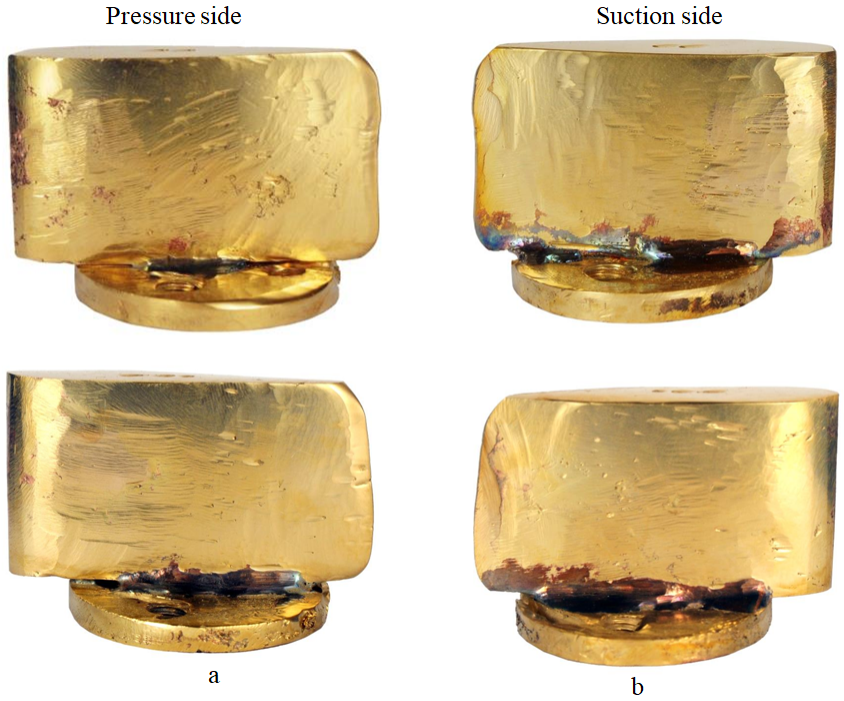

Figure 5.29: Erosion pattern of Brass GVs

The erosion-corrosion zone's development was examined using SEM analysis. Figure 5.30 is a SEM picture of the GV mid-stream surface constructed of brass. A careful examination of the magnified picture reveals that there are various types of indents on

the surface. The indents in the SEM image point in a certain direction, indicating the slurry flow direction. In the image, the indents propagate from left to right, providing vital insights on the erosion-corrosion mechanism and the path travelled by the abrasive particles during the erosion process. The SEM observations contributed to a better knowledge of the precise erosion patterns and mechanisms involved in Brass GV's erosion-corrosion zones.

Figure 5.30 (a), (b), (c), (d), (e), (f), (g), and (h) shows indents, plough, pits, dimple, crack and holes, platelets, cutting and flaks. Indents are formed due to strike of particles on the surface. The ploughing marks are formed by particles striking the surface with acute impingement angle. The pits might be presented due to casting defects. Cracks and holes are formed due to melt of material during casting process. The dimple is formed due to plastic deformation in material's surface. Platelets are formed and removed due to the formation of normal impingement angle.

As shown in Figure 5.30 (e), some locations are not affected by erosion, and these regions are termed as no flow zones. Micro-cutting chips presented in Figure 5.30 (h) might also have formed during the casting process.

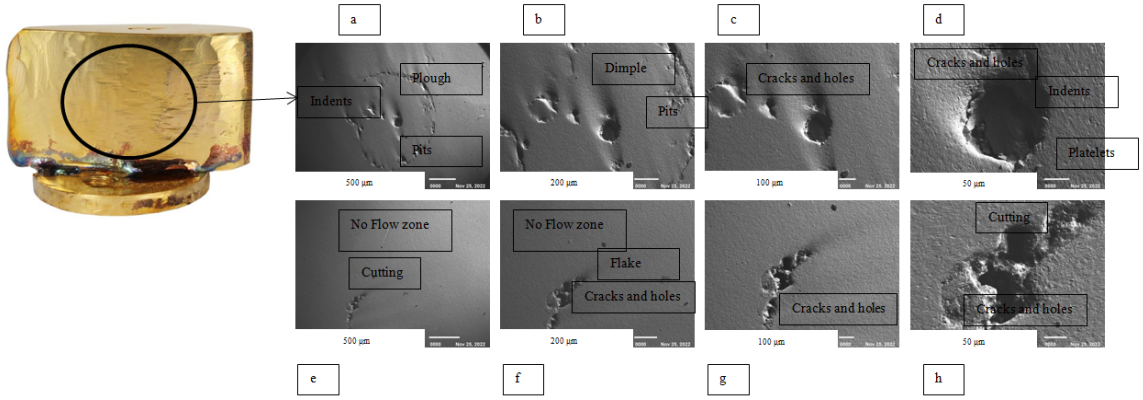

Figure 5.30: SEM images-mid-stream of Brass GV

Figure 5.31 shows SEM images of the eroded surfaces of leading edge of Brass GV. The sectors are divided into eight parts. Figure 5.31 (a), (b), (c) show cutting and plough, (d) shows cutting, platelet and indents, (e) and (f) show ripple formation, (g) shows plough and (h) shows plough, platelets and indents along the flow direction. Clearly, the specimens had similar erosive wear characteristics following slurry erosion at various velocities.

Figure 5.31 (h) shows several signs of particle impacts on the sample surface. This could be connected to the particles' impact velocity, impact angle, and the quantity of particles that impact the regions. Material removal by platelet mechanism is a slower process; it requires more impacts than micro-cutting or ploughing for the material

to be removed completely. Platelets flatten as a result of additional particle impacts following their creation.

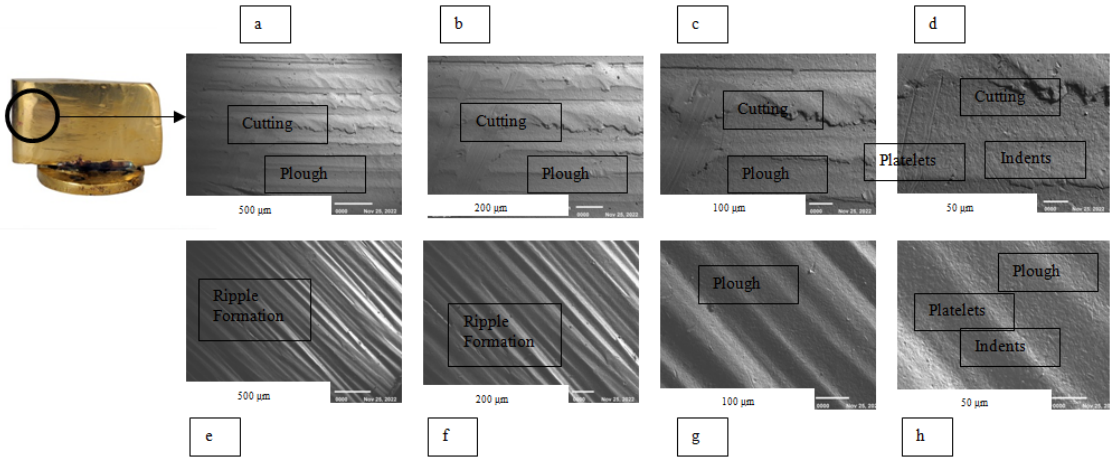

Figure 5.31: SEM images-leading edge of Brass GV

Figure 5.32 (a) shows plough, cutting and scratch, (b) shows debris, cutting, plough and cracks and holes, (c) shows debris, cutting and cracks and holes and (d) shows indents, scratch, cracks and holes and debris respectively of the trailing edge region of Brass GV.

The erosion morphologies were found to vary among regions. There were indents and scratches from particle strikes in all places; however, the extent of the damage varied. The gouging action of the abrasive particles resulted in the development of lips with cracks and holes. The original regions around the cracks and holes were no longer apparent, which may be attributed to the angle and quantity of internal particles impacting the regions.

In the images (a), (b), (c), and (d) of Figure 5.32 there were numerous debris marks and micro cuts. It was because the materials were moved and gathered at the point where the particles escaped. Moreover, the cutting signs were mainly caused by the sharp edges and corners of the particles pressed into the materials, which caused the materials to be cut to accumulate on both side of the scratch.

The specimens of Mild Steels from both pressure and suction sides are shown in Figure 5.33.

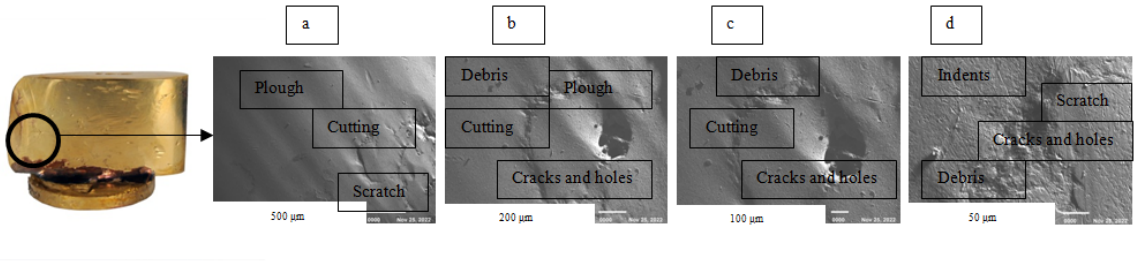

Figure 5.32: SEM images-trailing edge of Brass GV

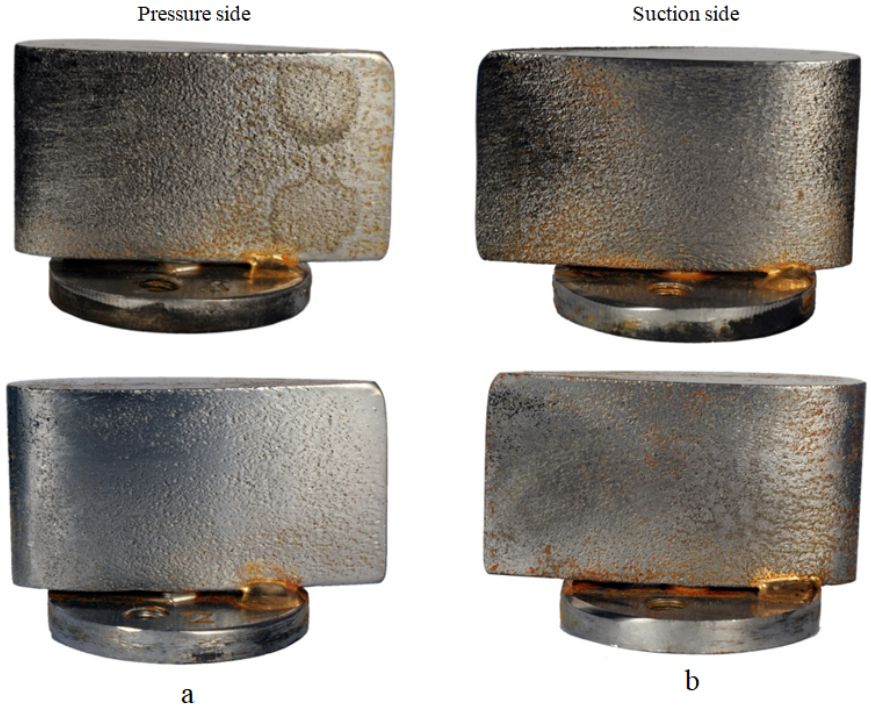

Figure 5.33: Erosion pattern of Mild Steel GVs

Figure 5.34 depicts SEM images of Mild Steel, which clearly demonstrate significant corrosion and mechanical degradation. The carbon percentages found in carbon steel make it more prone to corrosion when exposed to corrosive conditions. When carbon steel reacts with oxygen in the presence of moisture, it oxidizes, resulting in corrosion products and severe corrosion attacks. Corrosion-affected portions weakened and became more susceptible to mechanical erosion induced by abrasive particles. This combination of corrosion and mechanical erosion contributed to the extreme erosion. Figure 5.34 (a), (b), (c), (d) and (d) show the corrosion attack, micro cracks, flake, indents, and platelets. These micro cracks are observed might be with low ductility even though the crystalline structure of material that imparts good quality of ductility. These fractures appeared as tiny cracks on the surface. Particles with varying impact

velocities interact differently, as a result of which, the damage area on the material surface changes accordingly.

Figure 5.35, the prominent erosion mechanism was observed to be the formation and removal of material in the form of cracks and holes as well as platelets. Figure 5.35 (a), (b), (c), (d), (e), (f), (g), and (h) were shown corrosion attack as well as pits, indents, debris and cracks and holes.

From Figure 5.36 the SEM micrographs of the eroded surfaces of (a), (b), (c) and (d) carbon mild steel, trailing edge are shown. It was also discovered that a surface eroded at moderate impact velocity was less plastically distorted than one degraded at high velocity. Excessive flattening forms cracks when the strain reaches the threshold amount. This process finally leads to the removal of material in the form of minute pieces, indicating the presence of fatigue phenomena.

In addition to the platelet mechanism, substantial plastic deformation played an important part in the high-velocity erosion process. The extensive indentation by the erodent particles at high velocity would have resulted in severe plastic deformation of the surrounding region, as illustrated in Figures 5.36, 5.35, and 5.34.

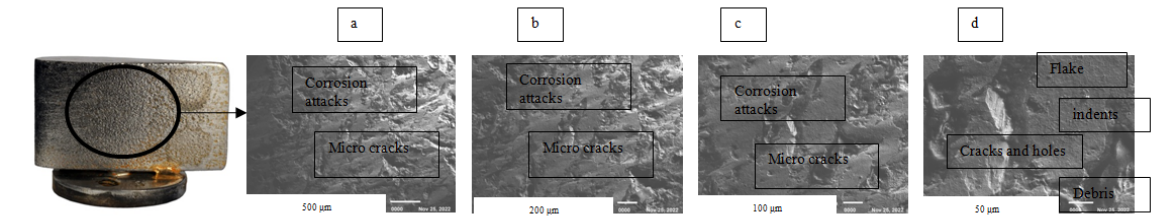

Figure 5.34: SEM images-mid-stream of Mild Steel GV

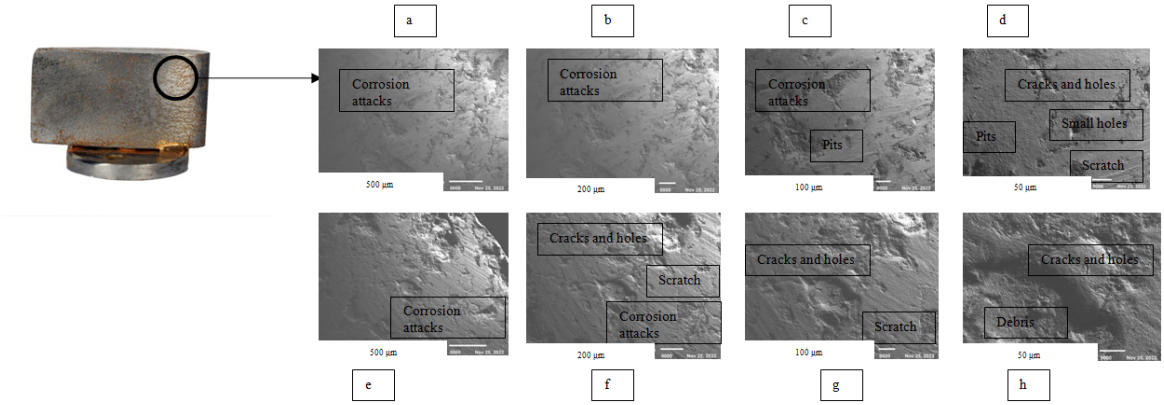

Figure 5.35: SEM images-leading edge of Mild Steel GV

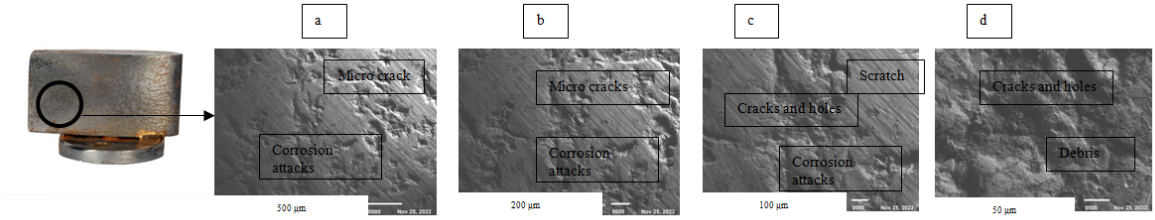

Figure 5.36: SEM images-trailing edge of Mild Steel GV

5.5 Chapter Summary

This chapter provided an overview of the research design with a single methodological framework. A technical implementation framework for each tasks viz. sediments characteristics and its consequences, 3D-scanning of eroded GVs and its consequences with CFD analysis, 3D-scanning of runner blades and its consequences with CFD analysis, GV loading curve with CFD analysis are performed. The results of the experiment in RDA were presented with analysis through SEM for Brass and Mild Steel guide vanes. Flow phenomenon with primary flow, secondary flow and vortex filaments in all above task with its consequences have been briefly discussed by considering the conceptual works formulated in Chapter 4. Similarly, data set preparation, necessary assumptions for simulations and analysis, tools and techniques used in the whole research have been presented with the overall steps of research work.

Chapter 6

Conclusions and Future Enhancement

6.1 Conclusions

Jhimruk hydrpower plant faces severe challenges due to sedimentation problems. The annual power generation from the plant has never reached its expected value since the date of the commissioning. This is because of the low efficiency of turbines after erosion due to high sediment load in wet seasons. From the average daily data of discharge, power output and sediment concentration; it was found that the plant is running at off-designed conditions for more than 50% of the operating time. For almost 100 days a year, the discharge in the River crossed 20 m^3/s which brought excessive sediments from the basin. The inefficient desilting basins in this run-off-river project cause fine sediment particles to remain suspended in water while flowing into the power house. Moreover, the constituent of quartz in the sediment in this river is above 70%. As a result, the components of the turbine where the velocity is high, such as GVs and runners undergo severe wear. Erosion in the turbine is further aggravated by the complex flow phenomena inside the GVs and runners. In this study, the flow field inside the turbines of Jhimruk was studied by using CFD. The erosion in the turbine components was found to have been in a good agreement from the results of the CFD. By using 3D scanning technology, the erosion in the GV was classified into four categories based on their location and type of secondary flow. Similarly, the erosion in the runner was classified into three categories, one at the inlet and two at the outlet. This study was primarily focused on characterizing the types of the erosion in the turbine based on the flow behavior, rather than on the properties of the sediments, such as their size and shape. It was found that the secondary flow induced from the GV's clearance gap was one of the important aspects to consider while developing a

relation between the flow behavior and erosion in Francis turbines.

Since this study aimed to find the means of verification for assuring the flow conditions of an experimental setup compared to that of the actual turbine. RDA was found to produce similar flow characteristics as that of the real turbine, when the test specimen consisted of a scaled down model of GVs of a Francis turbine. The development of the pressure and suction sides due to the flow behavior around the GV was verified through a blade loading curve. The pressure difference also resulted in the flow pattern around the tip region similar to the studies carried out in the past for the real turbine, or a cascade rig that was supposed to characterize the flow condition closely with the real turbine. It can be concluded from this study that RDA can be used as a standard experimental setup to develop erosion models applicable for GVs and compare the design, materials and coatings for performing any optimization. However, further research is necessary to make it more applicable to other components with special focus on the runner blades.

It was found that the prominent location of erosion was towards the trailing edge of the suction side. The mechanism of erosion in various portions of GVs was found to be closely related to the flow pattern in that part. The Brass GV showed plastic deformation, but the Mild Steel GV displayed corrosion attack. Erosion in both GVs was caused by the impact of sediment particles on the surface, resulting in platelets, cracks and holes, indents, and pits, while scratching was the primary source of material removal in the slope zone. The rate of erosion of Brass was found to have been higher than the Mild Steel. Out of the four GVs tested in the same apparatus for 390 minutes, the weight loss in Brass was found to be 5.27g and 4.94g, whereas 2.99g, and 1.88g in the Mild Steel.

The guide vane constructed of Mild Steel demonstrated a lower degree of erosive attack than the Brass. It is due to carbon steel's lower chromium concentration, which leads to high resistance to erosive attacks when exposed to erosive fluids. However, Mild Steel GVs showed crack formation and corrosion, whereas Brass GVs showed plastic deformations in overall process. It was also observed that the erosion scars in Mild Steel GVs were larger in both length and depth compared to Brass GVs. It can be inferred from this study that the experimental investigation of sediment erosion depends largely on the base material. Whereas the location of erosion is same in the GVs for both the materials, the surface morphology after erosion takes place differs depending upon the properties of the material. For accelerated erosion testing, Brass could be a suitable material, especially for estimating the erosion rate in relative scale. However, a correlation with the actual turbine material should be developed for predicting the actual erosion rates in GVs.

6.2 Future Enhancement

The clearance gap between GVs and facing plates were increased due to the pressure difference between the pressure side and suction side of GVs, due to which leakage flow occurred and when these leakage flow mixed up with stream line flow formed high turbulence vortices known as vortex filament. This study has investigated NACA0012 profile of eroded GVs and runner blades with 3D scanning technology and four scaled down GVs of NACA0012 at RDA.

Numerically, it has included the simulation of single phase flow. The most advanced erosion model with cavitation model can be used with multi-phase flow in the future to have more realistic picture of the flow phenomena inside Francis turbines.

Experimentally, research has included RDA investigation around four scaled down symmetric GVs with uniform clearance gap of 1 mm. The main aim of this experiment was to validate the numerical solutions with the real turbine case. Experimentally, Particle Image Velocimetry (PIV) technique of the flow in one GV cascade rig and in cambered hydrofoils was already done [77]. This technique could be used with the eroded model of GVs with cambered and without cambered hydrofoils.

The sediment erosion problem in Francis turbines in general, and the GV in particular, is a difficult operation and maintenance issue that presents significant hurdles in the planning, design, operation, and maintenance of hydro-power projects in high sediment-laden rivers. As described in this research, a variety of variables contribute to silt erosion damage inside the turbine. This study has investigated on sediment erosion in Francis turbine guide vanes. The current information and discoveries are insufficient to fully address this issue, but they can be used to make a significant advancement in erosion prediction and prevention.

The study of SEM analyses can be useful to material experts. The future researcher may conduct and in-depth study on material selection and experimentally explore all the mechanical properties of ploughing, cutting, crack and holes and pits. They may also explore GVs with different materials, sediment properties, velocity and duration of erosion.

References

[1] O. Edenhofer, R. Pichs-Madruga, Y. Sokona, K. Seyboth, S. Kadner, T. Zwickel, P. Eickemeier, G. Hansen, S. Schlömer, C. von Stechow *et al.*, *Renewable energy sources and climate change mitigation: Special report of the intergovernmental panel on climate change*. Cambridge University Press, 2011.

[2] J. D. Milliman and R. H. Meade, "World-wide delivery of river sediment to the oceans," *The Journal of Geology*, vol. 91, no. 1, pp. 1–21, 1983.

[3] N. N. E. Authority, "A year in review: Fiscal year 2017/2018," *NEA: Kathmandu, Nepal*, 2018.

[4] N. E. Authority and N. Kathmandu, "A year in review-fiscal year 2016/17," *NEA, Kathmandu, Nepal*, 2017.

[5] H. P. Neopane, O. G. Dahlhaug, and M. Cervantes, "The effect of sediment characteristics for predicting erosion on francis turbines blades," *Int. J. Hydropower Dams*, vol. 19, no. 1, pp. 79–83, 2012.

[6] B. Thapa, "Effect of particle separation and sand erosion in a hydraulic turbine," *International Journal of Fluid Mechanics Research*, vol. 37, no. 5, 2010.

[7] B. Chhetry and K. Rana, "Effect of sand erosion on turbine components: a case study of kali gandaki "a" hydroelectric project (144 mw), nepal," *Hydro Nepal: Journal of Water, Energy and Environment*, vol. 17, pp. 24–33, 2015.

[8] H. P. Neopane, O. G. Dahlhaug, and M. Cervantes, "Sediment erosion in hydraulic turbines," *Global Journal of researches in engineering Mechanical and mechanics engineering*, vol. 11, no. 6, pp. 17–26, 2011.

[9] S. Chitrakar, M. Cervantes, and B. S. Thapa, "Fully coupled fsi analysis of francis turbines exposed to sediment erosion," *International Journal of Fluid Machinery and Systems*, vol. 7, no. 3, pp. 101–109, 2014.

[10] M. Eltvik, "Sediment erosion in francis turbines," Master's thesis, Institute for energy process technique, 2009.

[11] S. Gautam, H. P. Neopane, N. Acharya, S. Chitrakar, B. S. Thapa, and B. Zhu, "Sediment erosion in low specific speed francis turbines: A case study on effects and causes," *Wear*, vol. 442, p. 203152, 2020.

[12] S. Chitrakar, H. P. Neopane, and O. G. Dahlhaug, "Study of the simultaneous effects of secondary flow and sediment erosion in francis turbines," *Renewable energy*, vol. 97, pp. 881–891, 2016.

[13] S. Chitrakar, B. S. Thapa, O. G. Dahlhaug, and H. P. Neopane, "Numerical and experimental study of the leakage flow in guide vanes with different hydrofoils," *Journal of Computational Design and Engineering*, vol. 4, no. 3, pp. 218–230, 2017.

[14] S. Chitrakar, "Secondary flow and sediment erosion in francis turbines," 2018.

[15] S. Chitrakar, O. G. Dahlhaug, and H. P. Neopane, "Numerical investigation of the effect of leakage flow through erosion-induced clearance gaps of guide vanes on the performance of francis turbines," *Engineering Applications of Computational Fluid Mechanics*, vol. 12, no. 1, pp. 662–678, 2018.

[16] R. Koirala, B. Thapa, H. P. Neopane, B. Zhu, and B. Chhetry, "Sediment erosion in guide vanes of francis turbine: A case study of kaligandaki hydropower plant, nepal," *Wear*, vol. 362, pp. 53–60, 2016.

[17] B. Thapa, "Sand erosion in hydraulic machinery," 2004.

[18] S. Chitrakar, B. S. Thapa, O. G. Dahlhaug, and H. P. Neopane, "Numerical investigation of the flow phenomena around a low specific speed francis turbine's guide vane cascade," in *IOP Conference Series: Earth and Environmental Science*, vol. 49, no. 6. IOP Publishing, 2016, p. 062016.

[19] W. Tsai, J. Humphrey, I. Cornet, and A. Levy, "Experimental measurement of accelerated erosion in a slurry pot tester," *Wear*, vol. 68, no. 3, pp. 289–303, 1981.

[20] A. Elkholy, "Prediction of abrasion wear for slurry pump materials," *Wear*, vol. 84, no. 1, pp. 39–49, 1983.

[21] B. Rajkarnikar, H. Neopane, and B. Thapa, "Development of rotating disc apparatus for test of sediment-induced erosion in francis runner blades," *Wear*, vol. 306, no. 1-2, pp. 119–125, 2013.

[22] B. Rajkarnikar, H. P. Neopane, and B. S. Thapa, "Comparative study of sediment erosion on alternative designs of francis runner blade," *International Journal of Fluid Machinery and Systems*, vol. 8, no. 3, pp. 183–192, 2015.

[23] R. Koirala, B. Zhu, and H. P. Neopane, "Effect of guide vane clearance gap on francis turbine performance," *Energies*, vol. 9, no. 4, p. 275, 2016.

[24] B. Naidu, "Developing silt consciousness in the minds of hydro power engineers," *Silting Problems in Hydro Power Plants*, pp. 1–34, 2020.

[25] I. B. Celik, U. Ghia, P. J. Roache, and C. J. Freitas, "Procedure for estimation and reporting of uncertainty due to discretization in cfd applications," *Journal of fluids Engineering-Transactions of the ASME*, vol. 130, no. 7, 2008.

[26] S. Aryal, S. Chitrakar, R. Shrestha, and A. K. Jha, "A case study of wear in a high head francis turbine due to suspended sediment and secondary flow in a hydropower plant of nepal," *International Journal of Fluid Machinery and System*, vol. 13, no. 4, 2020.

[27] S. Aryal, S. Chitrakar, R. Shrestha, and A. kumar Jha, "Credibility of rotating disc apparatus for investigating sediment erosion in guide vanes of francis turbines," in *IOP Conference Series: Earth and Environmental Science*, vol. 1037, no. 1. IOP Publishing, 2022, p. 012034.

[28] S. Aryal., S. Chitrakar, R. Shrestha, and A. kumar Jha, "Coating technology in hydro-turbines for sediment affected power plants: A review," in *IOP Conference Series: Earth and Environmental Science*, vol. 1037, no. 1. IOP Publishing, 2022, p. 012021.

[29] P. Bergeron, "Consideration of the factors influencing wear due to hydraulic transport of solid materials," in *Proceedings of the 2nd Conference on Hydraulic Transport and Separation of Solid Materials, Société Hydrotechnique de France, Paris, France*, 1952.

[30] C. Duan and V. Karelin, *Abrasive erosion and corrosion of hydraulic machinery*. World Scientific, 2003, vol. 2.

[31] G. Stachowiak and A. W. Batchelor, *Engineering tribology*. Butterworth-heinemann, 2013.

[32] J. T. Burwell Jr, "Survey of possible wear mechanisms," *Wear*, vol. 1, no. 2, pp. 119–141, 1957.

[33] B. Bhushan and P. L. Ko, "Introduction to tribology," *Appl. Mech. Rev.*, vol. 56, no. 1, pp. B6–B7, 2003.

[34] H. Meng and K. Ludema, "Wear models and predictive equations: their form and content," *Wear*, vol. 181, pp. 443–457, 1995.

[35] T. Bajracharya, "Efficiency deterioration in pelton turbines due to sand-particle-led bucket erosion," *Tribhuvan University*, 2007.

[36] K. Wellinger and H. Uetz, "Sliding, scouring and blasting wear under the influence of granular solids," *Vdi-Forschungsheft*, vol. 21, p. 449, 1955.

[37] W. Stauffer, "The abrasion of hydraulic plant by sandy water," *Schweizer Archiv Für Angew. Wiss. Technik*, vol. 24, no. 7/8, pp. 3–30, 1958.

[38] J. Goodwin, W. Sage, and G. Tilly, "Study of erosion by solid particles," *Proceedings of the Institution of Mechanical Engineers*, vol. 184, no. 1, pp. 279–292, 1969.

[39] P. Bergeron, "Similarity conditions for erosion caused by liquids carrying solids in suspension. application to centrifugal pump impellers," *La Houille Blanche*, vol. 5, pp. 716–729, 1950.

[40] R. Worster and D. Denny, "Hydraulic transport of solid material in pipes," *Proceedings of the Institution of Mechanical Engineers*, vol. 169, no. 1, pp. 563–586, 1955.

[41] W. Wiedenroth, "The influence of sand and gravel on the characteristics of centrifugal pumps, some aspects of wear in hydraulic transportation installations," in *Hydrotransport*, 1970.

[42] S. Bahadur and R. Badruddin, "Erodent particle characterization and the effect of particle size and shape on erosion," *Wear*, vol. 138, no. 1-2, pp. 189–208, 1990.

[43] L. Poudel, B. Thapa, B. Shrestha, and N. Shrestha, "Sediment impact on turbine

material: Case study of modi river, nepal," *Kathmandu University Journal of Science, Engineering and Technology*, vol. 8, no. 1, pp. 88–96, 2012.

[44] T. Bovet, "Contribution to the study of the phenomenon of abrasive erosion in the realm of hydraulic turbines," *Bull. Tech. Suisse Romande*, vol. 84, no. 3, pp. 37–49, 1958.

[45] Y. Shida and H. Fujikawa, "Particle erosion behaviour of boiler tube materials at elevated temperature," *Wear*, vol. 103, no. 4, pp. 281–296, 1985.

[46] H. Hojo, K. Tsuda, and T. Yabu, "Erosion damage of polymeric material by slurry," *Wear*, vol. 112, no. 1, pp. 17–28, 1986.

[47] W. Leith and W. McIlquham, "Accelerated cavitation erosion and sand erosion," in *Symposium on Erosion and Cavitation*. ASTM International, 1962.

[48] J. Bitter, "A study of erosion phenomena part i," *wear*, vol. 6, no. 1, pp. 5–21, 1963.

[49] R. Wood, "The sand erosion performance of coatings," *Materials & design*, vol. 20, no. 4, pp. 179–191, 1999.

[50] J. Zahavi and G. F. Schmitt Jr, "Solid particle erosion of polymeric coatings," *Wear*, vol. 71, no. 2, pp. 191–210, 1981.

[51] M. Matsumura and B. Chen, "Erosion-resistant materials," in *Abrasive erosion and corrosion of hydraulic machinery*. World Scientific, 2002, pp. 235–313.

[52] A. Bezinge and F. SCHAFER, "Pompes d'accumulation et eaux glaciaires," *Bulletin technique de la Suisse romande*, vol. 49, 1968.

[53] G. Truscott, "A literature survey on abrasive wear in hydraulic machinery," *Wear*, vol. 20, no. 1, pp. 29–50, 1972.

[54] J. Humphrey, "Fundamentals of fluid motion in erosion by solid particle impact," *International journal of heat and fluid flow*, vol. 11, no. 3, pp. 170–195, 1990.

[55] E. Bardal, *Corrosion and protection*. Springer, 2004.

[56] N. Tsuguo, "Estimation of repair cycle of turbine due to abrasion caused by suspended sand and determination of desilting basin capacity," in *Proceedings of*

international seminar on sediment handling technique, NHA, Kathmandu, 1999.

[57] G. Sundararajan, "A comprehensive model for the solid particle erosion of ductile materials," *Wear*, vol. 149, no. 1-2, pp. 111–127, 1991.

[58] S. Chitrakar, H. P. Neopane, and O. G. Dahlhaug, "A review on sediment erosion challenges in hydraulic turbines," *Sedimentation engineering*, p. 9, 2018.

[59] T. Bajracharya, B. Acharya, C. Joshi, R. Saini, and O. Dahlhaug, "Sand erosion of pelton turbine nozzles and buckets: A case study of chilime hydropower plant," *Wear*, vol. 264, no. 3-4, pp. 177–184, 2008.

[60] O. Dahlhaug, P. Skåre, V. Mossing, and A. Gutierrez, "Erosion resistant coatings for francis runners and guidevanes," *The international journal on hydropower & dams*, vol. 17, no. 2, p. 109, 2010.

[61] D. Felix, I. Albayrak, A. Abgottspon, and R. Boes, "Hydro-abrasive erosion of hydraulic turbines caused by sediment-a century of research and development," in *IOP Conference Series: Earth and Environmental Science*, vol. 49, no. 12. IOP Publishing, 2016, p. 122001.

[62] F. Antunes and N. Youlden, "Centrifugal pump wear and wear analysis," *FACTORY PLANT*, vol. 54, no. 3, pp. 34–35, 1966.

[63] I. Finnie, "Erosion of surfaces by solid particles," *wear*, vol. 3, no. 2, pp. 87–103, 1960.

[64] H. P. Neopane, B. Thapa, and O. G. Dahlhaug, "Particle velocity measurement in swirl flow, laboratory studies," *Kathmandu University Journal of Science, Engineering and Technology*, vol. 8, no. 1, pp. 1–14, 2012.

[65] B. S. Thapa, O. G. Dahlhaug, and B. Thapa, "Effects of sediment erosion in guide vanes of francis turbine," *Wear*, vol. 390, pp. 104–112, 2017.

[66] H. Brekke, "Konstruksjon av pumper og turbiner," *Waterpower laboratory, NTNU*, 2008.

[67] B. S. Thapa, O. G. Dahlhaug, and B. Thapa, "Sediment erosion induced leakage flow from guide vane clearance gap in a low specific speed francis turbine," *Renewable Energy*, vol. 107, pp. 253–261, 2017.

[68] R. Koirala, H. P. Neopane, B. Zhu, and B. Thapa, "Effect of sediment erosion on flow around guide vanes of francis turbine," *Renewable Energy*, vol. 136, pp. 1022–1027, 2019.

[69] L. J. Bakkevig, O. Hoftun, and H. Stensby, *Jhimruk Hydro Electric and Rural Electrification Project in Nepal: Experiences from the Project Implementation.* Norwegian Water Resources and energy Administration, 1996.

[70] A. K. Bastola and H. P. Neopane, "Mineral analysis and erosion potential of sediment samples from nepalese hydro power plant: A case study of lower marsyangdi hydropower plant," *Journal of Machinery Manufacturing and Automation*, vol. 3, no. 3, pp. 50–55, 2014.

[71] C. Trivedi, M. J. Cervantes, B. K. Gandhi, and O. G. Dahlhaug, "Experimental and numerical studies for a high head francis turbine at several operating points," *Journal of Fluids Engineering*, vol. 135, no. 11, 2013.

[72] B. P. Reif and P. Durbin, *Statistical theory and modeling for turbulent flows.* John Wiley & Sons, 2011.

[73] F. R. Menter, "Two-equation eddy-viscosity turbulence models for engineering applications," *AIAA journal*, vol. 32, no. 8, pp. 1598–1605, 1994.

[74] Z. Qian, Z. Zhao, Z. Guo, B. S. Thapa, and B. Thapa, "Erosion wear on runner of francis turbine in jhimruk hydroelectric center," *Journal of Fluids Engineering*, vol. 142, no. 9, p. 094502, 2020.

[75] S. Gautam, H. Neopane, B. Thapa, S. Chitrakar, and B. Zhu, "Numerical investigation of the effects of leakage flow from guide vanes of francis turbines using alternative clearance gap method," *Journal of Applied Fluid Mechanics*, vol. 13, no. 5, pp. 1407–1419, 2020.

[76] S. Chitrakar, H. P. Neopane, and O. G. Dahlhaug, "Development of a test rig for investigating the flow field around guide vanes of francis turbines," *Flow Measurement and Instrumentation*, vol. 70, p. 101648, 2019.

[77] S. .Chitrakar, H. P. Neopane, and O. G. Dahlhaug, "Particle image velocimetry investigation of the leakage flow through clearance gaps in cambered hydrofoils," *Journal of Fluids Engineering*, vol. 139, no. 9, p. 091201, 2017.

Appendix A

First Paper

A.1 A Case Study of Wear in a High Head Francis Turbine Due to Suspended Sediment and Secondary Flow in a Hydropower Plant of Nepal

Appendix B

Second Paper

B.1 Credibility of Rotating Disc Apparatus for Investigating Sediment Erosion in Guide Vanes of Francis Turbine

Appendix C

Third Paper

C.1 Coating Technology in Hydro-Turbines for Sediment Affected Power Plants: A Review

Appendix D

Fourth Paper

D.1 Erosion and Cavitation Induced Vibration in Kaligandaki A Hydropower Plant: A Case Study